CRUSTAL-SCALE SHEAR ZONES RECORDING 400 M.Y. OF TECTONIC ACTIVITY IN THE NORTH CARIBOU GREENSTONE BELT, WESTERN SUPERIOR PROVINCE OF CANADA

by

NETASHA KALBFLEISCH

B. Sc., University of Ottawa – Ottawa, Ontario, 2010

A THESIS SUBMITTED IN PARTIAL FULFILMENT OF THE REQUIREMENT FOR THE DEGREE OF

MASTER OF SCIENCE

in

THE FACULTY OF GRADUATE AND POSTDOCTORAL STUDIES

Department of Earth Sciences

We accept this thesis as conforming to the required standard

UNIVERSITY OF OTTAWA

September 2012

Crustal-scale shear zones recording 400 m.y. of tectonic activity in the North Caribou greenstone belt, western Superior Province of Canada

N. Kalbfleisch
Department of Earth Sciences, University of Ottawa, Ottawa, K1N 6N5 Canada

ABSTRACT

A series of crustal-scale shear zones demarcates the northern and eastern margins of the North Caribou greenstone belt (NCGB), proximal to a Mesoarchean terrane boundary in the core of the western Superior Province of Canada. The dominant deformation produced a pervasive steeply dipping fabric that trends broadly parallel to the doubly arcuate shape of the belt and was responsible for tight folding the banded iron formation host to Goldcorp's prolific gold deposit at Musselwhite mine. The shear zones in the North Caribou greenstone belt are of particular interest because of their ability to channel hydrothermal fluids with the potential to bear ore and cause alteration of the middle to shallow crust. Shear zones are commonly reactivated during subsequent tectonism, but exhibit a consistent and dominant dextral shear sense across the belt; fabric-forming micas and chlorite are generally Mg-rich. Although garnets samples from within the shear zones are dominantly almandine, they possess variable geochemical trends (HREEs of >2 orders of magnitude) and can be syn-, intra-, or post-tectonic in origin. *In situ* geochronological analysis of zircon (U-Pb) and monazite (total-Pb) in high strain rocks in and around the NCGB, interpreted in light of *in situ* geochemical analysis of garnet and fabric-forming micas and chlorite, reveals four relatively discrete events that span 400 million years. Metamorphism of the mid-crust was coeval with magmatism during docking of the Island Lake domain at c. 2.86 Ga and subsequent terrane accretion at the north and south margins of the North Caribou Superterrane from c. 2.75 to

2.71 Ga. Transpressive shear at c. 2.60 to 2.56 Ga and late re-activation of shear zones at c. 2.44 Ga produced a steeply-dipping pervasive fabric, and channeled fluids for late crystallization of garnet and monazite recorded in the Markop Lake deformation zone. These observations implicate a horizontal tectonic model similar to the modern eastern Pacific plate margin. Further, this study highlights the caution that should be exercised when using traditional rock forming metamorphic minerals (mica, chlorite, garnet) when attempting to vector into zones of hydrothermal alteration within midcrustal rocks.

Keywords: North Caribou, Superior Province, shear zone, metamorphism, garnet, monazite, zircon, geochronology

Word count (without references): 19,351
Word count (references): 23,201
Tables: 1
Figures: 17
Appendices: Sample descriptions, methods and data repository (7 data tables)

Zones de cisaillement à l'échelle de la croûte enregistrant 400 millions d'années d'activité tectonique dans la ceinture de roches vertes de North Caribou, Province du lac Supérieur occidentale du Canada

N. Kalbfleisch
Département des sciences de la Terre, Université d'Ottawa, Ottawa, K1N 6N5 Canada

RÉSUMÉ

Une série de zones de cisaillement à l'échelle de la croûte délimitent la ceinture de roches vertes de North Caribou au nord et à l'est, à proximité de la limite d'un terrane mésoarchéen au cœur de la Province du lac Supérieur occidentale du Canada. La déformation principale a produit une fabrique pénétrative à pendage abrupte et dont la direction est dans l'ensemble parallèle à la forme doublement arquée de la ceinture ; elle est aussi responsable du pli serré dans la formation de fer rubanée contenant les dépôts aurifères prolifiques de Goldcorp à la mine Musselwhite. Les zones de cisaillement dans la ceinture de roches vertes de North Caribou sont d'un intérêt particulier en raison de leur habileté à canaliser des fluides hydrothermaux ayant un potentiel de contenir des minerais et de causer l'altération de la croûte moyenne à peu profonde. Les zones de cisaillement sont fréquemment réactivées lors d'épisodes tectoniques ultérieurs, mais démontrent un sens de cisaillement dextre constant et dominant tout au long de la ceinture ; les micas et la chlorite formant la fabrique sont généralement riches en Mg. Bien que les échantillons de grenat provenant de l'intérieur des zones de cisaillement consistent principalement d'almandine, ils possèdent des tendances géochimiques variables (ETRD – « HREE » – de >2 ordres de grandeur) et peuvent avoir une origine syn-, intra- ou post-tectonique. Des analyses géochronologiques *in situ* de zircon (U-Pb) et monazite (Pb-total) dans des roches de hautes contraintes à l'intérieur et autour de la ceinture de roches vertes de North Caribou, interprétées à la lumière d'analyses géochimiques

in situ de grenat et de micas et chlorite définissant la fabrique, révèlent quatre événements relativement distincts s'étendant sur 400 millions d'années. Le métamorphisme de la croûte moyenne était contemporain au magmatisme lors de l'amarrage du domaine Island Lake à c. 2.86 Ga et de l'accrétion subséquente de terranes aux limites nord et sud du superterrane North Caribou de c. 2.75 Ga à 2.71 Ga. Un cisaillement transpressif à c. 2.60 à 2.56 Ga et une réactivation tardive des zones de cisaillement à c. 2.44 Ga ont produit une fabrique pénétrative à pendage abrupte et ont canalisé des fluides pour la cristallisation tardive de grenat et monazite enregistrés dans la zone de déformation de Markop Lake. Ces observations impliquent un modèle de tectonique horizontale similaire à la limite orientale actuelle de la plaque du Pacifique. De plus, cette étude met en évidence la prudence à exercer lors de l'utilisation de minéraux métamorphiques traditionnels (mica, chlorite, grenat) en ciblant des zones d'altération hydrothermale dans les roches de la croûte moyenne.

TABLE OF CONTENTS

LIST OF TABLES

LIST OF FIGURES

ACKNOWLEDGEMENTS

Throughout the course of this project I have developed and grown both as an academic and as an individual, and I have many people to thank for helping to ensure my success. This project was kindly co-funded through an NSERC CRD in cooperation with Goldcorp's Musselwhite mine. I was fortunate to participate in a MITACS-Accelerate internship program during my first summer of fieldwork at Musselwhite mine, and I would like to thank Chief geologist Rohan Millar for Goldcorp's contribution to the funding of this program. An expression of sincere gratitude goes to John Biczok for his unequivocal enthusiasm for the project and for sharing his wealth of knowledge of the regional geology.

My data-collection could not have been completed in such a timely fashion without the assistance of many technicians. I would like to thank George Mrazek for his patience and care in preparing a multitude of oriented polished thin sections at the University of Ottawa. Peter Jones is thanked for his help with mineral identification on the SEM at Carleton University. Thanks to Lynn Heizler for *in situ* EMPA of monazite and garnet at the New Mexico Institute of Mining and Technology. I would like to thank Glenn Poirier for sharing his knowledge and expertise on the SEM and EMPA at the University of Ottawa. Simon Jackson at the Geological Survey of Canada is thanked for his guidance and assistance with LAICP-MS of garnet. My deepest thanks goes to Chris McFarlane and Yan Luo for teaching me their system for *in situ* LAICP-MS of zircon at the University of New Brunswick, and for their limitless help with the data reduction that ensued.

I have several colleagues and professors at the University of Ottawa that I would like to acknowledge for their help and support over the past couple of years. Élise Cossette and Colter Kelly were wonderful field assistants, thank you for our stimulating discussions both

on the outcrop and back at camp. Jason Duff and Amanda Van Lankvelt have been the best project companions a girl could ask for, thank you for letting me bounce my thoughts about NCGB origin and geometry around with you. Keiko Hattori receives thanks for her insight and encouragement as co-supervisor of this project. I would also like to thank my defense committee, particularly Alex Zagorevski from the Geological Survey of Canada who worked closely with me to enhance the local geology section of my thesis, as well as the chair of my defense, André Lalonde, who helped me process my chlorite and mica geochemical data.

Thanks to everyone and anyone who bore witness to my rants and rambles about my thesis-writing process and accepted my need to disappear in order to get her done. Particularly, my Mom, my Dad and Cathy, my sisters, the Collins family, my ball hockey girls, my geo dudes and surrogates, and my best friend Nicole Williamson, who is my brightest of guiding lights. I have never been more aware of the value of the incredible support system you have provided for me, thank you. Thank you for being ever so proud.

I feel like there are truly no words to express my gratitude to my supervisor, Dave Schneider. From the day we met, he has seen potential in me and has gone to great lengths to see it achieved. If ever in the dark, Dave would nudge me back into the light, he helped me to learn the invaluable lesson of balance and the importance of yin and yang.

Last but certainly not least, I would like to thank my partner, Sarah Collins, for always putting things into perspective and pushing me to be more than I thought I could be. We share a dream much stronger than the burden of all my stresses, and I am so fortunate to have had her by my side throughout this journey.

1. Introduction

The North Caribou greenstone belt (NCGB) consists of a c. 3.0 to 2.8 Ga suite of metasedimentary and metavolcanic supracrustal assemblages situated at the northern margin of the North Caribou core (NCC) of the Superior Province of Canada (**Fig. 1A**). Originally distinguished on the basis of lithological and structural characteristics by Card and Ciesielski (1986), the Superior Province is now defined by Mesoarchean terranes and superterranes in light of modern aeromagnetic, isotopic, and geochronological data (Percival et al., 2006 and references therein). The amalgamation of terranes to the North Caribou superterrane (NCS) in the Mesoarchean strongly implicates horizontal tectonics as microcontinents were accreted from both north and south throughout the Kenoran orogeny (Percival et. al, 2006). Although a vertical tectonic model is invoked to explain the dome and keel structures that typify Archean granite-greenstone terrains (e.g. Goodwin and Smith, 1980; Gorman et al., 1978; Chardon et al., 1996, 1998; Lin, 2005; Parmenter et al., 2006; François et al., 2012), the compression that may precede lateral flow collapse in the production of keel structures (Harris et al., 2012) necessitates horizontal movement, suggesting the two processes may be synchronous (cf. Parmenter et al., 2006). Vertical displacement along granite-greenstone contacts appears to operate in synchroneity with regionally consistent strike-slip shearing in many Archean terranes (e.g. Choukroune et al., 1997; Chardon et al., 2002). In contrast, vertical tectonism, such as has been documented in the eastern Pilbara craton (Van Kranendonk and Collins, 1998), predated the strike-slip shearing and Lin (2005) contends the importance of understanding the nature and timing of shear zone relationships in order to model the tectonic processes driving their formation.

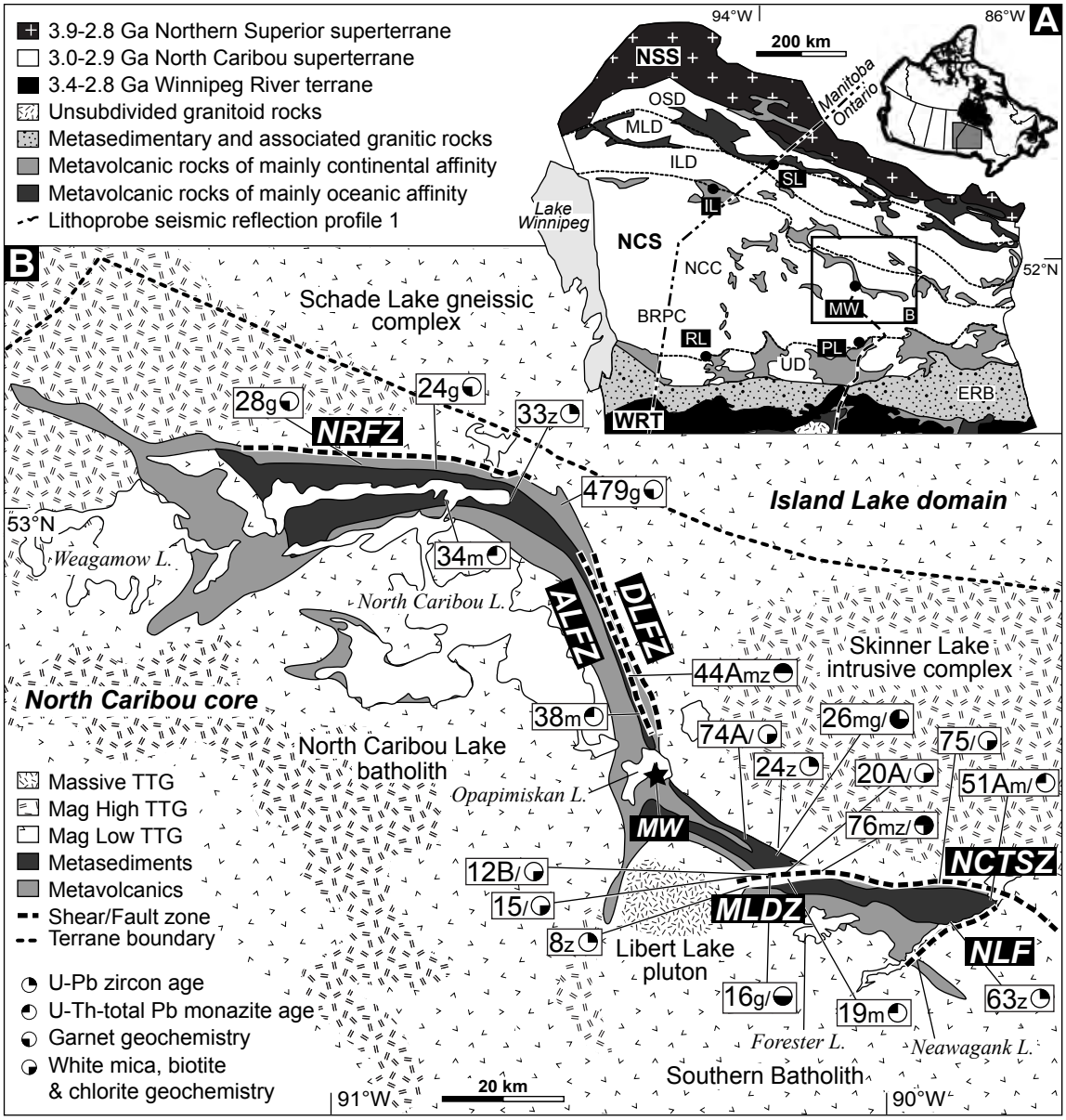

Fig. 1. Regional and local geology maps of the North Caribou greenstone belt in Northwestern Ontario (cf. Percival et al., 2006 and Breaks et al., 2001). (A) The location of the NCGB among the W-NW/E-SE trending terranes and superterranes of the Northwestern Superior Province. NSS: Northern Superior superterrane, NCS: North Caribou superterrane which encompasses the OSD: Oxford-Stull domain, MLD: Munroe Lake domain, ILD: Island Lake domain, NCC: North Caribou core, BRPC: Berens River plutonic complex, and UD: Uchi domain and is host to several gold deposits including thos in the SL: Stull Lake, IL: Island Lake, MW: Musselwhite, RL: Red Lake, and PL: Pickel Lake greenstone belts. A sediment trap formed during accretion of the WRT: Winnipeg River terrane to the NCS is identified as the ERB: English River basin. (B) The geometry of supercrustal metasedimentary and metavolcanic assemblages among TTG granitoids distinguished by aeromagnetic signatures (high vs. low), the locality of the NRFZ: North Rim fault zone, ALFZ: Akow Lake fault zone, DLFZ, Dinick Lake fault zone, MLDZ: Markop Lake deformation zone, NCTSZ: North Caribou-Totogan shear zone, NLF: Neawagank Lake fault, as well as the location of MW: Musselwhite mine. Sample locations are indicated (refer to Table 1 for sample number prefixes) and the type of analysis conducted is identified by filled quarters of a circle representing one of each of g: garnet geochemistry, m: total Pb monazite dating, z: U-Pb zircon dating, and /: geochemistry of chlorite and micas.

Shear zones are likely subject to reactivation during subsequent tectonism, which then can act as advective pathways for subjacent metamorphic fluids (McCaig and Knipe, 1990; Newton, 1990; Selverstone et al., 1991). These pathways expedite fluid flow by orders of magnitude greater than a rock's intrinsic permeability (Ingebristen and Sanford, 1998) and channel hydrothermal fluids, causing localized alteration throughout the middle and shallow crust. The North Caribou greenstone belt possesses a series of near-vertical shear zones that follow its northern and eastern margins in proximity to the suture zone that demarcates the accretion of the Island Lake domain during Mesoarchean tectonic assembly of the North Caribou superterrane (**Fig. 1B**). A tightly folded banded iron formation in the belt is host to a prolific gold deposit at Goldcorp's Musselwhite mine and these shear zones may have implications for transport of gold-bearing fluids as proximity to such crustal-scale structures is a major controlling factor in the development of many world-class orogenic gold deposits (cf. Weinberg et al., 2003).

The shear zones within the NCGB have been described in terms of their general size and orientation, as well as their first order rheology and kinematics (Breaks et al., 2001), yet our understanding of their importance is hampered by a lack of detailed mineralogical and geochemical characterization, and numerical age constraints. In an attempt to resolve the tectonometamorphic evolution of the North Caribou greenstone belt, I have conducted an integrated geochronologic and structural analysis of the major shear zones of this region. *In situ* zircon and monazite geochronology is coupled with major and trace element geochemical analyses of garnet and abundant fabric-forming phyllosilicates in hopes of distinguishing metamorphic ages from hydrothermal signatures. My results yield evidence for a 400 m.y. tectonic history that likely originated in a transpressive horizontal tectonic regime with the

docking of the Island Lake domain, highlighted by a 2.86 Ga metamorphic age of zircon, and terminated with re-activation of shear zones and channeling of fluids, particularly along the Markop Lake deformation zone (MLDZ, **Fig. 1B**), as evidenced by a c. 2.44 Ga recrystallization age of monazite. The nearby crustal-scale suture zone at the North Caribou-Island Lake boundary undoubtedly acted as a major fluid conduit with potential implications for hydrothermal alteration and mineralization.

2. Archean geodynamics of the Superior Province

The classic greenstone-granite terranes in the Superior Province of Canada have been the focus of many studies of Archean geology and tectonics for more than a century (Percival et al., 2006 and references therein). Originally, lithological and structural characteristics were used to distinguish linear NW- to WNW-trending subprovinces accentuated by subparallel boundary faults (Card and Ciesielski, 1986). These subprovinces have recently been re-classified into a series of Mesoarchean terranes and superterranes based on modern aeromagnetic surveys, crust formation ages, Nd isotopic signatures and other geochronological evidence for specific tectonothermal events relating to their assembly (Percival et al., 2006; Stott et al., 2007, 2010). A terrane represents a fragment of crust that existed tens to hundreds of million years prior to the development of ocean basins and a superterrane is a collage of terranes assembled prior to the amalgamation of the Superior Province. Five temporally discrete accretionary events, collectively referred to as the Kenoran orogeny, occurred during the Neoarchean to form the core of the Canadian Shield between 2.72 and 2.68 Ga (Percival et al., 2006). The now juxtaposed terranes and superterranes (**Fig.**

1A) are bounded by >1000 km long crustal welts exhibiting a distinct, yet similar, sequence of events at ~10 m.y. intervals (Percival et al., 2006).

Identified by Thurston et al. (1991) as an ancient cratonic nucleus, the North Caribou superterrane (NCS, **Fig. 1A**) is believed to have behaved as a dock to which younger island arcs and micro-continents were progressively accreted in a fashion resembling modern day plate tectonics (e.g. Langford and Morin, 1976; Williams, 1990; Percival et al., 1994). At the northern margin of the NCS, south-over-north shear-zone movement (Lin et al., 2006) and the occurrence of arc magmatic activity between 2.775 and 2.733 Ga across the Island Lake, Munroe Lake, and Oxford-Stull domains (**Fig. 1A**; Corkery et al., 2000; Skulski et al., 2000; Parks et al., 2006) indicate southward subduction. Docking of the c. 3.7 Ga Northern Superior superterrane (oldest remnant of Mesoarchean crust, Böhm et al., 2000, 2003; Skulski et al., 2000) trapped the c. 2.84 Ga oceanic volcanic rocks of the Oxford-Stull domain (Syme et al., 1999; Corkery et al., 2000) in which detrital zircon ages indicate isolation from northern Superior basement until after c. 2.72 Ga (Skulski et al., 2000; Lin et al., 2006). This northern-most region of the western Superior Province is the former Sachigo subprovince of Card and Ciesielski (1986) and Card (1990). White et al. (2003) attribute opposing shear zone vergence at the northern and southern margins of the NCS (imaged on Lithoprobe reflection Line 1, **Fig. 1B**) to a doubly vergent architecture. The southern margin of the NCS records arc magmatism across the Berens River plutonic complex and Uchi domain (**Fig. 1A**; formerly subprovinces) from c. 2.75-2.71 Ga (Corfu et al., 1995), evidence of northward subduction that led to the collision with the c. 3.4 Ga Winnipeg River terrane (**Fig. 1A**). Penetrative deformation at c. 2.72-2.71 Ga (Andrews et al., 1986; Sanborn-Barrie et al., 2001; Dubé et al., 2004) consists of steeply north-dipping surface structures along the south-central margin of

the NCS, potentially constraining the initiation of either subduction or collision (e.g. Corfu et al., 1995; Pan et al., 1999; Sanborn-Barrie et al., 2004; Hrabi and Cruden, 2006; Percival et al., 2006). Gold mineralization at the world-class Red Lake mining district, as well as in the Pickle Lake belt (**Fig. 1A**), is most likely associated with these regionally penetrative and generally synchronous tectonic fabric-forming events (Sanborn-Barrie et al., 2001; Dubé et al., 2003; Young et al., 2006).

The southward propagating accretion of terranes to this now composite Superior superterrane continued for 30 m.y. as the western Wabigoon, Minnesota River Valley, and Wawa-Abitibi terranes were juxtaposed through northward subduction, commonly trapping syn-orogenic sediments of the English River (**Fig. 1A**) and Quetico basins in the collision. Heaman et al. (2011) suggest the complex multistage Neoarchean metamorphic history of high-grade terranes of the Superior Province related to this progressive accretion may be a feature of Archean craton evolution and stabilization. Substantial crustal underplating of basaltic material (cf. Percival et al., 1992) is suggested as the most viable explanation for the global occurrence of widespread granulite terranes with U-Pb metamorphic zircon ages of c. 2700 to 2640 Ma (Heaman et al., 2011). Newton et al. (1980) relate carbonic metamorphism to crustal growth, in the sense that dehydration of a downgoing slab would have promoted the release of CO_2 vapour from carbonate-mica peridotite in the mantle wedge. Introduction of this CO_2 into the base of the crust generates a "granulitization front" (Newton et al., 1980). Potential evidence for this is present in the carbonic fluid inclusions described by Chi et al. (2009) in ankerite and associated quartz hosting gold at the Red Lake deposit (**Fig. 1A**).

The focus of this study is on the North Caribou greenstone belt (NCGB) of the North Caribou domain, at the core of the greater NCS (**Fig. 1A, B**). Major shear zones bound the

belt along its northern and eastern margins, possibly originating at the boundary between doming granitoids and sagducting greenstones of the vertical tectonic model (cf. Goodwin and Smith, 1980; Gorman et al., 1978; Chardon et al., 1996, 1998; Lin, 2005; Parmenter et al., 2006; François et al., 2012). The proximity of the NCGB to the suture zone between the North Caribou core and Island Lake domain (**Fig. 1A, B**) is of particular interest as transpressive forces generated in the crust during terrane accretion could give rise to such shear zones, focused along the contacts of contrasting lithologies. Preserving evidence of tectonism prior to 2.87 Ga, the North Caribou superterrane is interpreted as a Mesoarchean micro-continent, consisting of a c. 3.0 Ga juvenile crust unconformably overlain by c. 2.9 Ga quartz-rich metasedimentary rocks and mafic to ultramafic metavolcanic rocks thought to represent platformal or rift-type sequences (Thurston and Chivers, 1990; Thurston et al., 1991).

3. Geology of the North Caribou greenstone belt

The North Caribou greenstone belt is one of many small, arcuate and irregularly shaped metavolcanic-metasedimentary belts surrounded by voluminous younger granites and gneissic suites in the North Caribou superterrane (**Fig. 1A, B**). Detailed geochemical, geochronological and isotopic studies of greenstone belts in the NCS have shown that younger c. 2.8-2.7 Ga assemblages (e.g. Oxford-Stull and Monroe-Lake domains) are characteristic of subduction-derived island or continental arcs, while older c. 3.0-2.9 Ga sequences bear komatiites with plume-related signatures (Tomlinson et al., 1998; Hollings et al., 1999, 2000; Hollings and Kerrich, 2000; Hollings, 2002; Young et al., 2006). The early history of the North Caribou superterrane is obscured by younger plutonism (Stott, 1997), and

the belts of similar affinity and age may conceivably represent remnant fragments of a once continuous "megabelt" (Breaks et al., 2001).

3.1. Tectonostratigraphy

The NCGB represents a collage of distinct tectonostratigraphic units and the resulting suite of metavolcanic and metasedimentary rocks has been divided into five to eight supracrustal assemblages by various authors (e.g. deKemp, 1987; Thurston et al., 1991) as summarized in Breaks et al. (2001). The belt is defined by a doubly arcuate Z-shape with two E-W trending arms stretching outward from a central roughly N-S trending region and crustal-scale shear zones follow lithological contacts in the northern and eastern margins. On a first order, the belt is a ~150 km span of metasedimentary rocks bordered by metavolcanic rocks and bounded by metagranitoid rocks in the surrounding region (**Fig. 1B**).

The medial Eyapamikama Lake metasedimentary assemblage (ELS) comprises about 50% North Caribou greenstone belt (Breaks et al., 2001 and references therein). The ELS is flanked by South Rim metavolcanics (SRV) and North Rim metavolcanics (NRV), which overlie the Keeyask assemblage (KLS/V, Thurston et al., 1991; Breaks et al., 2001). Together these assemblages are bounded to the north and east by the Schade Lake gneissic complex (SLGC), and to the south and west by the North Caribou Lake batholith (NCLB) and the Southern batholith (Breaks et al., 2001; **Fig. 1B**).

3.1.1. Stratigraphy of the northern NCGB

The northern NCGB preserves volcanic and sedimentary sequences that span from c. 2.98 to 2.87 Ga. The oldest supracrustal rocks are found at the west end of the NCGB where the Agutua arm metavolcanic assemblage (AAV) is a felsic to mafic tholeiitic metavolcanic sequence that has been dated at 2981 ± 2 Ma (U-Pb zircon, deKemp, 1987). The 2980 ± 3 Ma

Keeyask Lake assemblage (KLS/V) unconformably overlies the AAV and comprises a thin basal unit of quartz arenite and stromatolite overlain by komatiitic massive, pillowed, and variolitic flows and rare hyaloclastic breccias (U-Pb zircon, deKemp, 1987; Breaks et al., 2001). Most of the major magnetite-grünerite-chert banded iron formation (BIF) units and significant gold mineralization are hosted within these komatiite-rich metavolcanic assemblages. The NRV and SRV comprise subaqueous, tholeiitic to Mg-tholeiitic mafic metavolcanic-rich sequences are found in both depositional and tectonic contact with the underlying rocks of the Keeyask assemblage (Thurston et al., 1991; Breaks et al., 2001). Lithologic and structural considerations led deKemp (1987) to interpret the SRV and NRV as correlative volcanic sequences based on lithological and structural considerations, however, they have not been dated and it is possible they are discrete units. The ELS stratigraphically overlies the NRV and SRV, and comprises basal meta-cobble- to quartz-pebble-conglomerates presumably waining upwards into quartz-rich wackes. Lack of exposure and the extent of deformation make it difficult to resolve the transition from conglomerate to wacke. Breaks et al. (2001) observe thick massive interbeds of ELS quartz- and plagioclase-rich metawackes and NRV/SRV metavolcanics higher in the stratigraphy and interpret this to infer rapid depostion prior to cessation of volcanism. Coeval NRV/SRV volcanism and ELS sedimentation is indicated by the presence of up to 12 km long mafic metavolcanic lenses that are entirely enclosed in ELS (Breaks et al., 2001).

In the most western portion of the belt, the rocks have witnessed lower strain. Quartz-carbonate-veined pillow basalts and tuffs of the NRV and SRV are common and cobbles in basal conglomerates of the ELS have experienced no evident flattening. Along the length of the northwestern arm, I observed primary bedding features in which normal grading indicated

tops to the south when proximal to the NRV and to the north when proximal to the SRV. This observation is in accordance with Breaks et al. (2001)'s interpretation of an E-W trending synform. Along the length of the northwestern arm, the metasedimentary rocks range from chlorite schist in the south to dominantly biotite schist approaching the NRV, which itself is dominantly amphibolite.

In the N-S trending portion of the belt, the rocks are highly deformed and locally mylonitic, exhibiting L>>S fabrics. The overall distribution of the volcano-sedimentary packages remains the same, however, they are tectonically thinned. Locally, the high strain intensity indicated by extreme grain-size reduction makes identification of primary lithologies very difficult.

3.1.2. Stratigraphy of the southern NCGB

The southeastern arm of the NCGB was not previously extensively studied, but appears to contain direct correlatives of the northern NCGB. The Forester-Neawagank metavolcanic (FNV) and Opapimiskan Lake metavolcanic (OLV) assemblages are hosts to local komatiites and BIFs and may be correlated with the KLV (Breaks et al., 2001). The Eyapamikama Lake metasedimentary assemblage is dominated by quartz pebble to cobble metaconglomerates in proximity to the OLV. Along the FNV, the poorly exposed ELS is dominated by finer-grained quartz-rich metawackes. The metasedimentary rocks are mainly exposed in regions of elevated strain, and it appears primary depositional features, such as bedding, may have been rotated into parallelism with foliation. Quartz stringers and veinlets are common and often fabric-parallel among flattened pebbles or cobbles and dominantly biotite schists (**Fig. 2A**). The metavolcanic rocks of the FNV are aerially extensive, especially at the southern margin and are dominated by foliated amphibolite. These amphibolites almost

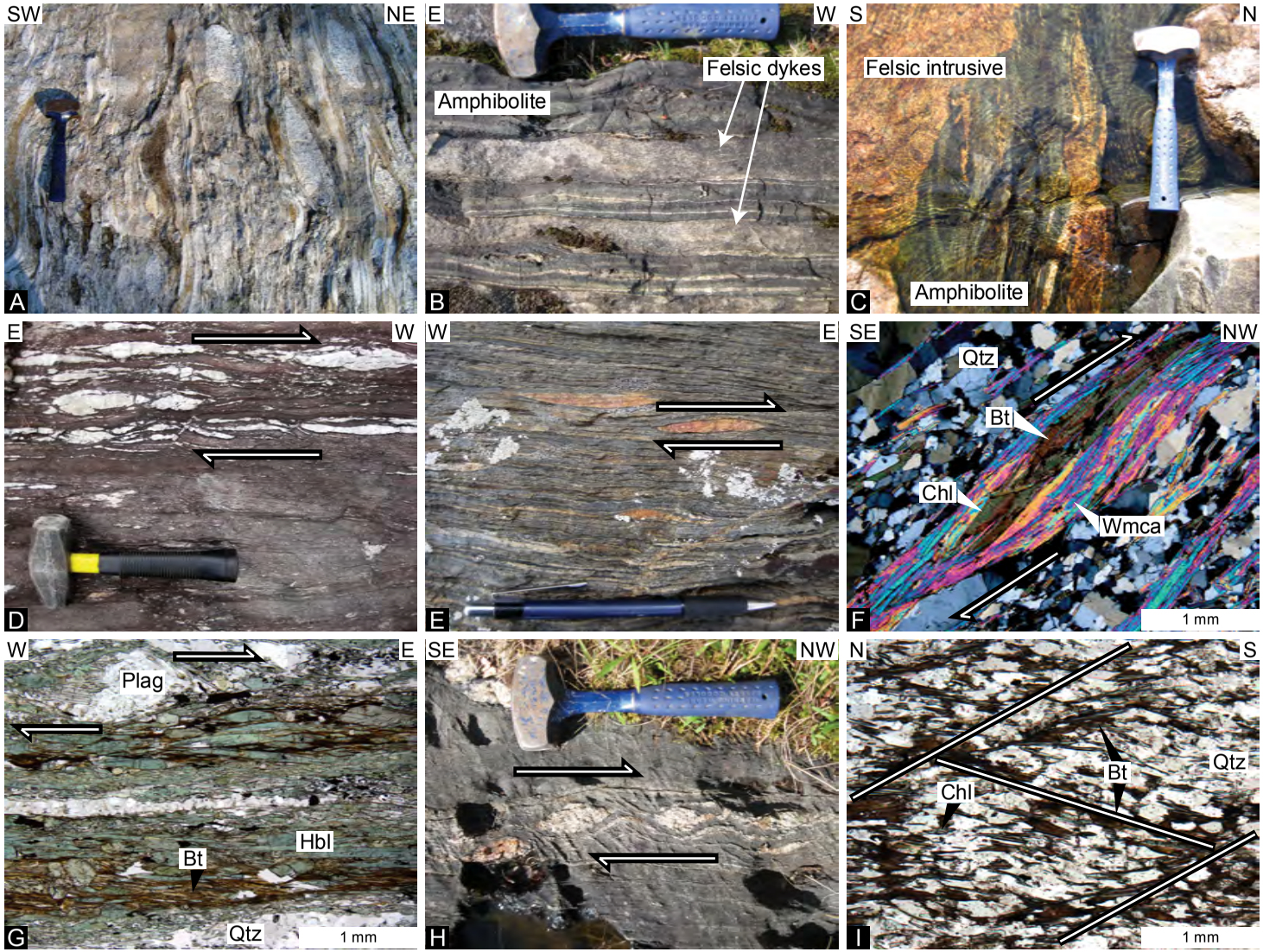

Fig. 2. Typical deformational features in the NCGB. (A) 3:1 flattening of cobbles in a metaconglomerate (NCTK10-26) north of the MLDZ.. (B) Transposed felsic dykes in amphibolite near the southern margin of the southeastern arm of the belt. (C) An amphibolite enclave surrounded by felsic material in the southern margin of the southeastern arm. (D) Dextral kinematics in deformed and boudinaged qtz stringers and veinlets in a coarse-grained metasediment (NCTK10-12) in the MLDZ. (E) Highly strained sigmoid qtz pebbles in a bt-schist (NCTK10-51) at the eastern extent of the belt in the NCTSZ. (F) Cross-polarized photomicrograph of a sigmoidal bundle of wm, bt, and chl surrounded by Q-domains of dynamically recrystallized qtz in a two-mica schist (NCTK10-76) from the transition of the NCTSZ and MLDZ. (G) Photomicrograph in plane-light of a plag porphyroblast displaying dextral kinematics among bands of hbld, dynamically recrystallized bt, and ribbon qtz in a sample from the NCTSZ. (H) Sigmoidal-boudinaged qtz-carb vein indicating dextral kinematics in amphibolite on the north shore of S. Neawagank Lake. (I) A plane-light image of SC-fabric in a bt-schist (NCTK10-38) from the ALFZ.

ubiquitously contain typically foliation parallel quartz-carbonate veins, are often host to highly transposed felsic dykes (**Fig. 2B**), and sometimes appear to be cut by late (un?)deformed pegmatite intrusions (**Fig. 2C**). The southeastern extent of the OLV is poorly exposed. Hornblende-porphyroblastic mafic metavolcanic rocks are common in the OLV and FNV supracrustal assemblages and have the same characteristics as the domains of higher-grade metamorphism and high-strain deformation in the NCGB (Breaks et al., 2001).

3.1.3. Plutonic rocks

Granitoid bodies surrounding the North Caribou greenstone belt are of tonalite-trondjhemite-granodiorite composition and range in age from c. 2.87 to 2.64 Ga. These include the c. 2.87-2.83 Ga North Caribou Lake batholith (NCLB) and the c. 2.86-2.84 Ga Schade Lake gneissic complex (SLGC), as well as c. 2.75-2.71 Ga and c. 2.68-2.64 Ga magmatism and metamorphism recorded in discrete plutons in the SLGC and the Southern Batholith.

The Schade Lake gneissic complex bounds the belt on the northern and eastern margins and is a highly deformed, recrystallized, commonly interbanded combination of massive to gneissic, and locally mylonitic, hornblende-biotite tonalite, biotite trondhjemite, biotite granite, and biotite-hornblende quartz diorite, with scattered amphibolite enclaves (**Fig. 1B**; Breaks et al., 2001). The Schade Lake gneissic complex is dated from 2858 ± 5 to 2841 ± 29 Ma (U-Pb zircon, Pers. Comm. A. Van Lankvelt, 2012). Van Lankvelt (2012) observed metamorphic rims (characterized by low Th/U) ranging in age from c. 2735 to 2678 Ma, as well as certain magmatic zircons with a similarly young age (c. 2642 Ma) as low Th/U rims on older (c. 2841 Ma) cores. Biczok et al. (2012) interpret a 2857 ± 2 Ma U-Pb upper intercept age of zircon from the contact with the NCGB to signify emplacement of the Schade

Lake gneiss and attribute an age of 2875 ± 2 Ma to inheritance of older zircon. These data indicate that determing the timing of the interplay of synchronous magmatism and metamorphism will be difficult to resolve.

On the opposite side of the belt, the North Caribou Lake batholith is of tonalite-trondhjemite-granodiorite composition. Breaks et al. (2001) purport diapiric emplacement of the tonalite-trondhjemite-granodiorite NCLB from 2870 ± 2 Ma (U-Pb zircon, Thurston et al., 1991; Ontario Geological Survey, 1992; Van Lankvelt et al., 2012) to 2864 ± 1 Ma (Davis and Stott, 2001) and suggest it is responsible for the pronounced orocline of the greenstone belt as it produced a contact metamorphic aureole in the SRV. Van Lankvelt et al. (2012) contend the NCLB was emplaced through multiple melt batches over 40 m.y. based on recent U-Pb zircon geochronology that yielded a range from 2870-2858 Ma in the marginal regions of the NCLB and 2852-2833 Ma in the center. Van Lankvelt et al. (2012) used the plagioclase-amphibole thermobarometer of Holland and Blundy (1994) and Anderson and Smith (1995) to determine the P/T conditions of the marginal granitoids to be roughly 6.3 kbar and 600°C and of the central granitoids to be roughly 7.5-6.7 kbar and 640-620°C. The southern margin of the southeastern arm is in continuous contact with an un-named batholithic complex locally referred to as the 'Southern Batholith' (**Fig. 1B**; Breaks et al., 2001). Aeromagnetic trends highlight the presence of at least two circular plutons, ~6-8 km across, with c. 2730-2700 Ma zircon crystallization ages (**Fig. 1B**; Biczok et al., 2012; Pers. Comm. A. Van Lankvelt, 2012). The less defined granitoids of the Southern Batholith contain a population of c. 2727 ± 12 Ma zircons as well as populations of c. 2853 ± 10 Ma cores and c. 2731 ± 13 Ma rims (**Fig. 1B**; Pers. Comm. A. Van Lankvelt, 2012).

3.2. Deformation, metamorphism, and mineralization

There is a complex history of deformation and metamorphism recorded in the North Caribou greenstone belt. Randy Hall (geologist, Esso Minerals Limited, 1984) and D. Rigg (geologist, Dome Exploration Limited, 1985) unraveled at least three ductile deformation events in the supracrustal rocks of the Opapimiskan Lake area (Breaks et al., 2001), with concominant mineralization during at least one of the tectonic episodes.

3.2.1. Deformation

As a result of pervasive D_2 overprinting, preservation of the earliest event (D_1) is limited to superposed folding observed only in banded iron formations. S_1 foliations have otherwise been obliterated or rotated into parallelism with the S_2 fabric but may be preserved as planar inclusion trains in helicitic andalusite, cordierite, staurolite, and garnet porphyroblasts, which lie at varied, but commonly high angles to, the enveloping S_2 foliation (Akow Lake, Breaks et al., 1985; Opapimiskan Lake, Hall and Rigg, 1986). A pre-D_2 layer parallel extension is evident in boudinaged quartz veins in mafic metavolcanic rocks that have since been overprinted by open D_2 mesoscopic folds. A moderately to strongly developed steeply-dipping planar fabric pervades the belt as a result of D_2, striking broadly parallel to the trend of the belt: E-W in the northwestern arm, N-S in the central region, and E-W again in the southeastern arm. The D_2 event is also characterized by variably developed mineral and stretching lineations that commonly follow the trends of associated, usually closed to open, asymmetric mesoscopic folds and thought to represent the most significant tectonic event affecting supracrustal rocks of the NCGB (Breaks et al., 2001). This phase of deformation is consistent with a flattening event that could be related to intrusion of the nearby crescent-shaped North Caribou Lake batholith (Fyon et al., 1992 and references therein; Stott and

Biczok, 2010). Alternatively, similarly penetrative and steeply north-dipping surface structures in the south-central margin of the NCS are interpreted to have developed during subduction or collision (Percival et al., 2006 and references therein). D_3 is a relatively weak event characterized by inhomogeneous strain and manifested as locally pervasive, mesoscopic, open to gentle, asymmetric F_3 warps and chevron crenulations of D_2 foliations and axial planar cleavage. Brittle D_4 fault zones provide a structural control for intrusion of late, unmetamorphosed, north- to northwest-striking diabase dykes and plutons of possible Proterozoic age (Hall and Rigg, 1986), possibly related to the Pickle Crow diabase dyke swarm (Sage and Breaks, 1992).

Several major ductile-brittle shear zones transect the NCGB, generally guided by zones of competency contrast and affecting all supracrustal assemblages (Breaks et al., 2001). The structural framework for this study is provided by four of these zones: (1) the North Rim fault zone (NRFZ); (2) the Akow Lake fault zone (ALFZ); (3) the right-lateral Markop Lake deformation zone (MLDZ); (4) the dextral North Caribou-Totogan shear zone (NCTSZ) (**Fig. 1B**; cf. Piroshco, 1986; Osmani and Stott, 1988; Breaks and Bartlett, 1991; Breaks et al., 1991). These shear zones generally cross-cut previous deformation and metamorphism in the NCGB, and any relationship to the mineralization at Musselwhite mine remains undetermined, yet likely as proximity to crustal-scale shear zones can have implications for orogenic gold deposits (cf. Weinberg et al., 2003).

North Rim fault zone

The North Rim fault zone is likely controlled by the competency contrast between the NRV and ELS north of Eyapamikama Lake (**Fig. 1B**). It is characterized by pervasive planar fabric and E-trending lineations defined by the alignment of isoclinal fold axes, hornblende,

biotite, and garnet-rich mineral aggregates (Breaks and Bartlett, 1991). A predominant feature of this shear zone is the manifestation of strain in foliation-parallel shear bands, observed in both metavolcanic and metasedimentary rocks. Grain size is reduced and foliation homogenized in these cm-scale features and to a lesser extent in the entire outcrop, which made protolith identification locally difficult. Quartz stringers and quartz-carbonate veinlets have been transposed and indicate dextral displacement. Together the tectonites defining the NRFZ define a dextral deformation zone 35 km long by 200 m wide. Under-exposure and inaccessibility has limited the previous study of this fault zone and the nature of its terminations remains unknown.

Akow Lake fault zone

The Akow Lake fault zone is also controlled by the contact of the North Rim metavolcanic rocks with the Eyapamikama Lake metasediments, and trends roughly N-S in the central region of the NCGB. It is near-vertical, 10 km long by 200 m wide and parallel to the 300 m wide, 30-km Dinnick Lake fault zone (DLFZ) that forced right-lateral displacement along the N-S trending contact between the NRV and the Schade Lake gneissic complex to the east. The deformation in the Dinnick zone is significantly greater than in the ALFZ, as it partially to completely mylonitized the tonalites of the Schade Lake gneissic complex at the eastern margin of the NCGB (Breaks et al., 1991). Similar to the NRFZ, the deformation is locally so intense it was difficult to distinguish metasedimentary from metavolcanic rocks in this central region of the NCGB. Quartz-carbonate veins in the Akow Lake fault zone are typically foliation-parallel and sigmoidal offset indicates dominantly dextral shear sense.

Markop Lake deformation zone

The Markop Lake deformation zone is characterized by an increase in thickness and abundance of near-vertical m-scale shear zones in which foliation is thinly spaced, planar, and homogenous, and grain size significantly reduced. Several drill holes across these shear zones have intersected sulphide-bearing mineral zones hosted by moderately deformed schistose rocks (Breaks et al., 2001 and references therein). The cobbles in a metaconglomerate just north of the MLDZ have experienced 3:1 length to width flattening, and were possibly transposed into parallelism with foliation (**Fig. 2A**). This localization of mesoscopic shear zones, and surrounding intensely foliated rocks, spans 13 km and transects the ELS across a thickness of 150-1500 m from the northern margin in the southeastern arm to the granitoids west of Pipestone River. Quartz stringers and veinlets are commonly sigmoidal or stretched and boudinaged en-echelon with a dextral displacement (**Fig. 2D**).

North Caribou-Totogan shear zone

The North Caribou-Totogan shear zone follows the northern margin of the southeastern arm of the NCGB and appears to terminate in the Markop Lake deformation zone. It is very poorly exposed, however, the quartz-pebble metaconglomerates and metawackes of the ELS proximal to the contact with the OLV metavolcanic rocks are highly deformed, as evidenced by elongate narrow lenses of quartz that have a sigmoidal shape indicating a dextral sense of shear (**Fig. 2E**). The dimensions of the NCTSZ are not known, however, it is believed to continue southeast of the belt (**Fig. 1B**).

3.2.2. Metamorphism

The current understanding of Abukuma type regional metamorphism in the NCGB is limited to a simple schematic isograd map of the N-S and northwestern E-W trending regions

produced by Breaks et al. (2001). Much like the geology, the metamorphism in the southeastern arm has been understudied to date. Breaks et al. (2001) report two discernible trends: (1) a general increase in metamorphic grade from the western arm toward the N-S trending portion of the belt (north of Opapimiskan Lake); (2) an increase in metamorphic grade from low to medium towards the northern margin within the western arm (only in the Eyapamikama Lake area), which opposes the isograd trend in the N-S stretch of the belt. Upper-greenschist to amphibolite facies metasediments bear index minerals such as garnet, staurolite, cordierite, grünerite, and more rarely, sillimanite, whereas lower-grade assemblages are characterized by chlorite and/or biotite (Breaks et al., 2001). A narrow hornfels contact aureole overprints the regional chlorite zone at the contact with the NCLB, providing possible evidence that emplacement post-dated the development of strike-parallel regional isograds that were deformed with the belt to follow the doubly arcuate shape observed today. Pre-Kenoran regional metamorphism affected the NCGB prior to emplacement of the North Caribou Lake batholith at c. 2870 Ma (Breaks et al., 2001). Easton (2000) identifies a region of the North Caribou core, the Whachusk metamorphic domain, affected by Mesoarchean metamorphism and likely armored from any significant subsequent metamorphism in the Northwestern Superior Province related to terrane docking. Using the chlorite-garnet-muscovite-staurolite-biotite-quartz isograd of Froese and Gasparinni (1975) and the staurolite-muscovite-quartz-Al_2SiO_5-biotite isograd of Hoschek (1969), Breaks et al. (2001) estimated peak metamorphic conditions of 400 to 500°C and 3 kbar or less. The peak metamorphic conditions reported by Otto (2002) based on the assemblage of garnet-hornblende-biotite-plagioclase-quartz in a mineralized unit beneath Opapimiskan Lake, range between 540 and 600°C and 6 to 7 kbar.

3.2.3. Mineralization

The North Caribou greenstone belt is host to the banded iron formation-hosted orogenic gold deposit of Goldcorp's Musselwhite mine. Despite the proximity of the belt to the purported suture zone between the North Caribou core and the accreted Island Lake domain (**Fig. 1A, B**), there is no evidence that gold mineralization is related to a through-going crustal-scale shear zone (Biczok et al., 2012). D_2 folding in the Opapimiskan Lake area produced a series of northwest-trending, subvertical folds comprised of a central synform, which exposes rocks of the OLV, flanked by antiforms cored by metasedimentary and lesser felsic volcaniclastic rocks of the underlying 'Lower Sediments' (Biczok et al., 2012). Plunging from 10° to 35° to the northwest beneath Opapimiskan Lake, these folds obscure the nature of the contact relationship with the South Rim and North Rim metavolcanic units. The mineralized structures have been interpreted as local high-strain zones that were developed along the steep limbs of the folded iron formation during fold development and commonly swelled in width at favorable inflection points (Biczok et al., 2012).

Gold occurs primarily within pyrrhotite-filled fractures in garnet grains, and less so as scattered grains in green amphibole, feldspar, pyroxene, and quartz veins (Biczok et al., 2012). Chlorite precipitated with pyrrhotite and gold in a fractured garnet from Musselwhite's mineralized unit is nearly $100\%_{Dph}$ and Otto (2002) used Walshe's (1986) chlorite geothermometer to determine formation occurred under reducing conditions at 210 to 250°C. Hall and Rigg (1986) describe an inclusion-filled, anhedral to subhedral stage of garnet growth followed by a second stage of euhedral, inclusion-free growth, either as new crystals or overgrowths on previous, inclusion-filled garnets. The later stage of garnet growth is confined to the commonly discrete, well defined and demarcated, mineralized and quartz-

veined high-strain zones that cut otherwise unaltered iron formation. Mine geologists believe this to be evidence that garnet rims are hydrothermal in origin and directly related to the mineralizing event (Biczok et al., 2012). Garnet is the most abundant mineral in the ore that can be dated and Biczok et al. (2012) report c. 2720-2660 Ma Sm-Nd age of whole rock-garnet in the mine. Garnets from mineralized garnet-grünerite-amphibole-chert meta-iron formation are Fe-rich (74-80%$_{Alm}$), Mn-poor (3-7%$_{Sps}$), and variable in terms of zoning such that Fe decreases towards the rim of some crystals and increases toward the rim of others (Otto, 2002). Generally, the garnets in mineralized rock have more Mn-rich (18-25%$_{Sps}$) cores and more Mg- (8-15%$_{Prp}$) and Ca-rich rims (Duff et al., 2012). Garnets from unmineralized garnet-biotite schist are also rich in Fe (78%$_{Alm}$), Mn-poor (2%$_{Sps}$), yet variability in zoning is negligible (Otto, 2002). Garnet is in equilibrium with biotite in both units and together they have grown along the S_2 foliation (Otto, 2002).

Biotite in mineralized garnet-grünerite-amphibole-chert meta-iron formation is Fe-rich (75%$_{Ann}$) and Mg-poor (2%$_{Phl}$), whereas fine-grained biotite in the matrix of the unmineralized unit is 50%$_{Ann}$, and relatively more Mg-rich (21%$_{Phl}$; Otto, 2002). Isaac (2008) reports a biotite chemistry that is distinctly more Fe-rich in unmineralized metasediments and metavolcanics from Musselwhite mine than in granitoids and ELS metasediments from the surrounding region. An unmineralized oxide-facies iron formation is locally altered to biotite similar in composition to the biotite in metavolcanics beneath Opapimiskan Lake with increased Fe (65-74%$_{Ann}$) and decreased Mg (4-10%$_{Phl}$, Otto, 2002; Isaac, 2008). Isaac (2008) observes a positive correlation of Mg with Si in biotite and whole rock gold concentration and invokes a relationship between such Mg-rich biotite with gold mineralization based on silica flooding. She reports an unusual abundance of Mg-rich biotite at 44%$_{Phl}$ in altered metabasalts

in the mine and suggests a hydrothermal origin for Mg-rich (62%$_{Phl}$) biotite in metasediments of the ELS southeast of Opapimiskan Lake, as biotite in the surrounding granitoids is Mg-poor (~14%$_{Phl}$, Isaac 2008). This is a potential vector that can be used to identify hydrothermal biotite elsewhere in the region, knowledge of which will help characterize shear zones in terms of fluid presence. Biczok et al. (2012) report a nearly 100 m.y. Ar-Ar age difference between biotite localized in foliation planes, sometimes replacing hornblende in the metabasalts that overlie the mineralized iron formation (plateau age: c. 2590 Ma), and biotite in the matrix of the unmineralized garnet-biotite schist unit (total gas age: c. 2490 Ma).

4. Petrography, microstructural analysis, and regional trends

Bounded to the north by major crustal-scale shear zones, the supracrustal assemblages in and the granitoids surrounding the NCGB preserve many features related to the pervasive deformation and metamorphism in the region. Although the size, general trend, kinematic sense, and certain meso- to macroscopic features characterizing the regions of high strain that provide a structural framework for my study have been investigated (e.g., Breaks et al., 2001 and references therein), little work has been done in terms of petrography and microstructural analysis. In order to better understand the geological and structural features that characterize the shear zones demarcating the northern margin of the NCGB, I conducted regional geologic mapping and sampling of all lithotypes over a range of strain intensities (correlatable to shear zone proximity) and variable metamorphic grades (from greenschist through amphibolite facies). More attention was given to the southeastern arm to obtain a more detailed petrologic framework of the North Caribou-Totogan shear zone, which, as a result of a paucity of outcrop, has been understudied to date. Here I present a summary of my detailed petrography

and microstructural analysis of samples, followed by a summary of the regional structural mapping and I focus primarily on rock units that contribute to better understanding trends of deformation and metamorphism.

4.1. Metasedimentary rocks

The metasedimentary rocks of the NCGB are host to an abundance of microstructures and textures that can be used to identify kinematic orientation. Foliation of metasediments results in a segregation of abundant quartz, plagioclase and rare potassium feldspar into microlithons (Q-domains) through preferential alignment of micas and chlorite into foliation planes (P-domains). Samples with abundant fabric-forming minerals are characterized by a coarse-grained foliation. Often micas are intergrown with one another and/or chlorite in sinuous foliation planes having aligned this way in response to strain (**Fig. 2F**). Alternatively, the micas and/or chlorite grow at angles to and cross cut one another within a foliation plane having had time to recover after cessation of strain. Sometimes where two types of mica are present, one will be aligned in the foliation having crystallized this way in response to strain, and the other will be coarser, more blocky, and oriented at oblique angles to the foliation, suggesting recovery. Chlorite is often present as an alteration mineral or a product of retrograde metamorphism. Hornblende or another dark green amphibole (i.e., ferrotschermakite) is sometimes present in higher strain metasediments commonly in proximity to the contact with metavolcanics (i.e., in the NRFZ). A highly strained metasedimentary rock from the Libert Lake area (south of Opapimiskan Lake, **Fig. 1B**) contains abundant epidote localized in silica-rich bands and potentially of hydrothermal origin. Common accessory minerals in the metasediments are apatite, tourmaline, rutile (often as inclusions in quartz), ilmenite, magnetite, zircon, and monazite. Higher-grade

metamorphism is indexed through the presence of garnet, staurolite, andalusite, and cordierite, the occurrences of which are rare and generally only local (**Fig. 3**). Upper-greenschist to amphibolite facies mineral assemblages are observed mainly in regions of high strain (e.g. andalusite and staurolite in the ALFZ, garnet in the MLDZ and NRFZ) or in proximity to late granitic intrusions as a result of contact metamorphism (e.g. cordierite nodules in proximity to both granitic and mafic dykes). Garnet is often localized in dilation zones or pods filled with alteration minerals, which can be interpreted as a hydrothermal derivation. Albite is commonly porphyro- or poikiloblastic, altered by sericite, and fractured in microlithons as a result of the strain that has induced dynamic recrystallization of or dissolution precipitation creep in quartz.

The intensity of strain is evaluated through the degree to which quartz has undergone recrystallization and/or recovery. Undulose extinction is prevalent in most samples more distal from high strain as well as in ribbon quartz segregated from fine-grained quartz in microlithons. Grain boundary migration leading to the formation of subgrains (**Fig. 2F**), which themselves are sometimes rotated into parallelism with foliation, is characteristic of the more highly deformed quartz. Elongate quartz and plagioclase sometimes form cusps in the direction of foliation and there are local occurrences of plagioclase growing locally between micas in the direction of foliation. These features are indicative of fluid-assisted dissolution precipitation creep. Banding, up to cm-scale, is sometimes prevalent in planar-foliated samples, developed through grouping of microlithons into Q-domains and foliation planes into P-domains, evidence of prolonged strain and metamorphism. Centimeter-scale quartz stringers and veinlets as well as small quartz sweats are commonly lined with fibrous chlorite and micas and transposed or deformed in most outcrops of metasediments. Most stringers and

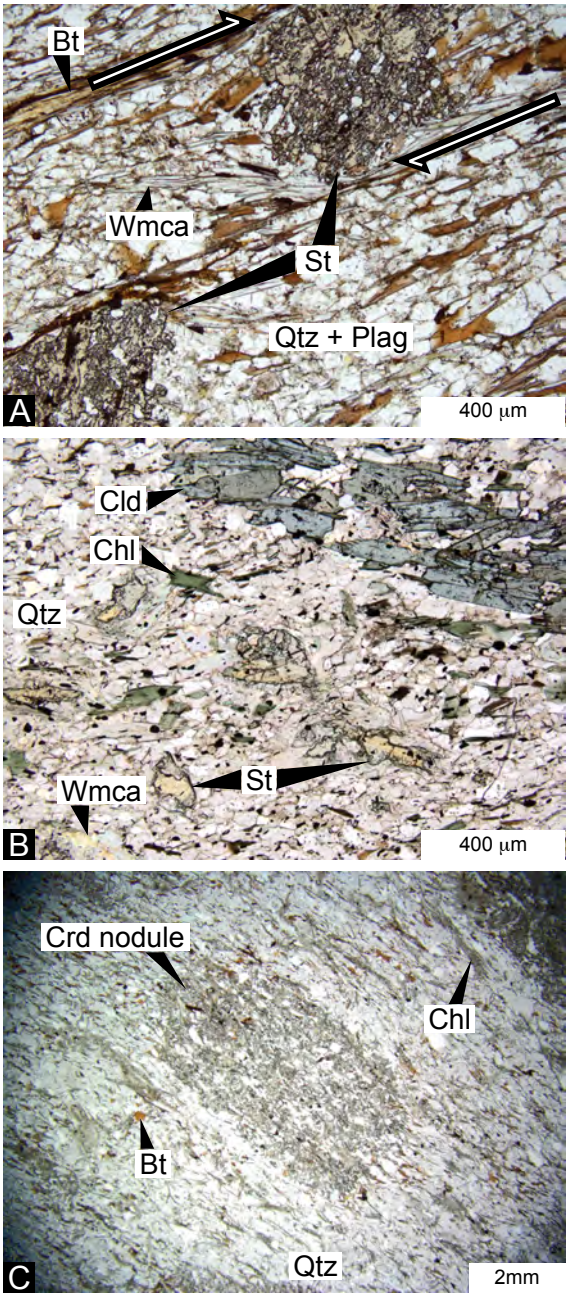

Fig. 3. Photomicrographs showing metamorphic minerals in the NCGB. (A) Staurolite porphyroblasts wrapped by sigmoidal foliation defined by biotite and chlorite indicating dextral kinematics in an andalusite-staurolite schist (NCTK10-44A) in the ALFZ. (B) shows weak alignment of fractured chloritoid and staurolite porphyroblasts in staurolite-chloritoid-chlorite schist (NCTK10-16A). (C) Cordierite nodules overprinting a fine-grained matrix of quartz, biotite, and chlorite in cordierite schist (NCB11-33) from the east end of Eyapamikama Lake.

veinlets are fabric-parallel with Z-shaped kinks, and sweats are commonly sigmoid in shape, an indication that the region is dominated by dextral kinematics (**Fig. 2D**). Where primary features such as bedding are observed in the outcrop (e.g. southern shore of Eyapamikama Lake, **Fig. 1B**), they are roughly parallel with the predominant foliation indicating either the principal stress direction was perpendicular to the bedding plane, or the bedding plane was rotated into parallelism with the foliation, or a combination of these. A conglomerate situated north of the main strand of the Markop Lake deformation zone is highly deformed with 3:1 roughly WSW-ENE flattening of tonalitic cobbles (**Fig. 2A**). A similar feature is observed on a smaller scale in a metasedimentary rock from Heaton Lake in which I interpret fabric-parallel lenses of quartz to be up to 4:1 flattened quartz pebbles. A conglomerate from the southern shore of Obabigan Lake, near the eastern extent of the northern margin and the North Caribou-Totogan shear zone (**Fig. 1B**), displays a similar flattening of pebbles into lenses of dynamically recrystallized quartz around which the foliation anastomoses (**Fig. 2E**), a commonality arising from heterogeneities in even the most highly deformed rocks of the NCGB.

4.2. Metavolcanic rocks

Dominantly metabasalts, most metavolcanic rocks of the NCGB are host to hornblende that preferentially aligns parallel to the fold axes in the region, defining a mineral lineation from which regional strain can be inferred. Metabasalts have often been metamorphosed to amphibolite facies, and are characterized by a mineral assemblage of hornblende, plagioclase, biotite, minor quartz, and chlorite most often as a product of alteration or retrogression (**Fig. 2G**). Calcite is commonly present and sometimes is pervasive, and plagioclase usually has sericite-altered cores. Bladed actinolite is found in some

hornblende-dominated amphibolite facies rocks, yet is more abundant in the far less common greenschist facies metabasalts found locally most proximal to the contact with metasediments and most distal to high-strain. As in the metasediments, metamorphic grade appears to increase with strain. An exception to this, however, is highly deformed and tightly folded actinolite-rich metabasalt situated in the Akow Lake fault zone. Minor and local epidote and relic volcanic pyroxene are sometimes present and common accessory minerals include titanite, rutile, apatite, magnetite, ilmenite, and traces of sulphide minerals (pyrite, pyrrhotite, chalcopyrite).

The metabasalts are often foliated through segregation of plagioclase and quartz into microlithons and of amphiboles and biotite into fabric-defining planes (**Fig. 2G**). Q-domains are isolated from strain-accomodating micro-shear zones that focus in P-domains containing grain-size reduced hornblende and biotite in the highest-strain metabasaltic rocks (**Fig. 2G**). In samples containing little to no plagioclase and quartz, a fabric may still be defined through segregation of coarser-grained from finer-grained varieties of the same minerals. Where hornblende and plagioclase are commonly matrix minerals, they are sometimes porphyro(/poikilo)blastic (e.g. plagioclase, **Fig. 2G**). Centimeter-scale quartz-carbonate veins are common in amphibolites of the southeastern arm but are also observed elsewhere in the NCGB. Often containing white mica, they have been transposed and ptygmatically folded, and sometimes boudinaged (**Fig. 2H**) with a Z-shape indicating dextral kinematics. A characteristic feature of the southern margin of this southeastern arm of the NCGB is the presence of elongate belt-parallel amphibolitic blocks that appear to be deformed by the felsic material that surrounds them (**Fig. 2C**). I interpret these as enclaves of amphibolite, or potentially as the result of nascent migmatization, however, the preferred orientation of sharp-

edged dm-scale felsic dykes in the Forester-Neawagank metavolcanics of the southeastern arm of the North Caribou greenstone belt (**Fig. 2B**) is interpreted to result from transposition. The rotation of previously crosscutting features into parallelism with the strain-induced fabric in the belt is an indication of the elevated strain experienced by this region.

4.3. Shear zones

Regional field mapping in the southeastern arm reveals mesoscopic shear zones characterized by homogeneous planar foliation that appear to increase on a m-scale in terms of thickness and abundance towards loci of crustal-scale deformation. Although exposure of the northern margin of the belt is rare in the southeastern arm, where exposed the supracrustal rocks reveal closely spaced planar fabrics and marked transposition of previously cross cutting features, consistent with the E-W-trending North Caribou-Totogan shear zone. The fabric, in terms of both orientation and homogeneity, is more variable at the center of this southeastern arm and tapers westward into the Markop Lake deformation zone. The stereogram in **Fig. 4** displays a minor shift in the trend of foliation from WNW-ESE (dominantly dipping to the north and striking ~280°) in the northern margin in the NCTSZ to roughly WSW-ENE (dominantly dipping to the south and striking ~80°) southeast of Opapimiskan Lake, where the MLDZ crosses the belt (**Figs. 1B, 4**). Dip angles are fairly steep (~72° on average), and some of the steepest dipping units are overturned. The variability in fabric orientation increases towards the center and eastern extremity of the southeastern arm of the NCGB, with fabrics in the supracrustal assemblages near the end of the belt striking ~340° and dipping ~60° on average. The pervasive foliation in the region of the Akow Lake and Dinnick Lake fault zones has a similar strike (~160° on average) but generally dips more steeply (~80°) with the opposite orientation (**Figs. 1B, 4**). The highest strain is recorded in

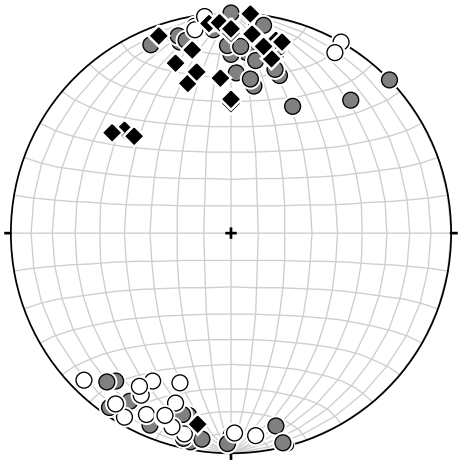

Fig. 4. Lower hemisphere projection of poles to foliation plotted on a Schmidt's equal-area net. Coloured symbols represent structural measurements in the southeastern arm of the NCGB. Black diamonds are in the MLDZ, grey circles are proximal to the MLDZ, and white circles are along the NCTSZ.

proto-mylonites, mylonites, and L>S tectonites, the majority of which are found in the N-S trending portion of the belt, in the Dinnick Lake fault zone. Micas and chlorite almost ubiquitously wrap around porphyroblasts and are rarely found as inclusion trails within (**Fig. 3**). Where most strain shadows have an augen shape, some are more sigmoidal and indicate dextral kinematics of the shear zone. SC-fabric is not uncommon in high-strain rocks (**Fig. 2I**) and also indicates dextral kinematics. Mineral lineations in the amphibolites plunge from shallow (~5°) to steep (~87°) and trend more commonly ~135-225° or ~315-45°, whereas the axes of ptygmatic, chevron, or re-folded folds trend more commonly ~225-315° or 45-135°, yet have a similar plunge range averaging to ~50°. This indicates that the regional folds imposing the preferential alignment of hornblende were derived from strain nearly perpendicular to that responsible for the microscopic to mesoscopic folds in the NCGB. A potential source for this distinction is the transposition of mineral lineation in dextral shear particularly in the central portion of the belt where motion is roughly N-S in contrast with a folding of cross cutting features in response to the same stress particularly in the E-W trending regions and/or the bends in the belt.

The pervasive vertical fabric and dominantly dextral kinematics observed in high-strain zones along the northern and eastern margins of the NCGB indicate development in response to a dominantly horizontal stress. Small (<100 μm) zircon and monazite grains are abundant in regions of high strain and I have dated them with the U-Pb and total-Pb geochronometers, respectively, to resolve the timing of separate tectonic events recorded in the shear zones of the NCGB. The locality of garnets in dilation zones and pods bearing signs of late-stage remobilization of fluids suggests their composition may reflect that of fluids channeled during deformation in these shear zones. Fabric-forming micas and chlorite are

similarly ubiquitous in the high-strain regions of the NCGB and their geochemistry may help reflect a metamorphic or hydrothermal derivation. I have characterized garnet, chlorite and micas in terms of trace (garnet only) and major element geochemistry to investigate the nature of the fluids associated with shear-zone localized events.

5. *In situ* LA-ICP-MS U-Pb geochronology of zircon

The slow diffusion rates (Cherniak and Watson, 2001) of preferentially incorporated U and Th in the $ZrSiO_4$ lattice, combined with preferential exclusion of Pb (Watson et al., 1997), make zircon an ideal candidate for geochronology. Stages of mineral growth and dissolution (Scharer et al., 1997; Corfu et al., 2003; Tichomirowa et al., 2005; Aleinikoff et al., 2006; Harley et al., 2007) are often recorded in zircon and can be observed with cathodoluminescence (CL) and back-scattered electron (BSE) imaging. By combining microanalytical methods, such as Laser Ablation - Inductively Coupled Plasma Mass Spectrometry (LA-ICPMS) U-Pb geochronology with imaging and microstructural analyses it is possible to obtain useful ages documenting tectonic episodes of a rock. Four samples of wacke to arkose composition (**Table 1**) from the ELS were selected to investigate metamorphism and deformation in the MLDZ, the ALFZ, and the NCTSZ and two samples of tonalitic to trondhjemitic composition were chosen to investigate the deformation in the Schade Lake gneissic complex at the contact with the southeastern arm of the NCGB (**Fig. 1B**). A detailed description of these samples is provided in **Appendix 1**.

5.1. Methods

I performed *in situ* LA-ICP-MS U-Pb geochronology to investigate zircon grains ranging in size from 25 to 100 μm in highly strained rocks. Since the abundance of zircon in

Table A1 Summary of the samples analyzed in this study, NCGB, NW Ontario

Sample ID	UTM Easting	UTM Northing	Datum/ Zone	Shear zone[a] affiliation	Rock Name	Mineralogy	Age (Ma)	MSWD	mnz	zrn	grt	chl	wmca	bt
NCTK10-8	689866	5820991	27 15	MLDZ	bt schist	qtz+pl+kfs+bt+wmca+ ap+zrn+ttn	2865 ± 4 2866 ± 8	1.1 1.4		x				
NCTK10-12B	690491	5821669	27 15	MLDZ	two-mica schist	qtz+pl+kfs+wmca+bt+ chl+tur						x	x	x
NCTK10-15	690680	5821772	27 15	MLDZ	mica schist	qtz+pl+kfs+wmca+bt+ chl+zrn+cal						x	x	
NCTK10-16A	690904	5821552	27 15	MLDZ	st-cld-chl schist	qtz+pl+kfs+chl+wmca +bt+tur+cld+st						x	x	
NCTK10-16B	690904	5821552	27 15	MLDZ	chl schist	qtz+pl+kfs+chl+wmca +bt+tur+grt					x			
NCTK10-19	692153	5821302	27 15	MLDZ	ab schist	qtz+pl+kfs+wmca+bt+ chl+mnz+zrn+rt+ilm	*2421 ± 49*	*13*	x					
NCTK10-20A	692076	5821726	27 15	MLDZ	two-mica schist	qtz+pl+chl+wmca+bt+ rt+ap						x	x	x
NCTK10-24A	694245	5824386	27 15	SLGC	bt-tonalite gneiss	qtz+pl+bt+pyx+ttn+ zrn	2871 ± 24	4.2		x				
NCTK10-26A	694428	5823783	27 15	MLDZ	grt-bt schistose conglomerate	qtz+pl+bt+chl+wmca+ clay+mnz+zrn++grt+ ap±tur	*2446 ± 26*	*6.2*	x			x		x
NCTK10-26B	694428	5823783	27 15	MLDZ	bt nest in alteration pods	qtz+chl+bt+grt+wmca +clay					x			
NCTK10-38	673555	5843971	27 15	ALFZ	bt schist	qtz+pl+kfs+bt+chl+ zrn+ilm	*2413 ± 29* *2556 ± 28*	*1.2* *1.8*	x					
NCTK10-44A	670289	5850342	27 15	ALFZ	and-st schist	qtz+pl+bt+wmca+chl+ sil*+and+st+mnz+ zrn+tur+ilm+mag	*2320 ± 37* *2579 ± 20* 2866 ± 14 2876 ± 17	 3.0 4.6	x	x				
NCTK10-51A	312525	5819101	27 15	NTCSZ	bt schist	qtz+pl+bt+wmca+chl+ mnz+zrn	*2570 ± 46*	*4.8*	x			x	x	x
NCTK10-63	308451	5816070	27 15	NLF	proto-mylonitic tonalite	qtz+pl+kfs+opx+bt+ chl+ttn	2861 ± 22	2.5		x				
NCTK10-74A	686874	5827529	27 15	NW of MLDZ	bt schist	qtz+pl+wmca+bt+chl+ sil?+ep?						x	x	x

Table A1 Summary of the samples analyzed in this study, NCGB, NW Ontario

Sample ID	UTM Easting	UTM Northing	Datum/ Zone	Shear zone[a] affiliation	Rock Name	Mineralogy	Age (Ma)	MSWD	mnz	zrn	grt	chl	wmca	bt
NCTK10-75	306991	5820283	27 15	NCTSZ	two-mica schist	qtz+pl+wmca+bt+chl+ zrn						x	x	x
NCTK10-76	702814	5821125	27 15	NCTSZ	two-mica schist	qtz+pl+bt+wmca+chl+ mnz+zrn	*2414 ± 79* *2600 ± 39* *2735 ± 20* 2858 ± 8	*1.0* *1.6* *6.2* 3.5	x	x		x	x	x
NCB11-24	646720	5871092	27 15	NRFZ	bt schist	qtz+pl+cal+bt+chl+w mca+dk.amph+grt+ttn +mag+ilm					x			
NCB11-28	638553	5871489	27 15	NRFZ	hbl schist	qtz+pl+ser+dk.amph+ bt+grt					x			
NCB11-33	657319	5867427	27 15	S Rim EYAP	crd schist	qtz+pl+kfs+chl+bt+ crd	2865 ± 15 2956 ± 17	3.6 4.8		x				
NCB11-34A	649138	5867125	27 15	S Rim EYAP	meta-granule conglomerate	qtz+pl+kfs?+cal+chl+ bt+mnz+ttn+zrn	*2196 ± 47* *2342 ± 20*	*2.7 1.2*	x					
E591 479	664565	5867407	27 15	E of EYAP	schist	qtz+felds+chl+bt+ clays					x			

[a] Shear zone abbreviations are as follows:
MLDZ: Markop Lake deformation zone, SLGC: Shade Lake gneiss complex, ALFZ: Akow Lake fault zone, NCTSZ: North Caribou-Totogan shear zone, NLF: Neawagank Lake fault, NRFZ: North Rim Fault zone, EYAP: Eyapamikama Lake.
Italics are used to distinguish U-Th-total Pb monazite ages from U-Pb zircon ages.
* Indicates a relatively local occurrence in fibrolite form.
? Indicates an uncertainty in mineral identification.

any rock thin section was inadequate to achieve statistically reliable U-Pb ages, five to six thick sections of each sample containing zircon were cut at spaced intervals through the rock to improve the number of targets for geochronology. I used the Resonetics M-50-LR 193 nm ArF Excimer laser ablation system coupled to an Agilent 7700x quadrupole inductively coupled mass spectrometer(ICP-MS) at the University of New Brunswick (UNB, Fredericton, Canada). A detailed description of analytical procedures is provided in **Appendix 2**.

The results of *in situ* LA-ICPMS analysis of zircon are presented in **Table A2**, and Isoplot v3.0 (Ludwig, 2003) was used to plot the concordant ages calculated from $^{206}Pb/^{238}U$ and $^{207}Pb/^{235}U$ ratios. Concordia age values are given at 2σ error (**Fig. 5A-F**). Anywhere from 50 to 70 single spot analyses were conducted for each of six metasedimentary and metagranitoid rock samples, however, only the analyses in which the $^{207}Pb/^{204}Pb$ ratio was greater than 350 were considered to limit the effects of common lead. For the samples of known sedimentary origin, only the results <30% discordant were considered. This is a moderate to generous cutoff but de-emphasizes highly discordant grains, yet not significantly biasing the dataset (cf. Gehrels, 2012). Spot analyses with a propagated 2σ error on $^{207}Pb/^{235}U$ >1 or $^{206}Pb/^{238}U$ >0.3 were omitted. I report upper and lower intercept ages in the Concordia diagrams in **Fig. 5**. In most samples, some analyses are excluded because they fall far from Concordia or a main discordia line and are not abundant enough to define a meaningful age. The discord was occasionally anchored at 0 Ma in order to yield the lowest MSWD associated with the upper intercept age. The Th/U ratios in **Table A2** are plotted against age in **Fig. 6** and display an absolute range from ~0.1-1.0 with the majority of values in the ~0.2-0.6 range. All zircons are small (30-100 μm), generally of one homogeneous population, commonly oscillatory zoned and most often in the matrix of quartz and feldspars (**Fig. 7**). Sector-zoned

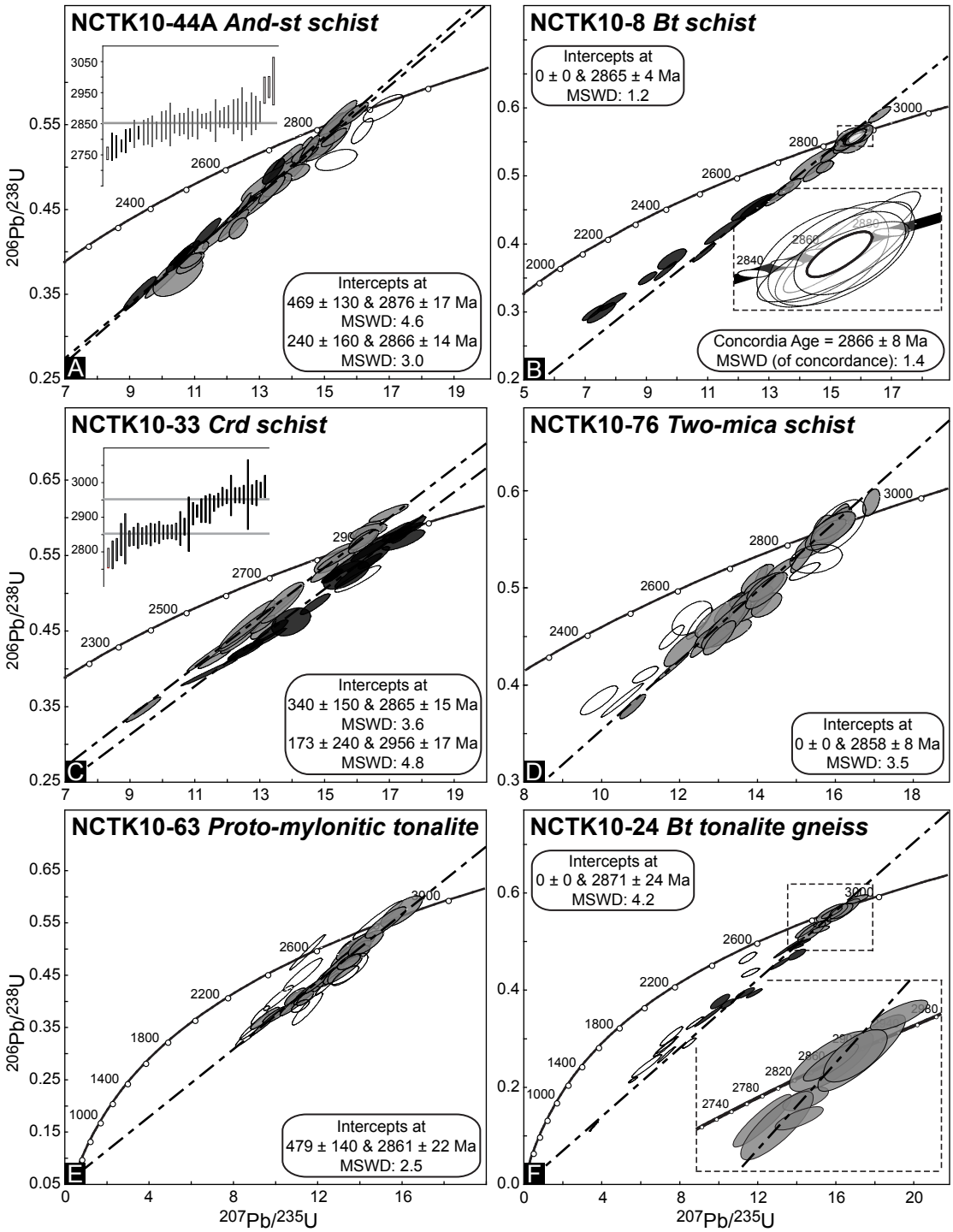

Fig. 5. Concordia plots of U-Pb analyses of zircons from high-strain metasedimentary and granitoid rocks from the North Caribou greenstone belt. Error ellipses shown at 2σ. Weighted mean plots are present in A and C and report $^{207}Pb/^{206}Pb$ ages along the y-axis. White ellipses are either too discordant or do not plot close enough to a discord to contribute positively to an upper intercept age. An extra discord is shown in A to demonstrate the shift in age and MSWD when the black ellipses are included. A cluster of concordant ages is highlighted in B, the grey ellipses are single spot analyses <12%, and the black ellipses >12% discordant. Discords in C lead to two separate upper intercept age populations, and the grey ellipses magnified in the inset in D define a discord (<8%) at the upper intercept of which, four ellipses plot on Concordia.

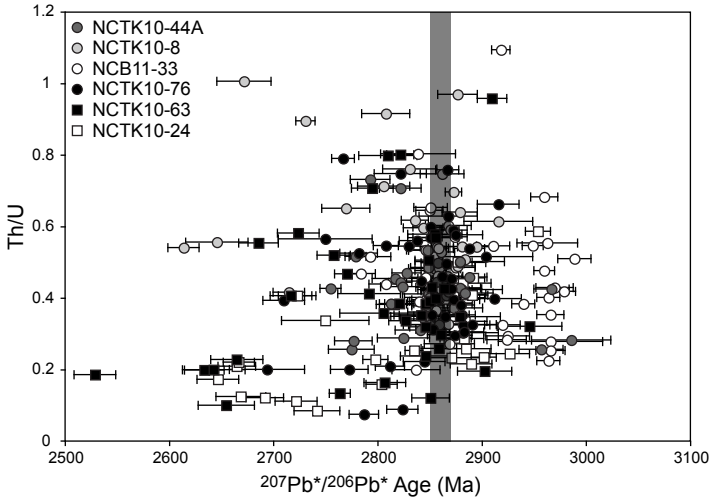

Fig. 6. Th/U values plotted against 207Pb/206Pb age (Ma) for zircons from the North Caribou greenstone belt. Error bars are at 1σ level. Vertical grey bar represents the dominant cluster around 2.86 Ga.

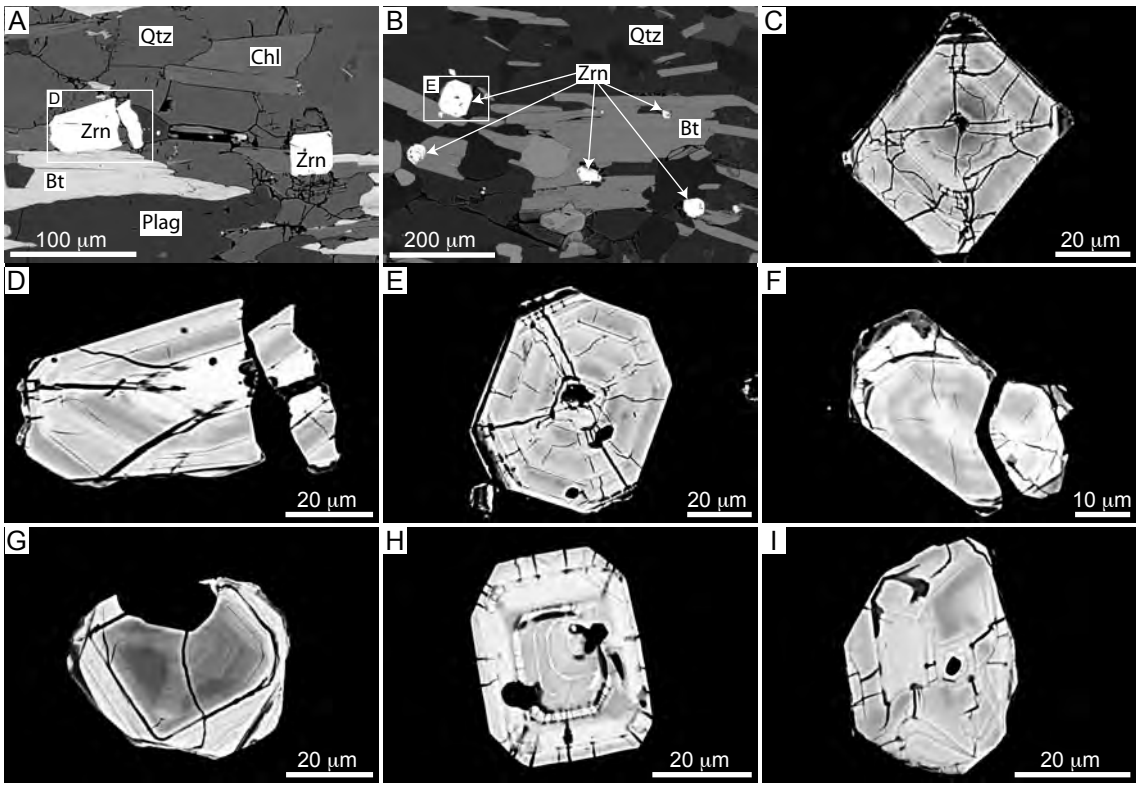

Fig. 7. Backscatter electron images showing a variety of zircon shapes and textures representative of those analyzed through U-Pb geochronology in this study. (A) Zircons in andalusite-staurolite schist (NCTK10-44A) from the ALFZ with their long axis oriented parallel to foliation, the broken grain is magnified in D. (B) Zircons in biotite schist (NCTK10-8) from the MLDZ in a similar context and the largest grain is magnified in E. (C) Patchy oscillatory zoning and F shows sector-type zoning in zircons from cordierite schist (NCB11-33), similar to the grain in E, both have a thin and discontinuous low-U rim. (G) A sector-zoned zircon in two-mica schist (NCTK10-76) from the NCTSZ. (H) A euheral grain from protomylonitic trondhjemite (NCTK10-63) in the NFZ that displays a distinction between core and rim. (I) A patchy-zoned grain from biotite-tonalite gneiss (NCTK10-24) north of the MLDZ.

zircons are few but present, and though some crystals appear to have a thin rim or overgrowth, the small size of the zircons make it nearly impossible to resolve different domains with the laser spot size. The potential of age domain mixing is therefore high, which may explain the occasional multiplicity of closely spaced discordia lines, from which it is hard to determine a single robust age.

5.2. Results

Sample NCTK10-44A possesses characteristics of a rock typical for high strain under amphibolite facies conditions. The rock is an andalusite-staurolite schist situated within the Akow Lake fault zone (ALFZ) that parallels the eastern contact of the ELS with the NRV north of Opapimiskan Lake (**Fig. 1B**). On the outcrop scale, porphyroblastic staurolite and andalusite are localized in tightly folded bands that cross cut bedding and/or axial-planar foliation (**Fig. 3A**). Zircons are dominantly euhedral and oscillatory-zoned, and where the c-axis is not perpendicular to the direction of principal strain, the grains are often fractured and slightly displaced in the plane of foliation (**Fig. 7A, D**). Pre-kinematic porphyroblasts displace a fairly planar biotite- and chlorite-rich foliation resulting in sigmoidal strain shadows that indicate localized sinistral rotation (**Fig. 3A**). U-Pb analysis yields 38 single ages for 36 zircons. The three oldest single ages (2957-2986 Ma) define a discord but are not abundant enough to draw a meaningful age. An upper intercept age of 2876 ± 17 Ma (MSWD: 4.6) results from all other spot analyses, excluding six of the youngest single ages (2755-2817 Ma) that results in an age of 2866 ± 14 Ma (MSWD: 3.0, **Fig. 5A**).

A sample of biotite schist (NCTK10-8) is situated within the projected termination of the MLDZ near the contact with the granitoids to the southeast (**Fig. 1B**). NCTK10-8 is thought to be of sedimentary origin, based on unpublished geochemistry of a similar sample

<100 m away (pers. comm. A. Van Lankvelt, 2012). Most of the zircons are euhedral prismatic, oscillatory zoning is common, and a small core is observed in certain grains (**Fig. 7B, E**). Similar to NCTK10-44A, the c-axis of the zircons is often in the plane of the fabric and roughly perpendicular to a lineation defined by preferential orientation of the blocky biotite in this sample. Six single spot analyses yield a Concordia age of 2866 ± 7 Ma (MSWD: 1.4). Eighteen single spot analyses on 14 zircons are <12% discordant and define a discord that, if anchored at 0 Ma and including the six concordant ages, yields an upper intercept age of 2865 ± 4 Ma (MSWD: 1.1, **Fig. 5B**). Ten of the youngest single ages (2614-2808, 2836, and 2844 Ma) are >12% discordant, do not fall on the dominant discord, and do not define a discord of their own.

A sample of cordierite schist (NCB11-33) of the ELS is situated in the contact metamorphic aureole at the southern border of the western arm with the North Caribou Lake batholith (**Fig. 1B**). Both granitic and aplitic mafic dykes cut through the metasedimentary rocks in the outcrop and mm- to cm-scale cordierite nodules have resisted weathering in proximal surfaces of the host rock. Retrograde chlorite alteration is concentrated in pseudomorphs of the fabric-elongate (2-3 mm x 5 mm) cordierite poikiloblasts (**Fig. 3C**). The matrix is fine-grained and foliated through weak alignment of fibrous chlorite and blocky biotite in planes that anastomose through variably recrystallized quartz grains and ribbons, as well as around the occasional albite poikiloblast. Zircons in this sample are mostly asymmetrical and subhedral, although a euhedral prismatic variety is present dominantly in the coarser-size fraction ~45-80 μm. Oscillatory zoning is prevalent (e.g. **Fig. 7C**), but sometimes patchy or faint, and sector zoning is also present, but to a much lesser extent (e.g. **Fig. 7F**). It is the only sample for which two distinct age populations are clearly discernible.

A young discordia trend defined by 20 single spot analyses on 17 zircons yields an upper intercept age of 2865 ± 15 Ma (MSWD: 3.6) and an older discordia trend defined by 17 single spot analyses on 16 zircons yields an upper intercept age, with a few discrete single ages clustering on Concordia at 2956 ± 17 Ma (MSWD: 4.8, **Fig. 5C**). The oldest single age (2989 Ma) does not plot on the older discord.

Sample NCTK10-76 is a two-mica schist from the ELS near the NCTSZ-MLDZ transition (**Fig. 1B**). This meta-arkose constitutes thick foliation planes of biotite, muscovite, and minor chlorite that anastomose through coarse-grained microlithons of highly strained, dynamically recrystallized quartz and sericite-altered albite. The subhedral to slightly rounded prismatic zircons are mostly found in association with fabric forming minerals, often with their c-axis in the plane of foliation. Whereas the zircons are most commonly oscillatory zoned, some also display a patchy sector zoning (**Fig. 7G**) and others a small distinct core. Thirty single spot analyses on 26 zircons define a discordia trend with an upper intercept age of 2858 ± 8 Ma (MSWD: 3.5) when the discord is anchored at 0 Ma (**Fig. 5D**). The six youngest (1694-2782 Ma) and three oldest (2904-2916 Ma) single ages do not plot on the dominant discordia trend and fail to define a significant discord of their own.

From the Neawagank Lake fault (**Fig. 1B**), a sample of proto-mylonitic trondhjemite (NCTK10-63) is banded through strain-induced segregation of mm-scale layers of biotite and mafic minerals from plagioclase-rich microlithons. Biotite is locally replaced by chlorite and aligned with hornblende and orthopyroxene in an anastomosing foliation that locally wraps around heavily altered poikiloblastic potassium feldspar and forms augen-shaped pods of alteration. Zircons are found in the matrix with a locally observed fabric-parallel orientation and, whereas a few are euhedral prismatic, most are subhedral with slightly rounded edges. A

common feature of these zircons is a weakly zoned core with a distinctly more strongly zoned and complex rim (**Fig. 7H**). U-Pb analysis through 29 single spots on 24 zircons yields a discordia trend with an upper intercept age of 2861 ± 22 Ma (MSWD: 2.5, **Fig. 5E**). In most cases, where the rim was large enough to ablate separately, single spot analysis of the rim yields a 40 to 150 m.y. older age than single spot analysis of the core. Analysis can yield an apparent older age when there is an abundance of common Pb. Only one analyzed core-rim pair yields a rim that is younger than the core, by about 50 m.y. (**Table A2**). Seven of the youngest single spot ages (2529-2686 & 2758 Ma) and five of the oldest single spot ages (2859, 2861, & 2903-2946 Ma) do not plot on the dominant discord and do not themselves define discordia trends that bear any meaning to an age.

Sample NCTK10-24 is a biotite-tonalite gneiss from just north of the MLDZ in the Schade Lake gneissic complex (**Fig. 1B**). Gneissic banding is observed from the thin-section scale to the outcrop-scale through segregation of biotite-rich from biotite-poor fabrics. The mostly subhedral zircons (e.g. **Fig. 7I**) in this sample often display weak oscillatory zoning and, though commonly in contact with biotite, a preferred orientation is less evident in this least deformed of all samples analyzed for U-Pb geochronology. Nineteen single spot analyses (up to 30% discordant) on 17 zircons define a discordia trend from which, if the ten >8% discordant (ranging from 2750-2954 Ma) are omitted, the MSWD is reduced from 10.9 to 4.2. Anchored at 0 Ma, explain why in methods section a cluster of four single ages plot on Concordia at the upper intercept of 2871 ± 24 Ma (**Fig. 5F**). Eleven single spot analyses on ten zircons yield ages >30% discordant (2647-2798 & 2891-2902 Ma) that do not plot on the discord.

6. *In situ* U-Th-total Pb EMPA of monazite

To complement the U-Pb zircon ages, I performed U-Th-total Pb Electron Microprobe Analysis (EMPA) of monazite. Monazite [$(Ce,La,Th)PO_4$] is nearly ubiquitous in pelitic and psammitic metamorphic rocks, and an overwhelming majority of monazite grains contain distinct compositional zones (Zhu and O'Nions, 1999a, 1999b; Williams et al., 2007) representing different stages of growth. *In situ* analysis provides a means for specific dates to be linked to specific structural or textural domains, and the high spatial resolution of the EMPA (~1 μm in diameter) allows for age determination of the associated growth or recrystallization of monazite. Growth events reflect reactions that led to the production of monazite (e.g. Zhu et al., 1997; Williams et al. 1999; Schmitz and Bowring, 2000). The crystallization or breakdown of garnet, for example, is a major control of the abundance of HREE and Y available for crystallization of monazite (Williams et al., 2007 and references therein). Seven of my samples from the Eyapamikama Lake metasedimentary assemblage contain monazite grains large enough for EMPA analysis and a description of these samples can be found in **Appendix 1**. One is a relatively undeformed meta-granule conglomerate from the south shore of Eyapamikama Lake and six others are from three brittle-ductile shear zones in the NCGB: (1) staurolite-andalusite schist and two-mica schist from the region of the ALFZ; (2) biotite schist in the MLDZ and garnet-biotite schistose conglomerate just north of it; and (3) two-mica schist and biotite schist from the NCTSZ (**Table 1**, **Fig. 1B**).

6.1. Methods

I used the Cameca SX-100 electron microprobe at New Mexico Institute of Mining and Technology (NMT, Socorro, USA) to obtain *in situ* U-Th-total Pb ages for <100-μm anhedral resorbed to euhedral monazite grains that exhibit clear microstructural relationships

with fabric elements (cf. Williams et al., 1999). A description of the two-part EMPA portion of the investigation is provided in **Appendix 3**.

The results of *in situ* U-Th-total Pb geochronology of monazite from seven high-strain Eyapamikama Lake metasedimentary samples are presented in **Table A3**. After single-spot total-Pb ages were calculated, dates were plotted on relative probability diagrams using Isoplot v3.0 (Ludwig, 2003) to assess the major populations of mineral-age domains for a given sample (i.e. 'peaks'). Once populations were identified, total-Pb dates were sorted by increasing age and plotted on weighted average diagrams in order to calculate domain age and error (**Fig. 8**). Weighted-mean ages were calculated using the standard error from individual analyses of similar age domains and are reported at the 1σ level (**Fig. 8**). Age populations are displayed in terms of Pb vs. Th* in **Fig. 9**; Th* combines the U content converted into the equivalent Th that would have produced the same amount of Pb and the actual Th (Cocherie et al., 1998). This approach allows us to assess monazite populations and the robustness of their ages.

6.2. Results

Sample NCB11-34 is a meta-granule conglomerate near the contact of the ELS with the SRV on the southern shore of Eyapamikama Lake (**Fig. 1B**). The strain is localized along bedding planes and zones of lithological contrast in very coarse-grained and thick-bedded metasediments. Matrix grains are found in tightly spaced microlithons segregated by pervasive foliation planes that wrap around granules of albite ± quartz to form a heterogeneous fabric. Ribbon quartz is highly strained and partially dynamically recrystallized. The monazite grains are 50-60 μm long and only 10 μm wide, often kinked but roughly parallel to the very fine-grained foliation, and they have convoluted edges and sieve

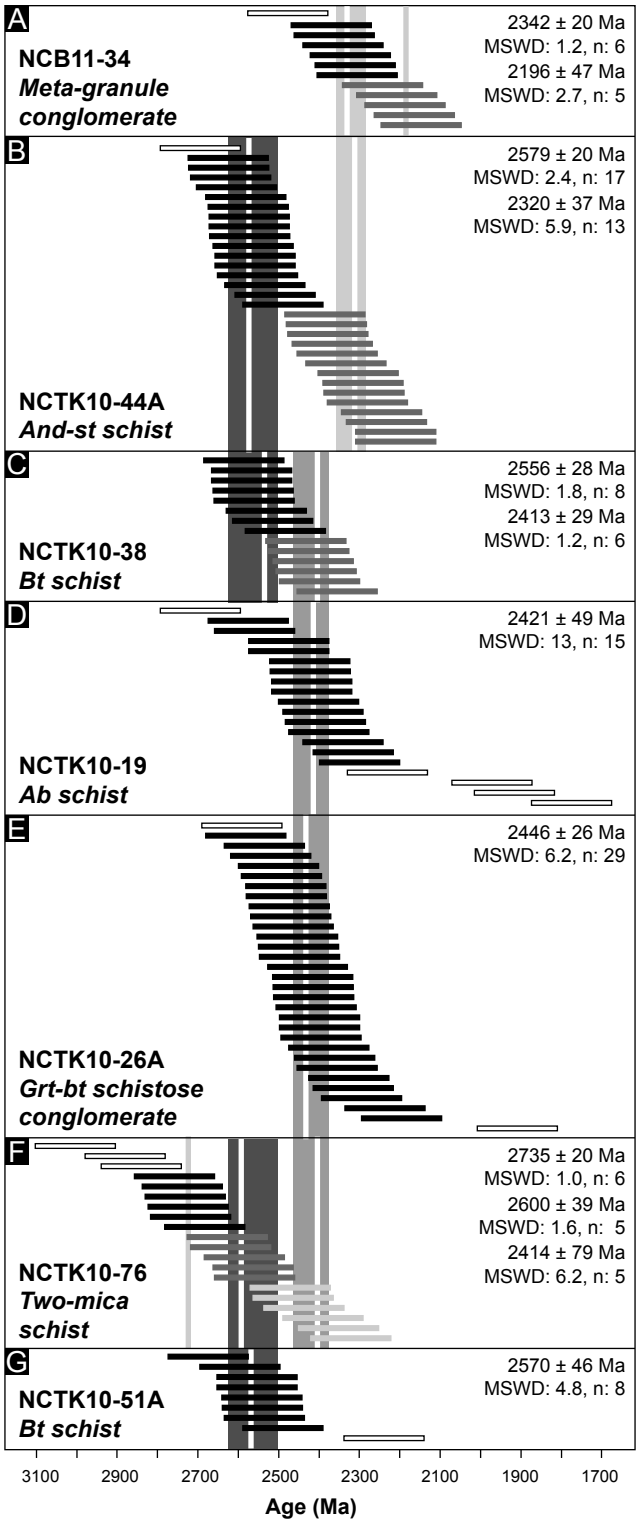

Fig. 8. Weighted mean ages of U-Th-total Pb analyses of monazites from high-strain metasedimetary and granitoid rocks from the North Caribou greenstone belt. Error bars shown at 2σ. Single spot analyses were sorted by age and populations are distinguished by colour. Each vertical white bar is a population mean correlatable to other population means within the bounds of the vertical grey bars. Means that are not correlatable are pale grey and sit outside the bounds of grey bars.

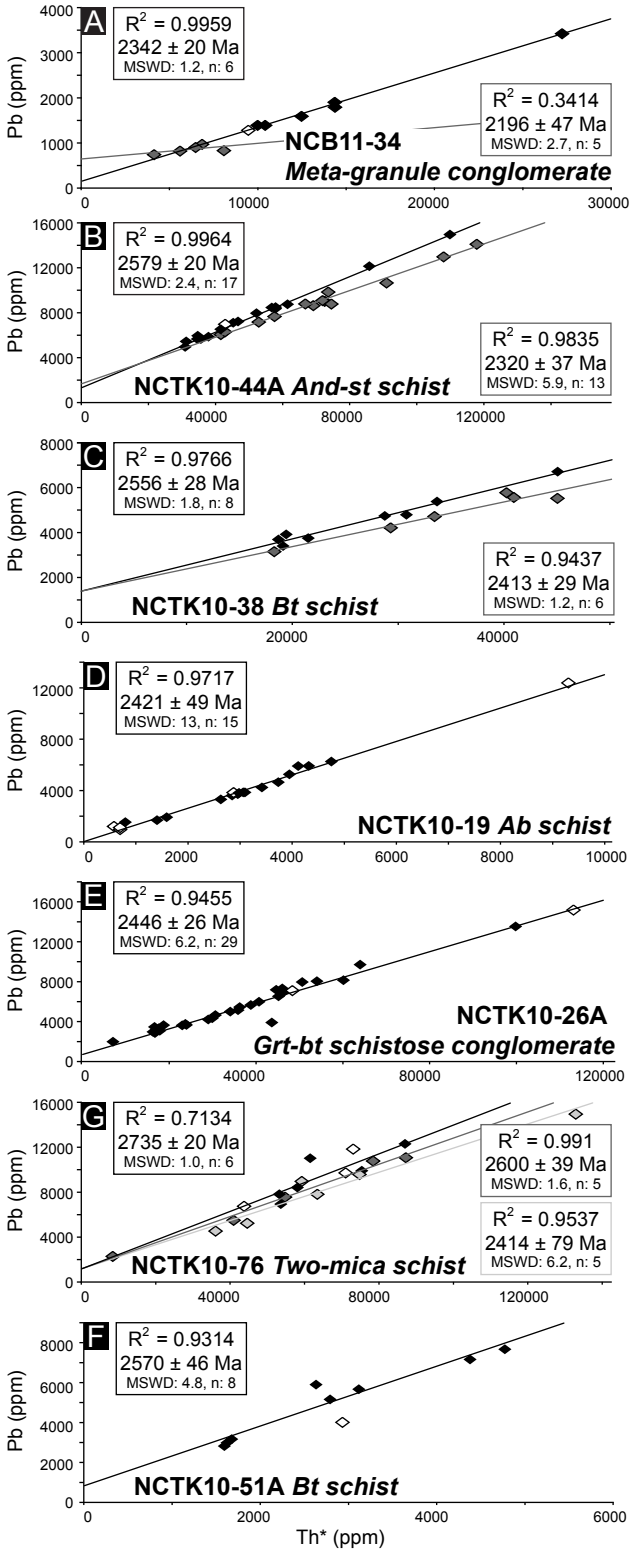

Fig. 9. Scatter plots showing how Pb content varies with Th* to demonstrate robustness of age populations. Thorium* values include the contribution from U converted into Th that would have produced the same amount of Pb. Age populations are distinguished by different shades of grey and R^2 values are shown for the lines defined by each. Empty diamonds represent analyses that were not included in the determination of the age populations.

textures. A non-monazite Ce-bearing phase is prevalent in this sample and some grains have an inclusion with a high-Y content, potentially xenotime. Monazites show a decrease in U, Th, and Y at the rims, and a slight positive correlation of Th content with age. Two age populations are reported from 12 single spot analyses of four monazite grains from NCB11-34; the older and more significant is 2342 ± 20 Ma (MSWD: 1.2), a weighted-mean average of six spot analyses for which Pb/Th* yields an R^2 value of 0.9959, and the younger is 2196 ± 47 Ma (MSWD: 2.7), a weighted-mean of five single spot analyses for which Pb/Th* yields a very low R^2 value of 0.3414 (**Figs. 8, 9A**).

An andalusite-staurolite schist (NCTK10-44A) from the ALFZ, yielding a 2866 ± 14 Ma U-Pb zircon age, also contains monazite. One of six 30-40 μm monazite grains analyzed is an inclusion in poikiloblastic andalusite (**Fig. 10A, B**), while the remaining are found in the matrix of plagioclase ± quartz, often in contact with (and more rarely embedded in) fabric forming micas (biotite ± muscovite or chlorite; e.g. **Fig. 10C, D**). Monazites display a patchy zoning in terms of U, Th, and Y and there is no correlation within the grains between the abundance of these with age. Yittrium is relatively more abundant in the monazite grain included in andalusite and the grains generally contain high Y (~11620 ppm, **Fig. 11**). The weighted mean age of the 13 youngest single ages is 2320 ± 20 Ma (MSWD: 2.4) and the Pb/Th* values define a line with an R^2 of 0.9835 (**Figs. 8, 9B**). The 17 oldest single ages yield a weighted mean age of 2579 ± 20 Ma (MSWD: 5.9) with an R^2 value for Pb/Th* of 0.9964 (**Figs. 8, 9B**). All six grains contain domains of both age populations except for the grain that is included in poikiolitic andalusite, which surprisingly yields only ages of the younger population (**Table A3**; **Fig. 10A**).

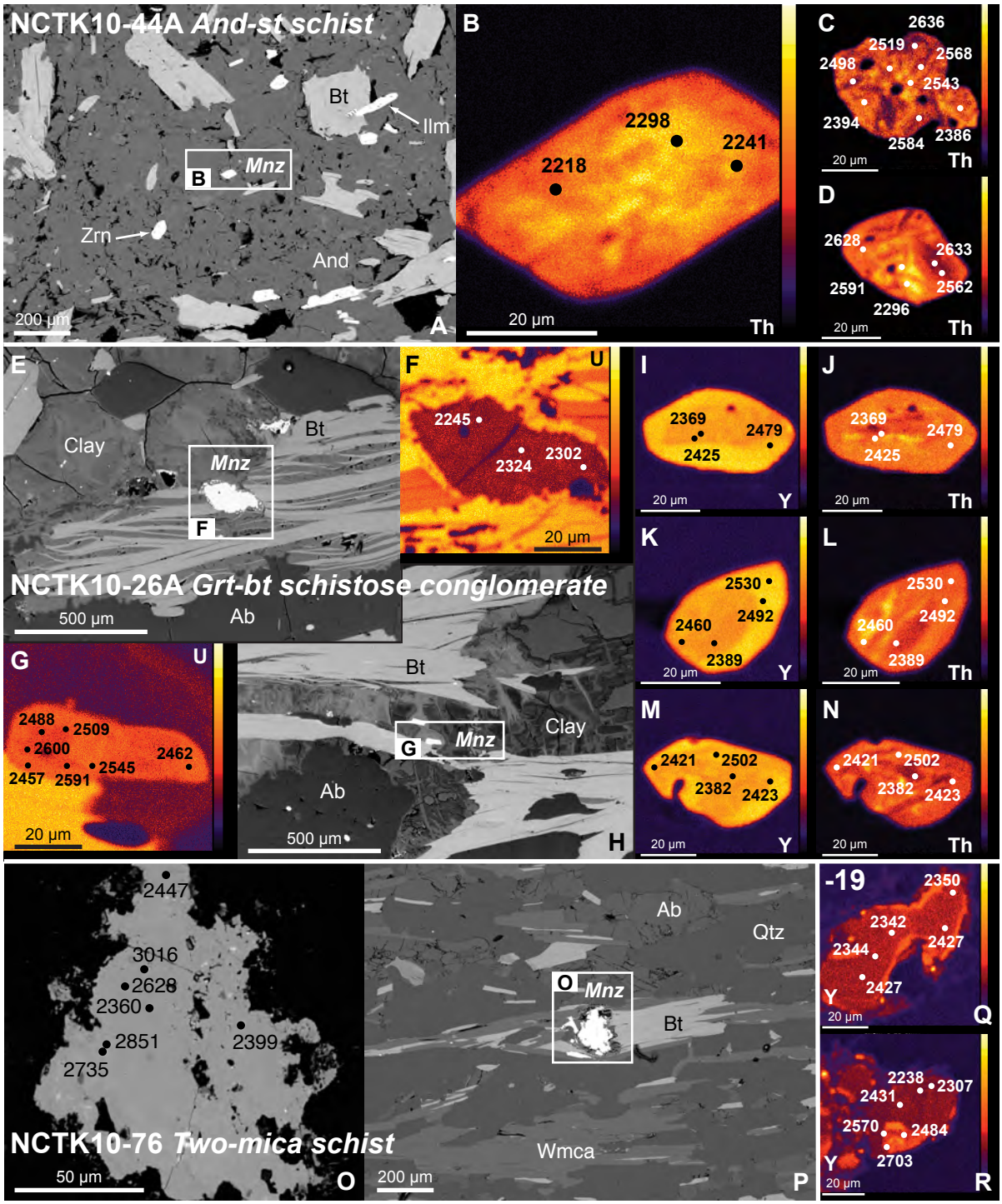

Fig. 10. Collage of backscatter electron images and Xray maps of monazite grains from high strain metasedimentary rocks in the NCGB. Boxes in low magnification images (A), (E), (H), & (P) surround monazite grains for which xray maps are also shown. (A-D) is sample NCTK10-44. (E-N) is sample NCTK10-26A. (O-P) is sample NCTK10-76. (Q-R) is sample NCTK10-19. All maps, as well as the high magnification BSE image of O show spot locations and associated ages (Ma).

NCTK10-38 is a sample of biotite schist situated about 4 km south of NCTK10-44A, strongly deformed in the ALFZ (**Fig. 1B**). The level of strain is indicated by dynamically recrystallized quartz isolated with albite in microlithons through segregation by penetrative SC-foliation planes defined by biotite and chlorite. Three small foliation-elongate monazite grains are characterized by patchy Th zoning and relatively low overall abundances of U, Th, and Y and reside either at the boundary between quartz and albite or in contact with biotite ± ilmenite. These yield two significant age populations; the older 2556 ± 28 Ma (MSWD: 1.8) age is the weighted-mean average of eight single spot analyses, has a Pb/Th* R^2 value of 0.9766, and is similar to the older population of NCTK10-44A, whereas the younger 2413 ± 29 Ma (MSWD: 1.2) age is averaged over six single spot analyses, defines a Pb/Th* line with an R^2 of 0.9437, and is older than the youngest age of NCTK10-44A (**Figs. 8, 9C**).

An albite schist (NCTK10-19) situated within the MLDZ (**Fig. 1B**) is characterized by a weak SC-fabric, and sigmoidal strain shadows cast by albite porphyroblasts indicate dextral sense of deformation. One of the 40-70 μm-long fabric-elongate monazite grains in this sample is broken and deformed and single spot analyses yielded anomalously low Th values (5120-7420 ppm, **Table A3**), so it was omitted from the probability plot. The remaining three grains form a group that parallels local foliation bundles of biotite and white mica and sparsely peppered blocky biotite throughout the matrix and found at the boundary between a plagioclase matrix and a foliation sub-parallel quartz ribbon. The monazite grains have diffuse boundaries and are surrounded by a combination of allanite and clay minerals. The monazite is chemically zoned in terms of Th, U, and Y and the age domains appear to be somewhat controlled by this chemistry (e.g. Y, **Fig. 10Q, R**). There is a slight positive correlation of Th content with age, and a general decrease in age in the same direction across each of the grains.

A robust single population of 2421 ± 49 Ma (MSWD: 13) is reported as a weighted mean average of 15 single ages and this age is represented through linear variation of Pb with Th* with an R^2 of 0.9717 (**Figs. 8, 9D**).

Sample NCTK10-26A is situated just north of the main strand of the MLDZ (**Fig. 1B**) and constitutes a garnet-biotite schistose granule to cobble conglomerate that has experienced increased levels of strain, evidenced in 3:1 length to width flattening of cobbles (**Fig. 2C**), and garnet zone metamorphism. Eight monazite grains were analyzed, most of which are fabric-elongate, range in size from 25 x 20 μm to 80 x 50 μm, are found either at the boundary between albite grains in the matrix or surrounded by clay minerals, and sometimes in contact with or proximity to fabric-forming biotite ± chlorite. Grains in the matrix are fairly euhedral, free of inclusions, zoned in terms of Th and Y (e.g. **Fig. 10I-M**), and while age does not vary with Y content, it generally increases with Th content (**Fig. 11**). EMPA analysis of monazite in this sample yields a single robust total-Pb age with a weighted-mean average of 2446 ± 26 Ma (MSWD: 6.2) over 29 single spot analyses and Pb vs. Th* yields a linear relationship with an R^2 of 0.9648 (**Figs. 8, 9E**). The grain that yields the youngest ages differs from the other grains in that it has diffuse edges and is found in the foliation plane alongside biotite surrounded by "clay" (**Fig. 10E, F**). The grain that yields some of the oldest ages is found in a similar microfabric context but the "clay" appears to differ slightly in terms of U content (**Fig. 10G, H**).

The two-mica schist (NCTK10-76) of the NCTSZ-MLDZ transition, yielding a U-Pb zircon age of 2858 ± 8 Ma, was also investigated for U-Th-total Pb geochronology of monazite. Of the five monazite grains analyzed, two are small in size (~20 μm), have fairly smooth grain boundaries, display weak Th zoning, and yield four single ages that cluster

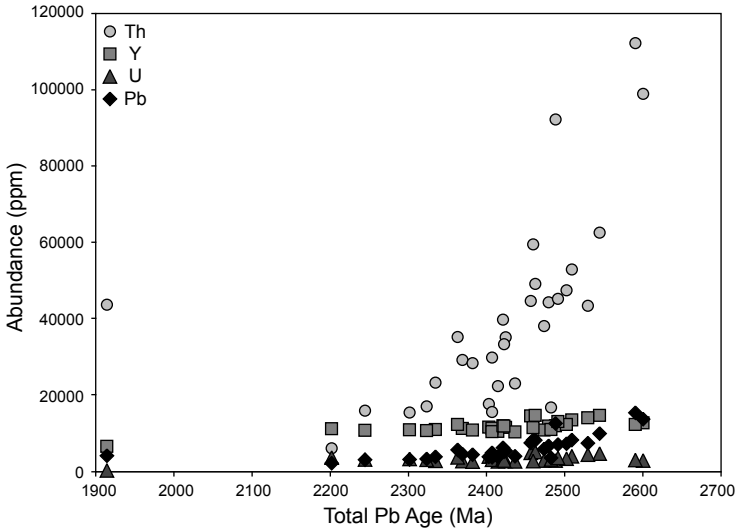

Fig. 11. Plot demonstrating variation among Y, Th, U, and Pb abundance (ppm) in single spot monazite ages from garnet- and biotite-bearing schistose conglomerate (NCTK10-26A) from north of the MLDZ.

within a 2600 ± 39 Ma (MSWD: 1.6) total-Pb age population (**Table A3**; **Fig. 9F**). In contrast, the remaining three grains range in size from ~40 x 30 μm to >100 μm in diameter, have resorbed boundaries, have relatively low yet highly variable U, Th, and Y contents (e.g. Y, **Fig. 10**), and together yield 16 single ages that span the three populations displayed in **Fig. 8**. The largest monazite grain is oriented perpendicular to the fabric, completely immersed in a bundle of biotite and muscovite (**Fig. 10P**), and the seven single spot analyses of this grain range in age from 2360 ± 50 to 3016 ± 50 Ma (**Fig. 10O**). There is no obvious trend among the three single spot analyses yielding ages >2800 Ga with respect to chemical zones and they have not been considered in tabulation of the significant age populations. The oldest population is defined by a weighted-mean average of six single ages at 2735 ± 20 Ma (MSWD: 1.03) and Pb varies with Th* only weakly linearly with an R^2 of 0.7134 (**Figs. 8, 9F**). The youngest population consists of a weighted-mean average over six single ages at 2414 ± 79 Ma (MSWD: 6.2) and the plot of Pb/Th* weakly defines a line with an R^2 value of 0.9537 (**Figs. 8, 9F**). The most robust population of this sample has a weighted mean age of 2600 ± 39 Ma (MSWD: 1.6) over 5 spot analyses and Pb vs. Th* is linear with an R^2 of 0.991 (**Figs. 8, 9F**). The three lines on the Pb/Th* diagram are close together and there is some overlap between single spot ages of the different populations (**Fig. 9F**).

Sample NCTK10-51A consists of a high-strain biotite schist from the ELS at the eastern extremity of the belt in the NCTSZ (**Fig. 1B**). Alignment of blocky biotite is a pervasive feature and long sinuous dextral bundles of biotite, chlorite, and muscovite weave between dynamically recrystallized microlithons of quartz and plagioclase feldspar among sweats of recovered quartz. Magnetite and ilmenite are accessory phases in this sample. Four small (~20 μm) grains, situated at the junction between plagioclase grains, are somewhat

elongate in the direction of foliation and in contact with biotite. The grains are characterized by patchy zoning of Th, U, and Y and the abundance of these elements are variable (e.g. Y, **Fig. 10**). As a result of the small grain size of the monazite in this sample, only nine analyses could be conducted over the four grains and the youngest of these was omitted from the weighted-mean age because of low Th content. The reported age population of 2570 ± 46 Ma (MSWD: 4.8) is a mean weighted average of 8 single ages and similar to the older age populations of monazite in the ALFZ (**Figs. 8, 9F**). Despite a few outliers, Pb is weakly related to Th* in a linear fashion with an R^2 of 0.9314 (**Fig. 9G**).

7. *In situ* major element EMPA and trace element LA-ICP-MS of garnet

The trends and patterns of garnet geochemistry are of particular interest due to the link between the Y and Zr that can be mobilized during garnet dissolution or fracturing and the potential for monazite and zircon crystallization (McLelland and Chiarenzelli, 1990; Fraser et al., 1997; Scoates and Chamberlain, 1997; Gaides et al., 2008). Five garnet-bearing samples (summarized in **Table 1**) of uppergreenschist to lower amphibolite metasediments displaying a range of deformation features, such as 3:1 flattening of cobbles, fold hinges and limbs, and micro-shear zones, were analyzed *in situ* to identify and determine geochemical variability within. A description of these samples is provided in **Appendix 1**.

7.1. Methods

Garnets in ~100 μm-thick sections were analyzed via core-rim or rim-rim multiple-spot transects for major element concentrations. Two samples, chlorite schist from the MLDZ and garnet- and biotite- bearing metaconglomerate from north of it (**Fig. 1B**) were analyzed *in situ* by EMPA with a Cameca SX-100 operated by the Bureau of Geology and Mineral

Resources, New Mexico Institute of Mining & Technology (Socorro, USA). Three additional samples, were analyzed *in situ* at the University of Ottawa (Ottawa, Canada) using the JEOL JXA-8230 SuperProbe. The garnets in two of these samples (biotite schist and hornblende schist) are microshear zone-hosted in the ELS at the North Rim fault zone (**Fig. 1B**), and garnets in the other are porphyroblastic in a very fine-grained matrix of potential felsic volcanic origin where the N-S stretch meets the northwestern arm of the NCGB (**Fig. 1B**). Furthermore, two X-ray maps of Fe, Mg, Mn, Ca, and Y in garnets from the alteration pod in schistose cobble conglomerate were produced using both the wavelength dispersive spectrometer (WDS) as well as the energy dispersive spectrometer (EDS) of the JEOL JXA-8230 SuperProbe at the University of Ottawa (Ottawa, Canada). A complete description of the analytical procedures is provided in **Appendix 4**.

The garnets from all five samples were also analyzed *in situ* for trace element concentrations using a Photon-Machines Analyte 193 μm ArF excimer laser ablation system coupled to an Agilent 7700x quadrupole ICP-MS at the Geological Survey of Canada (Ottawa, Canada). A complete description of the analytical procedure is provided in **Appendix 4**.

The results of *in situ* EMPA of garnet are summarized in **Table A4a** where wt% oxide, atom per formula unit (on the basis of 12 oxygens), and % endmember compositions are reported for the core, mean, and rim analyses of grains. Transect wt% profile plots of FeO_T, MnO, MgO, and CaO are presented in **Fig. 12**, and a two-ternary plot showing relative endmember compositions in **Fig. 13**. Data with either a high (due to quartz inclusion) or low (due to chlorite inclusion) Si, or high (due to rutile inclusion) Ti content were omitted. All garnets are almandine-rich whereas the contribution of the other endmembers is more variable

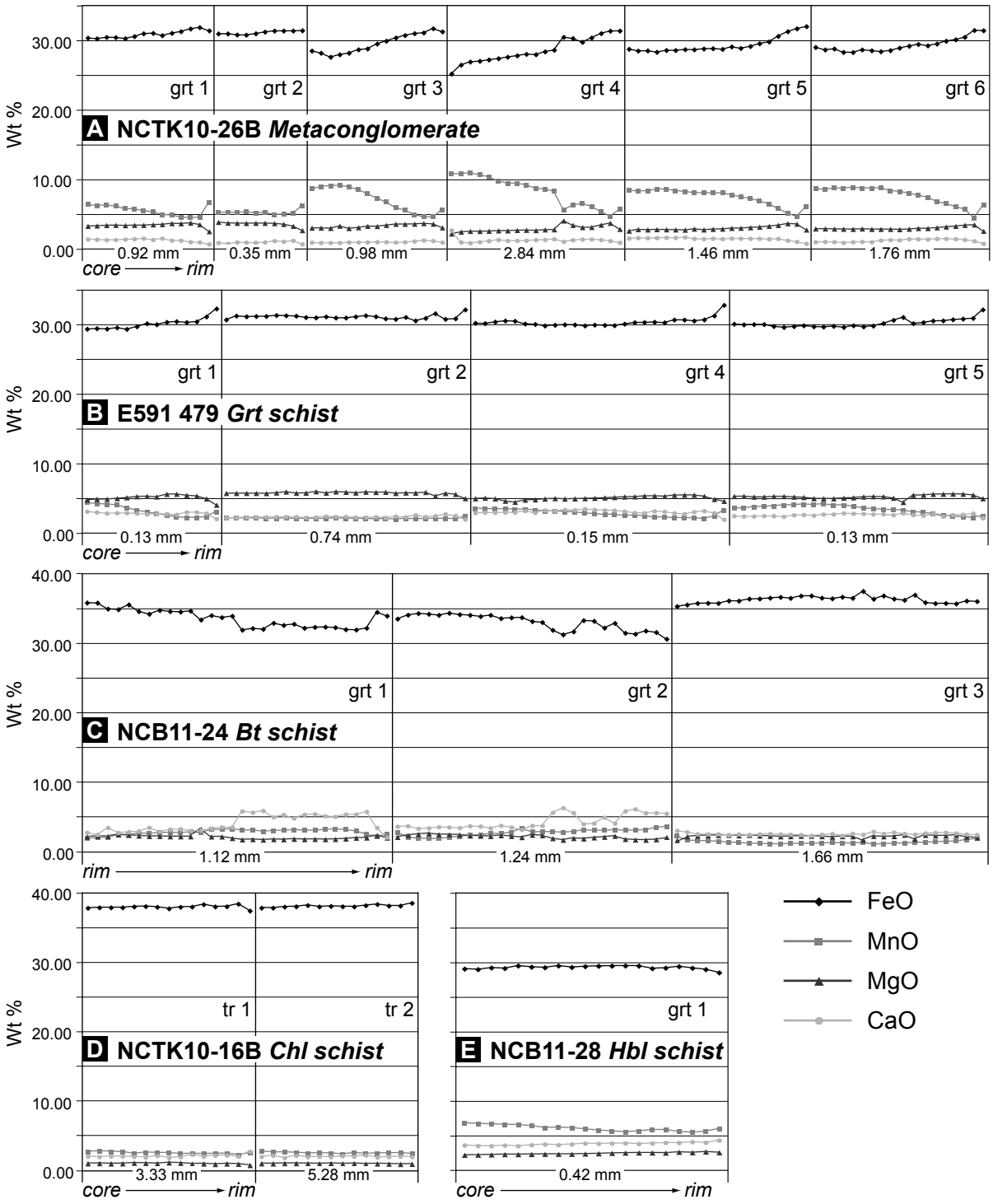

Fig. 12. Major element transects of garnet in supracrustal rocks of the North Caribou greenstone belt. Abundances of FeO, MnO, MgO, and CaO are plotted in terms of Wt% across garnets from core to rim in (A), (B), (D), and (E), and from rim to rim in (C). Perpendicular transects were conducted on the garnet in D (tr1, tr2).

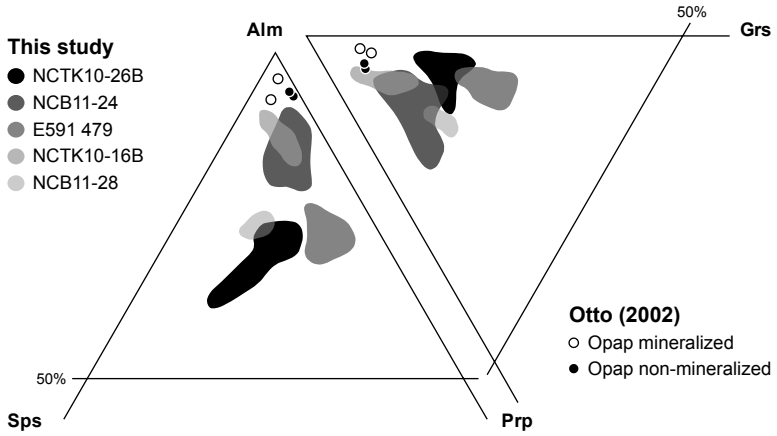

Fig. 13. Compositional variability among Fe, Mg, Mn, and Ca end members of garnets in supracrustal rocks of the North Caribou greenstone belt. Shades of grey are used to differentiate samples (descriptions are given in Table 1) and Otto's (2002) major element garnet geochemistry is shown as white (mineralized unit) and black (non-mineralized unit) circles.

between samples. The results of *in situ* LA-ICPMS of garnet are presented in **Table A4b** and trace element abundances normalized to chondrite (cf. McDonough and Sun, 1995) are plotted on a logarithmic scale for each of the rare earth elements **Fig. 14**. Lanthanum was not plotted in some samples because the values were below the detection limit.

7.2. Results

Sample E591 479 comprises schist containing many (~7%) 2-mm round to ellipsoid euhedral garnet porphyroblasts within an ultra-fine-grained siliceous matrix bearing abundant phyllosilicate minerals. Situated in the NRV at the northern bend of the NCGB (**Fig. 1B**), this high-strain sample contains local ribbons or sweats of coarser-grained quartz that has partially recrystallized through grain-boundary migration and formation of small subgrains, abundant fine-grained chlorite, and minor amounts of biotite. The long axes of ellipsoid garnets roughly parallel foliation and garnets present in strain shadows are oriented more randomly with respect to principal strain. Strain partitioning is evident as the foliation wraps around some garnet grains, and though on occasion with a sigmoidal shape as shown in **Fig. 15A**, dextral kinematics are also evident. Complete garnet transects were conducted on four garnets and only one half of each is plotted in **Fig. 12** to represent core-rim profiles. The major element profiles differ from those of NCTK10-26B in that the abundance of FeO_T increases at the rim by up to ~5 wt% (**Fig. 12**). The slight (~1 wt%) decrease in MgO and corresponding increase in MnO at the rim are, however, similar to those of NCTK10-26B, whereby the mirroring and mimicing roles of MnO and MgO appear to have switched with respect to the FeO_T profile (**Fig. 12**). The FeO_T profile of garnet 4 increases to a point and steps back down before increase once again at the rim and that of garnet 2 displays a similar feature but to a lesser extent (**Fig. 12**). There is no zoning in terms of wt% CaO except at the rim where it decreases

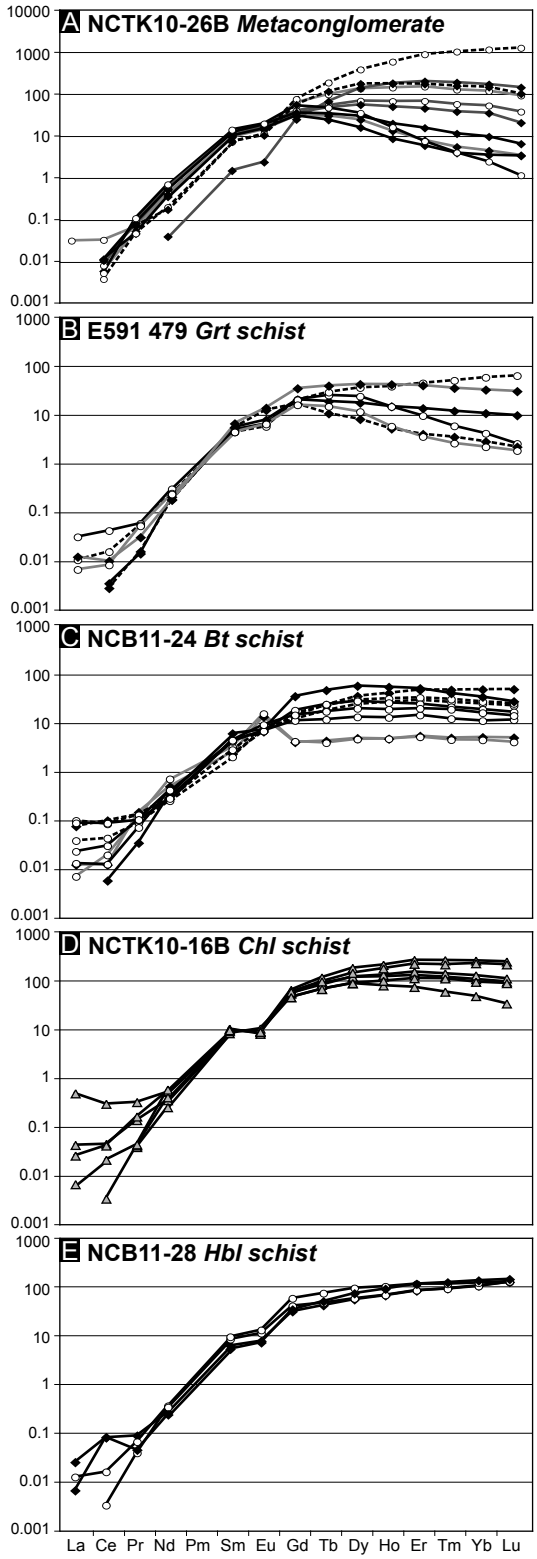

Fig. 14. Chondrite-normalized rare earth element patterns of garnet in supractustal rocks of the North Caribou greenstone belt. Black diamonds represent rim analyses, white circles represent core analyses, and grey triangles represent analyses that could not be differentiated. Different line colours correspond to different garnets in a sample.

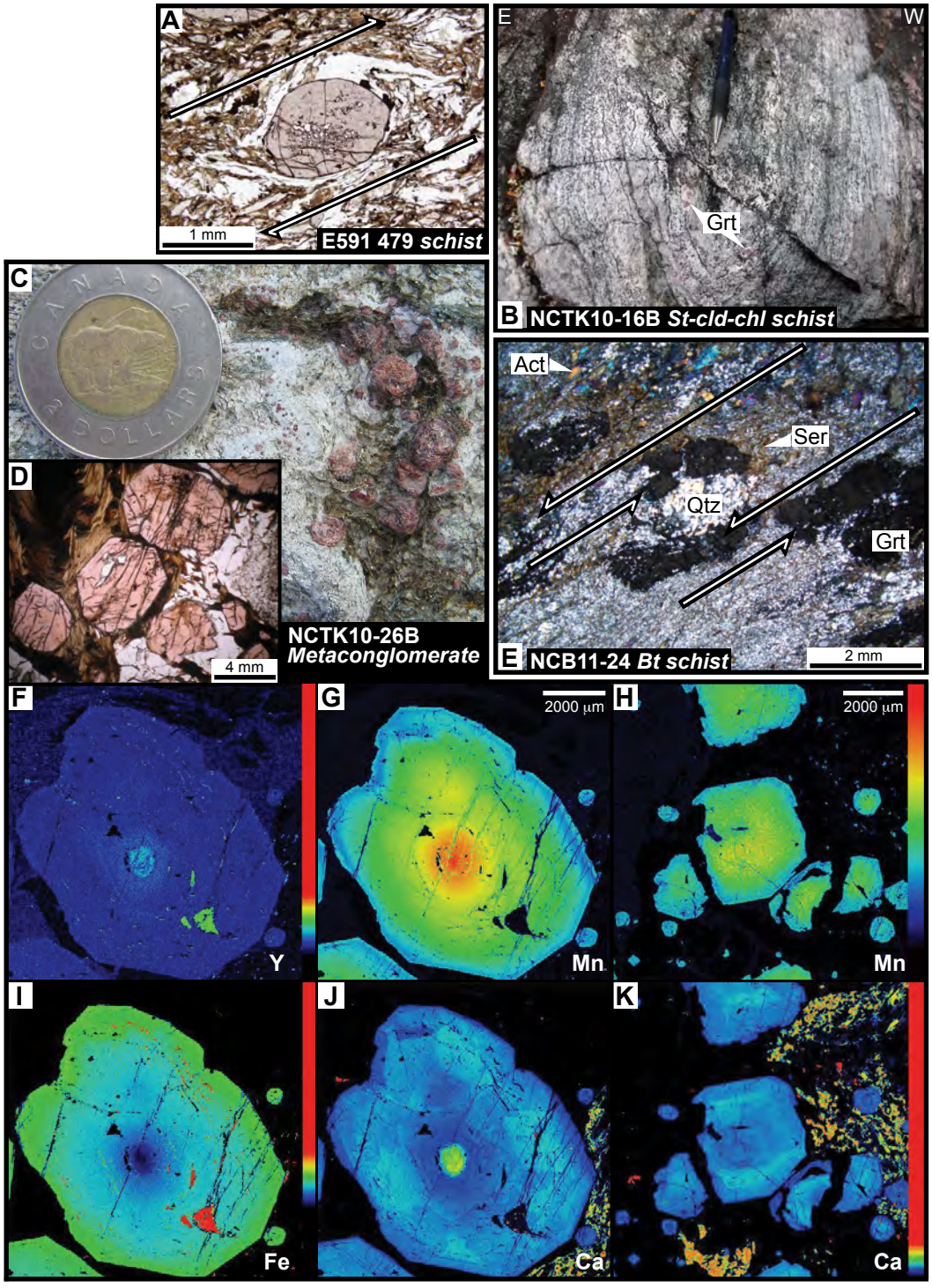

Fig. 15. Images of garnet in highly deformed rocks of the North Caribou greenstone belt. (A) Plane light photomicrographs of σ shaped strain shadows providing kinematic information in garnet-bearing schist (E591 479). (B) Tight and upright fold with garnet with quartz sweats in the limbs and hinge zone of chlorite schist (NCTK10-16B). (C and D) Plane light photomicrograph and field photograph of euhedral garnets in a nest of biotite within a pod of hydrothermal alteration among cobbles of a highly deformed conglomerate north of the MLDZ (NCTK10-26B). (E) Syn- to pre- tectonic garnets in a biotite schist from the NRFZ (NCB11-24). (F-K) Chemical maps of Y, Fe, Mn and Ca in euhedral hydrothermal garnets from a metaconglomerate (NCTK10-26B).

by <1 wt%. The garnets are zoned through chondrite normalized REE abundance as well, although where the core of one garnet is more enriched in HREEs relative to the rim, the rim of another garnet is equally enriched relative to the core (**Fig. 14**).

A chlorite schist (NCTK10-16B) is situated within the MLDZ, and garnet is associated with quartz sweats in the limbs and hinge zones of tight mesoscopic folds (**Fig. 15B**) that plunge 35° to the ENE. This sample is peppered with fine-grained chlorite that defines a fairly heterogeneous foliation through a matrix of mostly fine-grained quartz. Sample NCTK10-16A from the same outcrop contains other metamorphic index minerals such as chloritoid and staurolite (**Fig. 3**). One garnet in the thin section is at least 5 mm in diameter and full of inclusions of mostly quartz. Two perpendicular major element EMPA core to rim transects show flat profiles with the highest Fe content of the five garnet-bearing samples, ~80%$_{Alm}$ and <6%$_{Spes}$ (**Figs. 12, 13**). As a result of the inclusion-rich morphology of the garnet, the core was difficult to differentiate from the rim during LA-ICPMS analysis of this sample. Six of eight spots yield trace element abundances that are quite similar (within ~1 order of magnitude on a log scale) in terms of HREEs, have a subtle depletion in Eu, and vary by up to 2 orders of magnitude in terms of the lightest rare earth elements (e.g. La, Ce, **Fig. 14**). The remaining two trace element analyses hit inclusions, so were omitted from the spider diagram.

The sample containing garnet that is most likely to be of hydrothermal origin is NCTK10-26B, a pod of alteration situated within the highly deformed cobble conglomerate of NCTK10-26A, which was itself sampled for total-Pb dating of monazite, just north of the main strand of the MLDZ. This biotite is also found aligned in certain foliation planes of the cobble conglomerate and garnet is found there as well. EMPA analysis reveals some variance in major element patterns among the six garnets analyzed. The core to rim profile of the first

two garnets is relatively flat with only a slight 1-3 wt% increase in FeO_T towards the rim, in comparison with the remaining four in which the FeO_T increases on the order of 5-10 wt%. The MnO content roughly mirrors, and that of MgO mimics (on a smaller scale), the pattern of FeO_T, and where the decrease in FeO_T at the rim is minimal (or absent), the corresponding increase in MnO and decrease in MgO are more obvious and on the order of 1-2 wt%. X-ray maps for Fe, Mn, Mg, Ca, and Y were conducted on three garnets of this sample in order to observe a second dimension of the apparent zoning present. One 400 x 400 pixel map of one >7 mm garnet and one 500 x 500 pixel map of a cluster centered on a ~3 mm garnet was produced for each of the five elements and a representation is presented in **Fig. 15F-K**. The garnet appears to be sector zoned in terms of Ca, strongly concentrically zoned in terms of Mn, and less so in terms of Fe, Mg, and Y (**Fig. 15F-K**). This zoning is more evident in the larger garnet. Trace element analysis of four garnets in NCTK10-26B yields log values of chondrite normalized HREEs that span 3-orders of magnitude (**Fig. 14**). The Y content of these garnets is overall higher than most other garnets analyzed in this study (**Table A4b**). The difference between cores and rims of the same garnet, in terms of the heaviest REEs, ranges from 0.3 to 1.5 orders of magnitude, and although cores are more commonly enriched with respect to rims, this is not always the case (**Fig. 14**). The light REE patterns are nearly indistinguishable from one another (**Fig. 14**).

The remaining two garnet-bearing samples, biotite schist (NCB11-24) and hornblende schist (NCB11-28), are part of the ELS and situated near North Rim shear zone at the regional contact with the NRV in the northwestern arm of the NCGB (**Fig. 1B**). The rocks are highly deformed, and lithological contrasts and bedding planes are an obvious focal point for strain. Hornblende schist was obtained from a sliver of ELS sediments among the NRV and

localization of garnet growth appears to be controlled by the shear planes in the contact between the two units. Whereas the garnet in biotite schist displays a similar localization in shear planes, the morphology of the garnets differs significantly between the two samples. In the biotite-schist the fabric-elongate subhedral garnet grains are fractured and have been displaced along slip planes (**Fig. 15E**). Commonly accompanied by aggregates of smaller euhedral crystals and locally bearing some inclusion trails, the garnets appear to have grown preferentially and been brittly deformed and boudinaged in response to the same stresses that formed the penetrative foliaiton (**Fig. 15E**). The grains and/or fragments range in size from 1 to 3 mm. Very fine-grained biotite aligns in the matrix of equally fine-grained quartz but is a bit coarser-grained and occurrs at random orientations, sometimes with needle-like blue-green amphibole, in regions surrounding garnet blasts. The same amphibole, similar to the coarser-grained biotite, occurs with no preferred orientation surrounding, and between some, fragmented garnet blasts. Bundles of sericite locally radiate from the fragments of garnet, commonly in proximity to carbonate-altered domains within the shear band. In sample NCB11-28, the garnet is euhedral, relatively inclusion-free, and shows no preferential alignment. It is situated among abundant, potentially hydrothermal, coarse-grained biotite and dark green amphibole within a fabric-parallel dilation crack. Samples NCB11-24 and NCB11-28 differ significantly in terms of major element geochemistry. The average contribution from almandine is about 10% higher in NCB11-24 and the garnets are significantly more zoned (**Figs. 12, 13**). The CaO profile roughly mirrors that of FeO_T, and in garnets 1 and 2 there is an evident zoning from core to rim in which FeO_T decreases by ~2-4 wt% CaO increases accordingly (**Fig. 12**). The FeO_T abundance in garnet 3 broadly increases moving from core to rim and contribution and consistently higher than 35 wt%, most similar to NCTK10-16B in

terms of major element geochemistry. The profile plot of garnet in NCB11-28 is very flat with only a slight (<2 wt%) decrease in FeO_T accompanied by a mirroring increase in MnO at the rim. In the garnet from both of these samples, the abundance of Ca is more significant than in garnet from other samples with 10 and 11%$_{Grs}$ for NCB11-24 and NCB11-28 respectively. NCB11-28, however, has a greater abundance of Mn with 14 vs. 5%$_{Sps}$ in garnet from NCB11-24 (**Table A4a**; **Fig. 13**). The same three garnets of NCB11-24 were ablated in trace element analysis and display relatively flat HREE patterns. In garnet 1, there is no difference between core and rim despite the zoning observed in major element abundances, a positive Eu anomaly and low HREE relative to the other two garnets in which the core appears to have a slightly lower HREE abundance than the rim, and there is no positive Eu anomaly. Garnet 2 has more abundant light REEs and the trace element concentrations increase through the middle REEs and continue increasing across the heavy REEs to Lu (**Fig. 14**). The garnet from NCB11-28 is fairly homogeneous in terms of chondrite-normalized REE abundance. Two ablation craters near the rim and two ablation craters near the core yield roughly the same chondrite normalized REE plot. The HREE trend is similar to that of garnet 2 from NCB11-24, there is a weak negative Eu anomaly, and the four analyses vary most in terms of LREEs.

8. Major element EMPA of fabric forming minerals

The composition of abundant fabric forming minerals in the shear zones of the NCGB is investigated to compliment garnet geochemistry and monazite geochronology and lend insight into the nature of the fluids present during crustal-scale deformation. Chlorite is commonly aligned or intergrown with, and/or replaces micas in the penetrative foliation planes and commonly SC-fabrics that demarcate the high-strain zones of the NCGB. Blocky

micas define a less obvious and less homogeneous foliation as they pepper the matrix of more silicious coarser-grained samples, situated in planar contact with, or cross cutting chlorite. The micas are differentiated by colour and results for both white mica and dark mica (biotite) are presented. Endmembers for micas are muscovite [$KAl_2(AlSi_3)O_{10}(F,OH)_2$], paragonite [$NaAl_2(AlSi_3)O_{10}(F,OH)_2$], Mg-Al-celadonite [$K(MgAl)Si_4O_{10}(OH)_2$], Fe-Al-celadonite [$K(FeAl)Si_4O_{10}(OH)_2$], pyrophyllite [$Al_2Si_4O_{10}(OH)_2$], annite [$KMg_3(AlSi_3)O_{10}(OH)_2$], and phlogopite [$KFe_3(AlSi_3)O_{10}(OH)_2$] (cf. Parra et al., 2002) and chlorite in terms of daphnite [$(Fe_5Al)(AlSi_3)O_{10}(OH)_8$], clinochlore [$(Mg_5Al)(AlSi_3)O_{10}(OH)_8$], Mg-amesite [$(Mg_4Al_2)(Al_2Si_2)O_{10}(OH)_8$], and Mg-sudoite [$(Mg_2Al_3)(AlSi_3)O_{10}(OH)_8$] (cf. Vidal et al., 2001). A detailed description of the nine samples analyzed is provided in **Appendix 1**. They consist of various biotite and two-mica schists, a staurolite-chloritoid-chlorite schist, and a garnet-biotite schistose conglomerate from within and proximal to the MLDZ and NCTSZ (**Table 1**).

8.1. Methods

The JEOL JXA-8230 SuperProbe at the University of Ottawa (Ottawa, Canada) was used for *in situ* EMPA of chlorite and micas in ten metasedimentary rock samples from in and around the Markop Lake deformation zone as well as the North Caribou-Totogan shear zone. A complete description of the analytical procedures is provided in **Appendix 5**. Biotite-schists, mica-schists, two-mica schists, garnet-biotite schistose conglomerate, and staurolite-chloritoid-chlorite schist are all fairly highly foliated through preferential alignment of chlorite, dark mica (biotite) and/or white mica.

The results from EMPA of chlorite and micas are summarized in **Table A5**. The endmember components that contribute significantly to white mica chemistry are Parra et al.'s

(2002) muscovite, paragonite, Fe-Al-celadonite, and pyrophyllite, and are presented in **Table A5** as a percentage of their total. The endmember components that contribute significantly to dark mica chemistry are annite, phlogopite, and Al-Fe-celadonite and are likewise presented in **Table A5** as a percentage of their total. Chlorite is a combination of all four endmembers of Vidal et al.'s (2001) solid solution model and the individual percentages are with respect to the combination of these.

8.2. Results

All three phyllosilicates define the foliation in six of the nine analyzed samples, where dark mica was not analyzed in samples NCTK10-15 and NCTK10-16A, and white mica is absent from NCTK10-26B. The ternary plots in **Fig. 16** display variability in atoms of Al, Mg, Fe, and K per formula unit of chlorite, white mica, and biotite in samples from within the Markop Lake deformation zone and along the contact of the North Caribou greenstone belt with the Schade Lake gneissic complex to the north that runs along the North Caribou-Totogan shear zone.

Two-mica schists (NCTK10-12B and -20A), mica schist (NCTK10-15), and tightly folded staurolite-chloritoid-chlorite schist (NCTK10-16A) from the same location as NCTK10-16B (analyzed for geochemistry of garnet) are found in the high-strain MLDZ (**Fig. 1B**). These samples generally contain less biotite, and the composition of chlorite is somewhere between the chlinochlore and daphnite endmembers. NCTK10-16A is an exception, however, with chlorite of nearly $100\%_{Dph}$, and the chlorite of NCTK10-20A plots distinctly closer to the chlinochlore endmember. Outside of the MLDZ, Two-mica schists (NCTK10-75 and NCTK10-76) and biotite schist (NCTK10-51A), also analyzed for total-Pb dating of monazite, are situated within the NCTSZ (**Fig. 1B**) and generally more Mg-rich,

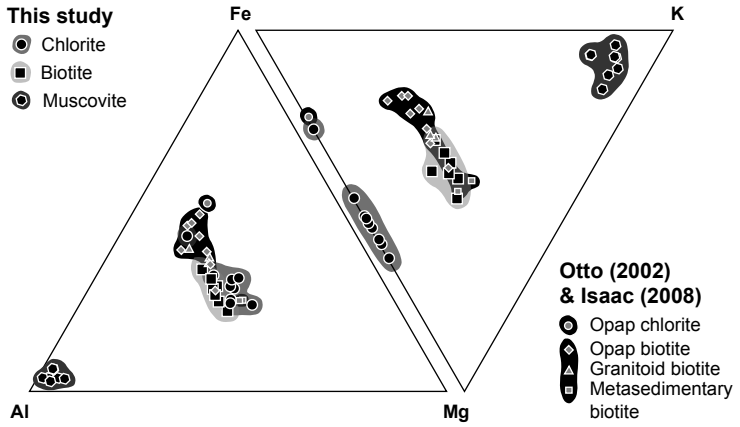

Fig. 16. Compositional variability among Fe, Al, Mg, and K in fabric-forming chlorite, biotite, and white mica in metasedimentary rocks of the North Caribou greenstone belt. Black symbols represent results obtained in this study wheras small grey symbols represent previous studies by Otto (2002) and Isaac (2008). Opap chlorite and biotite are from Musselwhite mine, while granitoid and metasedimentary biotite are from the surrounding region.

save NCTK10-75 which is more Fe-rich, with mica chemistry nearly identical to that of NCTK10-12B from the MLDZ (**Fig. 16**). Biotite schist (NCTK10-74A) near the NRV east of Opapimiskan Lake (**Fig. 1B**) contains the most Mg-rich chlorite and biotite with a mean of 81.3%$_{Clin}$ and 64.5%$_{Phl}$. Sample NCTK10-26A is host to the alteration pod bearing hydrothermal garnet of NCTK10-26B and was also analyzed for total-Pb dating of monazite. A garnet and biotite-bearing schistose conglomerate, situated north of the main strand of the MLDZ, this sample is most chemically similar to the northern-most sample in the MLDZ (NCTK10-20A) trending slightly towards Mg on the ternary diagram (**Fig. 16**). The composition of chlorite in all samples (excluding NCTK10-16A) varies most significantly across the daphnite and chlinochlore endmembers, from 6-58% and 29-82%, respectively (**Table 6**). The contribution of Mg-sudoite is never greater than 9% and that of Mg-amesite is only >15% in two samples, peaking at 18% in NCTK10-26A in which there are two distinct clay mineral species. The white mica is mostly muscovite, varying from 83-89%$_{Musc}$. Minor contributions come from the paragonite and Fe-Al-celadonite endmembers. Dark mica contains a significant amount of Fe-Al-celadonite, with an endmember composition ranging from 20-33%. The annite and phlogopite contributions vary from 15-48% and 18-65%, respectively, with phlogopite more commonly acting as the greater contributor. Both the biotite and chlorite of sample NCTK10-75 are more Fe-rich, and in general, the relative abundance of Mg and Fe in biotite mimics that of chlorite on a sample-by-sample basis (**Fig. 16**).

9. Discussion

The major high-strain zones that accommodated the protracted tectonic evolution of the North Caribou greenstone belt preserve dominant dextral kinematic signatures, and

commonly exhibit localized strain partitioning. Zircon and monazite are abundant in many metasedimentary rocks in, and metagranitoids surrounding, the belt and were used as geochronometers capable resolving the timing of tectonothermal events via *in situ* dating of these accessory phases within a microtextural context. Of the samples analyzed, U-Pb zircon age populations range from 2871 to 2858 Ma, with an older age population of 2956 Ma from a cordierite schist in the northern region of the belt (**Fig. 1B, 5**). Three significant total-Pb monazite age populations include c. 2735 Ma, c. 2600-2556 Ma, and a younger and robust c. 2441 Ma (**Figs. 1B, 8, 9**).

Garnets were analyzed from five samples within structural settings including an alteration pod, dilation crack, shear band, fold hinges and limbs in high-strain supracrustal rocks of the NCGB. Major element compositions of all these garnets, regardless of setting, are dominantly almandine (65-81%$_{Alm}$). Chondrite-normalized trace element plots of garnet in samples bearing evidence for remobilization of silica and/or circulation of hydrothermal fluids generally display variability in HREEs of >2 orders of magnitude (**Fig. 14A, D**). Syn- to inter-tectonic garnets localized in a foliation-parallel shear band are not zoned in terms of trace elements, but zoned in terms of major elements through a decrease in Fe and increase in Ca across the grain from one rim to the other (**Fig. 12C**). Ellipsoidal garnet porphyroblasts with inclusion-rich cores are from the rock most distal from crustal shear zones and have a greater pyrope component of 21%, in comparison with the other garnets in this study. The chlorite and micas that define the pervasive fabric in the metasediments of high-strain zones of the NCGB plot are more Mg- than Fe-rich, with the exception of a tightly-folded staurolite-chloritoid-chlorite schist from the MLDZ in which chlorite is nearly 100%$_{Dph}$ (**Fig. 16**). The

sample with the highest Mg-content is the most proximal to Musselwhite Mine, northwest of the Markop Lake deformation zone (**Fig. 1B**).

Based on petrographic and microstructural analysis of highly strained rocks in the NCGB combined with the results of zircon and monazite geochronology and garnet, chlorite, and mica geochemistry, I was able to identify four periods of tectonism spanning over 400 m.y. (**Fig. 17**). Below I discuss metamorphism of the supracrustal assemblages in the NCGB recorded in zircon at 2.86 Ga followed by 2.75-2.71 Ga transpression-influenced tectonism recorded in rims on zircons as well as in monazite domains (**Fig. 17A, B**). I believe I have also identified two later stages of tectonism in re(?)-crystallized monazite grains as a result of dextral transpression and related fluid flux at 2.60-2.56 Ga in the ALFZ, NCTSZ, and MLDZ and c. 2.44 Ga, focused mainly in the MLDZ (**Fig. 17 C, D**).

9.1 Metamorphism at 2.86 Ga

Uranium-Pb dating of zircon from four metasedimentary and two metaplutonic rocks from the high-strain margins of the North Caribou greenstone belt yielded consistent and robust age populations of c. 2.86 Ga. This is particularly peculiar for metasedimentary rocks collected across a regionally extensive basin as one would instead expect a detrital age population that more accurately reflects the protracted and punctuated nature of the surrounding batholith construction (Gehrels et al., 2012 and references therin). The morphology and internal structural of the zircons is fairly consistent across the samples, regardless of the host rock type and grade of metamorphism. Most grains are equant and commonly display oscillatory zoning although it is often blurry and patchy. When grains are elongate, the zircons are aligned within the fabric. From a simplified perspective, the growth of zircon is classified as a metamorphic process when the mineral is grown by solid-state

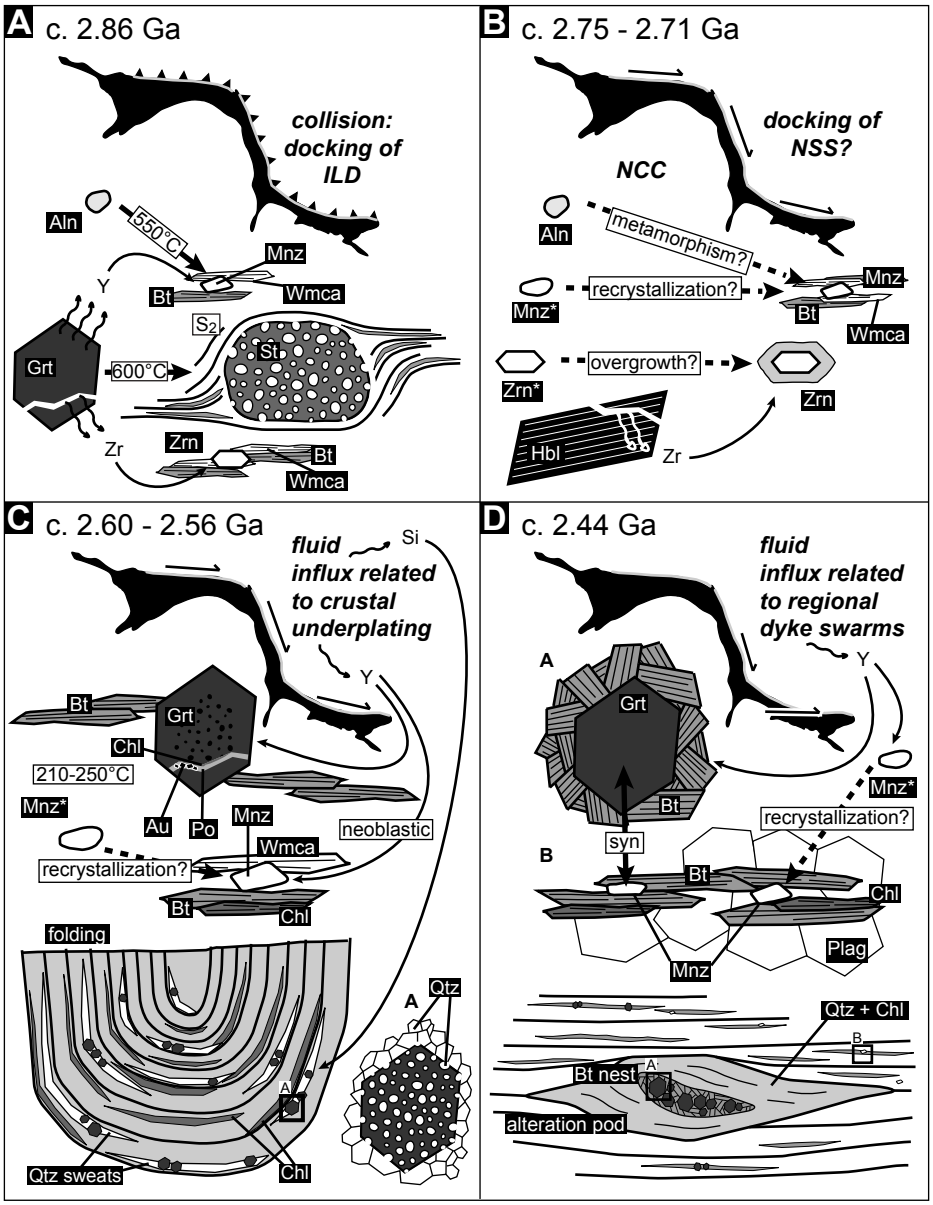

Fig. 17. Schematic diagram illustrating a tectonic progression that highlights the interplay of garnet and/or hornblende with the growth or recrystallization of monazite and zirrcon in the NCGB. (A) During 2.86 Ga metamorphism related to the docking of the Island Lake domain (ILD), staurolite is crystallizing at the expense of garnet, foliation-elongate monazite grows and incorporates the Y released in this process, Zr is being released during mechanical breakdown of garnet and incorporated into foliation-parallel metamorphic zircon, and there is a potential for monazite to crystallize at the expense of alanite at 550°C . (B) During docking of the Northern Superior superterrane (NSS) that also involved metamorphism and magmatism from 2.75-2.71 Ga, it is unlikely the temperatures reached 550°C (required to breakdown alanite and form monazite), so monazite that was generated during 2.86 Ga tectonism may have been recrystallized during deformation along the northern margin of the belt, and zircon locally developed metamorphic overgrowths. (C) During a protracted period of tectonism also involving transpression and fluid influx potentially related to crustal underplating beginning at 2.69 Ga, garnet brittley fractures and hosts gold, pyrrhotite, and chlorite which crystallized at 210-250°C (Otto, 2002), garnet at Musselwhite mine have inclusion-rich cores and inclusion-poor rims thought to have crystallized from a hydrothermal fluid, and quartz-inclusion-rich garnet is found in quartz sweats in the limbs and hinge zones of tight folds, and monazite recrystallize becoming elongate in the direciton of foliation. (D) During tectonic reactivation of MLDZ at 2.44 Ga and intrusion of regional mafic dykes potentially related to a large igneous province or mantle plume, garnet crystallizes from hydrothermal fluids among biotite nests within dilation zone containing abundant chlorite- and silica-alteration, and Y in the fluid is also incorporated during monazite recrystallization.

reactions, as an igneous or magmatic derivation when crystallized from a melt, and as a hydrothermal origin when crystallized from a fluid-dominated system (cf. Möller et al., 2003). There are obvious exceptions, which blend the categories, such as migmatitic rocks. Internal structure that exhibits oscillatory zoning is typically a characteristic of igneous zircon, reflecting compositional variation of major and trace-elements. Subsolidus growth or recrystallization of zircon can lead to distortion or overprinting of pre-existing internal structures and give rise to secondary textures that may be difficult to interpret (Corfu et al., 2003). Gradual homogenization and fading of original growth zoning, accompanied by Pb loss, is attributed to subtle metamorphic recrystallization (Connelly, 2001). Thus, moderate to high temperature metamorphism drives progressive convoluting, blurring, and thickening of original oscillatory zoning, which has been documented in Precambrian rocks that have been metamorphosed to at least amphibolite facies (e.g. Hoskin and Black, 2000). Metamorphism is generally also responsible for external changes to the zircon morphology, namely rounding and resorption of crystal faces, however, fluid-rich systems such as those involving the breakdown of chlorite, biotite and hornblende help to preserve a quasi-euhedral shape characteristic of magmatic zircons (Corfu et al., 2003). If you recall, the rocks analyzed in this study are products of upper-greenschist to amphibolite facies metamorphism of hydrous-bearing sedimentary rocks, suitable conditions likely to contain an abundance of fluid. Most zircons in this study are equant and subhedral, probably as a result of metamorphism.

Because of the sometimes-equivocal nature of zircon's structure, some workers (Williams et al., 1996; Rubatto et al., 2001) have suggested metamorphic zircons can be chemically distinguish from magmatic zircons by their low Th/U values (<0.1). The Th/U values reported in this study range from 0.1-1.0 with the majority around 0.4 (**Fig. 6**). In the

absence of other phases competing for Th during metamorphism, it is entirely possible that, should the zircons undergo subsolidus recrystallization, the Th/U signature could be inherited from the original systematics of the igneous population (cf. Möller et al., 2003; Wu and Zheng, 2004). It would be expected that the Th/U values of neoblastic zircon be influenced by the chemistry of the fluid and co-existing minerals.

Metamorphic reactions occurring at grades of upper-amphibolite facies and above involve the breakdown of Zr-bearing phases, such as garnet and hornblende (Fraser et al., 1997; Degeling et al., 2001), ilmenite (Bingen et al., 2001), biotite (Vavra et al., 1996), zirconolite ($CaZrTi_2O_7$) and pre-existing igneous zircon (Pan, 1997). In this study, for example, the 2866 Ma zircon population in an andalusite-staurolite schist from the Akow Lake fault zone (NCTK10-44A, **Fig. 1B**) potentially grew from, and incorporated zirconium during, the breakdown of garnet to form staurolite (**Fig. 17A**). Moreover, an outcrop of fine-grained metasedimentary rock at the east end of Eyapamikama Lake (**Fig. 1B**) was intruded by granitic dykes and is host to cordierite nodules (**Fig. 3C**) indicating high-temperature metamorphism. The peak metamorphic temperature of 540-600°C (Easton, 2000; Otto, 2002) in the NCGB is high enough to initiate subsolidus zircon growth, and also likely prompted intra-grain "reworking" and Pb loss. This resulted in the small, subhedral and equant, blurry-zoned zircon structure, with occasional thin rims.

The consistency and unimodality of the age population of small (<100 μm), equant zircons from both metaigneous and metasedimentary rocks of the NCGB leads me to believe I have dated a metamorphic event at c. 2.86 Ga. Due to the small zircon size, the *in situ* LAICP-MS often required ablation of the entire grain, and the potential for mixing of subdomains may help to explain the scatter and discordance of the single spot analyses. In

contrast, a provenance study in the North Caribou belt involving U-Pb dating of coarser size fractions (>200 μm) of metasedimentary rocks yielded a spread of single spot zircon ages typical of a detrital sedimentary population (pers. comm. J. Duff, 2012). An alternative explanation for the single robust age population acquired in this study would be that the zircons were all derived from the same magmatic event, manifested as either plutonic granitoids or volcanoclastic sequences, both subsequently metamorphosed. However, the >60 km span of sample locations (**Fig. 1B**) likely had more than one source, and rapidly cooled zircons in volcanic rocks tend to be narrow and prismatic as a result of rapid nucleation in one direction (Corfu et al., 2003).

Emplacement of the North Caribou Lake batholith (**Fig. 1B**) took place from c. 2870 to 2833 Ma (U-Pb zircon, Thurston et al., 1991; Ontario Geological Survey, 1992; Davis and Stott, 2001; Van Lankvelt et al., 2012) with the youngest episode of emplacement preserved in the center of the batholith (Van Lankvelt et al., 2012). Magmatism continued across the region, although localized, until c. 2730 Ma. The similarity in P-T conditions reported by Van Lankvelt et al. (2012) for the NCLB of 6.7-7.5 kbar and 620-640°C and those reported by Otto (2002) in the Opapimiskan Lake area of the greenstone belt of 6-7 kbar and 540-600°C are suggestive of regional tectonism (D_2/M_2) within the greenstone belt was occurring at the same structural level as the batholith was being emplaced. If the 2.86 Ga zircon ages reported here are indeed metamorphic, then the P-T constraints coupled with the geochronology indicates magmatism and metamorphism were roughly synchronous and intimately linked.

9.2. Magmatism and metamorphism at c. 2.75-2.71 Ga

Total-Pb dating of monazite from one metasedimentary sample in the North Caribou-Totogan shear zone yields a few age populations, the oldest of which is c. 2.74 Ga. Monazite

has two morphologies in this sample: big (~100 μm) with convoluted and cuspate grain boundaries, which yield single spot analyses that span 600 m.y. (**Fig. 10O, P**), and small grains that possess a fabric-preferred orientation, yielding similar single spot ages. Monazite is relatively stable across a range of metamorphic grades, and it can be quite challenging to implicate a meaning to the dates. The most commonly cited monazite-in reaction is the breakdown of allanite at 550°C (**Fig. 17B**; Overstreet, 1967; Smith and Barreiro, 1990; Parrish, 1990; Kingsbury et al., 1993; Wing et al., 2003). If allanite was present in the rocks it could have been a reactant to form monazite at c. 2.75-2.71 Ga during progressive metamorphism. Alternatively, monazite potentially formed during c. 2.86 Ga metamorphism (**Fig. 17A**) and acted as a precursor for the monazite that recrystallized during this subsequent event (**Fig. 17B**). The 2.72-2.66 Ga hydrothermal garnets in the mineralized high-strain limbs of the tightly folded BIF at Musselwhite mine (Sm-Nd [w.r.-granet], Biczok et al., 2012) were potentially also generated at this time. Evidence for tectonism within the NCGB during this period is evident as discrete plutons present among voluminous metagranitoids that surround the North Caribou greenstone belt. Discrete magmatism is recorded south of Musselwhite mine at 2729-2723 Ma (Biczok et al., 2012). The Southern Batholith is host to narrow (l:w of 1:4 to 1:7) zircons that are c. 2727 Ma as well as c. 2731-2710 Ma zircon rims on older cores (pers. comm. A. Van Lankvelt, 2012). The Schade Lake gneissic complex also possesses low Th/U value rims on zircon cores (c. 2758-2702 Ga) and A. Van Lankvelt (pers. comm. 2012) interprets these dates to indicate coeval magmatism and metamorphism. I interpret this oldest monazite age population to record the same tectonometamorphic event, and it is preserved in this sample because the larger monazite grains contain domains that were not completely reset during subsequent tectonism.

9.3. Deformation and mineralization between c. 2.60 and 2.56 Ga

Monazite grains from four high-strain metasedimentary rocks, two in the Akow Lake fault zone and two in the North Caribou-Totogan shear zone, yield age populations in the range of c. 2.60 to 2.56 Ga (**Fig. 8, 9**). The event recorded by monazite at this time postdates c. 2.86 Ga and c. 2.75-2.71 Ga tectonism by over 100 million years. Most monazite grains are surrounded by quartz and plagioclase in the rock's matrix and many are in contact with, though rarely embedded in, fabric forming micas and chlorite (e.g. **Fig. 10**). Often roughly elongated within foliation and exhibiting resorbed and cuspate grain boundaries, the grains commonly display patchy chemical zoning (e.g. **Fig. 10**).

Similar to zircon, the crystallization of monazite from a melt typically results in concentric or sector zoning and because the solid-state element diffusion of U, Th, and Pb is low (e.g. Zhu and O'Nions, 1999b; Cherniak et al., 2000; Gardes et al., 2006), older age domains with sharp boundaries are preserved through metamorphism even at high temperatures (Williams et al., 2007). The isotopic system is, however, sensitive to deformation-induced recrystallization, regulated by intracrystalline deformation mechanisms and the presence of fluids (Lanzirotti and Hanson, 1996; Poitrasson et al., 1996; Krohe and Wawrzenitz, 2000; Seydoux-Guillaume et al., 2002; Ayers et al., 2006; Harlov et al., 2011; Williams et al., 2011). Patchy zoning of Th, U, and Pb and the development of elemental domains are commonly the result of elemental redistribution within a monazite in response to strain and in the presence of fluid during a process described by Warwenitz et al. (2012) as dissolution-precipitation creep (DPC). Fluid-assisted dissolution and (re)precipitation of minerals operates at strain levels that are insufficient for initiation of dislocation creep and is an efficient mechanism for isotope resetting of monazite even at very low-grade conditions

(cf. Frost and Ashby, 1982; Carter and Tsenn, 1987; Wawrzenitz et al., 2012 and references therein).

The monazite-bearing samples dated in this study were collected from crustal scale shear zones, in which the monazites possess fabric-preferred orientation and abundant microstructural features indicative of DPC. I interpret the chemical domains within monazite grains that yield single spot ages of c. 2.60-2.56 Ga as the result of fluid-induced dynamic recrystallization. These ages bracket the c. 2.59 Ga $^{40}Ar/^{39}Ar$ age of foliation-bound biotite in metabasalts that stratigraphically overlie a mineralized unit at Opapimiskan Lake, yet ~ 10 m.y. younger than the c. 2.72-2.66 Ga Sm-Nd [w.r.-garnet] age of garnets host to gold in the mineralized unit at Musselwhite mine (Biczok et al., 2012). The second "hydrothermal" stage of garnet growth may in fact be related to the c. 2.75-2.71 Ga event discussed in the previous section, which further implicates a channeling of hydrothermal fluids bearing high field strength elements and silica at this time. It is possible that the subsequent tectonism (strain, heat, fluids) responsible for monazite recrystallization, gave rise to brittle fracturing (at temperatures as low as 210-250°C based on chlorite thermometry; Otto, 2002) of the garnets in the higher strain limbs of folded BIF units, providing a structural trap for gold deposition (**Fig. 17C**).

Poikiolitic garnet growth in a chlorite schist (NCTK10-16B) of the Markop Lake deformation zone, is potentially correlative to the "hydrothermal" stage of garnet growth at Musselwhite mine as it is associated with silica remobilization and predominantly restricted to the limbs and hinge zones of tight folds (**Figs. 15B, 17C**). The high Fe content (~80%$_{Alm}$; **Fig. 13**) of these garnets is similar to garnets (72-82%$_{Alm}$) in the mineralized unit at Musselwhite mine (**Fig. 13,** Otto, 2002) yet would be expected for crystallization in the KFMASH system

of a staurolite-chloritoid-chlorite assemblage. This poikiolitic garnet is fairly homogeneous in terms of trace elements (**Fig. 14**), however, only one garnet was analyzed and there very well could be some variability between garnets. The pattern resembles those observed by Spry et al. (2007) for garnets in samples affected by remobilization. The genesis of the quartz sweats and relative timing of garnet growth in this outcrop remain unknown, and the end-member possibilities have quite contrasting implications. If the garnet and quartz were generated prior to folding, and folding presumably occurred no later than c. 2.72 Ga, "peak" metamorphism may very well have occurred at c. 2.86 Ga. On the other hand, if the quartz was remobilized during folding, and the garnet crystallized synchronous with or after folding, it may be related to the c. 2.75-2.72 Ga event, or the younger c. 2.60-2.56 Ga fluid-related shearing. The localization of garnet in the outcrop, and to the tight fold, leads me to believe the latter to be true, yet I was unable to determine whether the fluid flux was synchronous with, or occurred after the folding event. The potential genetic link between this poikiolitic garnet and the garnets hosting gold at Musselwhite mine presents a means for further resolving the timing of mineralization, as both events appear to be directly related to remobilization of silica in the mid to shallow crust.

Garnet occurrences in the North Rim fault zone similarly appear to be preferentially located in shear bands accommodating regional strain. In sample NCB11-28, euhedral garnet apparently crystallized in a relatively strain free system, within a dilation crack parallel to a planar fabric in the hornblende schist (**Fig. 1B**), possibly during a fluid overpressure episode. The garnets from this sample are relatively homogeneous in comparison with the syn-tectonic garnets that were subsequently deformed along slip-planes within a biotite schist (NCB11-24, **Fig. 1B**, **15E**), recording progressive phases of growth and deformation. These garnets

display across-grain variability with respect to decreasing FeO_T and increasing CaO (from <2 to 4 wt%, **Fig. 12**) and are less deformed in their cores than in their rims. These observations are consistent with Storey and Prior's (2005) observation that Ca-highs represent the stable garnet composition that grew during deformation. There is a significant (~ 2 orders of magnitude) variation in trace element abundance across these garnets, which could arise during syn-deformational growth, or may implicate a fluid evolution over the crystallization history of the garnet, which is generally an indication of hydrothermal genesis. These garnets may have begun crystallizing during the c. 2.75-2.71 Ga period, once again implicating deformation accompanied metamorphism at this time, and deformed more brittly during the c. 2.60-2.56 Ga period of deformation similar to the garnets at Musselwhite mine. Only kilometers away, and in the same deformation zone, the homogeneous euhedral garnet of NCB11-28 clearly crystallized strain-free, which sheds some light on the relative timing of deformation in the North Rim fault zone and implicates post-tectonic conditions capable of crystallizing garnet. Despite the evident restriction of garnet growth in the NRFZ to mesoscopic manifestations of strain accomodation, the geochemistry remains variable, both in terms of major and trace elements (**Fig. 12, 13, 14**). Moreover, the non-systematic variability makes it difficult to distinguish a metamorphic signature from a hydrothermal one, even in light of microtextural considerations.

9.4. Deformation and fluid influx at 2.44 Ga

A single and robust monazite age population of c. 2.44 Ga is recorded in two metasedimentary rocks from the Markop Lake deformation zone, and also observed elsewhere in samples proximal to it within the North Caribou-Totogan and the Akow Lake shear zones. The morphology, internal zoning, and patching chemical nature of the monazite grains is

similar to those discussed in the previous section, and I believe this age similarly records a discrete late tectonic pulse.

Monazite from garnet-biotite schistose conglomerate (NCTK10-26A&B, **Fig. 1B**) near the Markop Lake deformation zone exhibits high concentrations of Y (mean: 11730 ppm, **Table A3**), typically an indication that its growth preceded garnet nucleation (Zhu and O'Nions, 1999b), potentially at the expense of allanite or a previous generation of monazite (**Fig. 17D**). This garnet-bearing conglomerate is the only sample in which the single spot ages from the monazites display a positive correlation of Th with age (**Figs. 10I-M, 11**), which may indicate inheritance of a magmatic (monazite) component as monazite in granitoids typically have significant quantities of Th (Franz et al., 1996; van Emden et al., 1997).

Any monazite-altering event that occurs at temperatures <800°C (closure temperature for Pb diffusion in monazite) is thought to be strongly dependent on fluid (Williams et al., 2007). The euhedral garnets from a pod of alteration (**Figs. 15 C, D; 17D**) found among the flattened cobbles in the garnet-biotite schistose conglomerate are concentrically zoned in terms of Mn (decreasing towards the rim, **Fig. 15G, H**) and sector zoned with respect to Ca (outward from a small high-Ca core, **Fig. 15J, K**). The major element zonation of these garnets is most similar to Duff et al.'s (2012) garnets in which the core is Mn-rich (18-25%$_{Sps}$) and the rim is more Mg-rich (8-15%$_{Prp}$), and similar to Otto's (2002) results in which the rims are Fe-rich. Despite these similarities, both biotite and chlorite in the garnet-biotite schistose conglomerate contain more Mg than Fe, which is in contrast with the Fe-rich chemistry of both mineralized and non-mineralized samples from Opapimiskan Lake (Otto, 2002; Isaac, 2008). These garnets also contain increased abundances of Y (mean: 150 ppm, **Table A4b**) relative to the garnets from all but one other sample in the MLDZ. Chondrite-

normalized HREE concentrations of individual garnets vary by up to 3 orders of magnitude, evidence for crystallization during fluid evolution and remobilization (cf. Spry et al., 2007). There is a slight positive correlation of Y with age across single spot analyses of monazite grains in the conglomerate host to this pod (**Fig. 11**). The event that gave rise to the older age population in monazite (c. 2.60-2.56 Ga) may precede garnet growth as the monazites of this age are more Y-rich, and the MLDZ-localized fluid that crystallized garnet likely contributed to the alteration of monazite at c. 2.44 Ga as Y would have been preferentially incorporated into garnet at this stage.

The 2.44 Ga monazite ages, are broadly coeval with the c. 2.49 Ga $^{40}Ar/^{39}Ar$ age of biotite in an unmineralized garnet-biotite schist unit at Musselwhite mine (Opapimiskan Lake; Biczok et al., 2012). This observation suggests late recrystallization of biotite in response to the same tectonic strain accommodated dominantly by displacement in the Markop Lake deformation zone responsible for recrystallizing monazite. Micas and chlorites are easily recrystallized in response to strain even at low temperatures and, as they are a pervasive component defining the fabric of the high-strain metasedimentary rocks in the southeastern arm of the NCGB, it is likely they were recrystallized by the latest reactivation of crustal-scale shear focused in the MLDZ. Relative abundances of Fe and Mg generally mimic each another in biotite and chlorite of the same sample (**Table A5**), possibly indicative of the conditions and fluid chemistry during crystallization, although this is difficult to discern without reference to the bulk rock chemistry. Two of the three samples from the NCTSZ bear monazite used for U-Th-total Pb geochronology and yield similar chlorite chemistries of ~60%$_{Clin}$ in contrast with the monazite-barren sample that yields significantly more Fe-rich biotite and chlorite with end-member compositions of ~49%$_{Ann}$ and ~57%$_{Dph}$. This correlation

is consistent with the elevated Mg (~67%$_{Clin}$) in chlorite of NCTK10-26A, another monazite-bearing metasedimentary rock. Isaac (2008) interprets Mg-rich biotite as hydrothermal in origin based on a positive correlation of Mg with Si in mineralized rock and probable derivation during silica flooding. There is no significant distinction between MLDZ and NCTSZ schists with respect to major fabric forming minerals. The distinction between chlorite and biotite compositions of otherwise similar NCTSZ schists bearing versus barren of monazite suggests a link between the recrystallization of monazite and the development of the fabrics in these high-strain zones, although, this may be a reflection of the bulk rock chemistry. There is no discernible pattern among geochemical signatures of chlorite and micas of metasedimentary rocks, despite the evident difference in shear-zone activity (i.e. broad restriction of the c. 2.44 Ga to the MLDZ) in the southeastern arm of the NCGB. Similar to garnet, it was not possible to distinguish a metamorphic from a hydrothermal genesis through geochemical analysis of these minerals.

9.5. Tectonic synthesis and summary

The shear zones in which my study is focused have the likely potential to be repeatedly reactivated during long-lived tectonism in the North Caribou region. During the occurrence of such events they are the ideal conduits for crustally-derived hydrothermal fluids, through interaction with which new growth of zircon, monazite, garnet, and abundant fabric forming minerals is likely initiated or at least catalyzed. These shear-zone conduits are known to enhance the transportation of gold-bearing fluids and play an important role in the genesis of many high-grade gold deposits. Below, I discuss a plausible tectonic evolution that may explain my results; it is not the only history that is possible, but one that explains the data simply and parsimoniously.

Widespread lower amphibolite facies metamorphism produced small (<100 μm), equant, often subhedral, and patchy oscillatory-zoned zircons in the NCGB under the same P-T conditions (6-7.5 kbar and 540-600°C) and roughly the same time (c. 2.86 Ga) as the emplacement of the surrounding granitoids. Metamorphism was likely driven by crustal thickening, and locally regional-scale contact metamorphism, resulting from collision in the north as the Island Lake domain was accreted to the North Caribou core (**Fig. 1A, 17A**; cf. Percival et al., 2006). One of few preserved occurrences of classic amphibolite facies index minerals is an andalusite-staurolite schist from the Akow Lake fault zone. The Y and Zr released during breakdown of garnet to form staurolite could have been incorporated into metamorphic zircon and monazite. Alternatively, precursor phases underwent recrystallization through progressive metamorphism at this time.

Monazite that may have been generated during 2.86 Ga metamorphism was completely recrystallized by subsequent episodes of deformation within the ALFZ. However, a few discrete domains in a ~100 μm monazite grain displaying random alignment relative to fabric in a two-mica schist, may recorded this earliest tectonometamorphic event at the transition of the Markop Lake deformation zone to the North Caribou-Totogan shear zone. This grain is also host to several single spots that contribute to the 2.74 Ga age population, only observed in this sample and dominantly in the smaller more euhedral grains, which has implications for successive recrystallization of precursor monazite and preservation of age domains within a single grain. Magmatism and metamorphism at c. 2.75-2.71 Ga was potentially driven by c. 2.72 Ga docking of the Northern Superior superterrane at the northern margin of the NCS (**Fig. 1A, 17B**; cf. Percival et al., 2006). The Berens River plutonic complex and Uchi domain (**Fig. 1A**) in the southern margin of the NCS, ~200 km to the south

record c. 2.75-2.71 Ga arc magmatism, potentially correlative with similar events in the NCGB (Percival et al., 2006). Gold mineralization at the world-class Red Lake mining district, as well as in the Pickle Lake belt at c. 2.71 Ga (**Fig. 1A**) is believed to be associated with the regionally penetrative fabrics formed in response to accretion to the NCS from the south (Sanborn-Barrie et al., 2001; Dubé et al., 2003; Young et al., 2006).

Deep-seated fluid circulation is invoked during crystallization of hydrothermal garnet at Musselwhite mine at c. 2.72-2.66 Ga (Sm-Nd w.r.-garnet, Biczok et al., 2012) and via recrystallization of monazite at c. 2.60-2.56 Ga during initiation or reactivation of crustal-scale deformation zones that parallel the northern margin of the NCGB. Poikiolitic garnet associated with quartz sweats in the limbs and hinge zone of a tightly folded schist in the MLDZ is thought to have also crystallized during either of these events. A potential source for the fluids at this time may be the significant crustal underplating in the Neoarchean, a process suggested by Heaman et al. (2011) as the most viable generator of global c. 2700 to 2640 Ma granulite terranes.

Deformation and the recrystallization of monazite at 2.44 Ga, apparently focused in the MLDZ and potentially associated with the transposition of earlier fabrics, is evident in sigmoidal deformed quartz sweats and veins, coinciding with an $^{40}Ar/^{39}Ar$ age of c. 2.49 Ma recorded in biotite from Musselwhite mine. The only correlatable tectonic source possibly responsible for the (partial) disturbance of these isotopic systems at this age is the emplacement of several Large Igneous Provinces, such as the c. 2.47-2.45 Ga Matachewan swarm in the Southeastern Superior Province (Heaman, 1997; Stott and Josey, 2009) and c. 2.51 Ga Irsuaq swarm in the far Northeastern Superior Province (Maurice et al., 2009). While there are no surface expressions of this period of magmatism in the Northwestern Superior

Province, dykes of Proterozoic age, potentially related to the Pickle Crow diabase dyke swarm (Sage and Breaks, 1982), are controlled by brittle fault zones in the NCGB (Hall and Rigg, 1986). The deformation related to the c. 2.49-2.44 Ga event is probably a far-field effect of the crust accommodating extension during super plume activity.

Late recrystallization of monazite at c. 2.44 Ga invokes a strong fluid presence evidenced further in the geochemical signature of strain-free euhedral garnets present in a pod of alteration situated in the matrix surrounding flattened cobbles of a MLDZ conglomerate. These garnets vary in terms of HREE by 3 orders of magnitude occur in nests of biotite within pods of alteration and believed to have crystallized from a hydrothermal fluid. Monazite grains in the garnet- and biotite-bearing metaconglomerate host to these pods are dominated by the c. 2.44 Ga population and independently interpreted as a fluid-induced deformation age. The strain did not apparently affect the garnets or the nests of biotite and I conclude the garnets crystallized from fluids channeled in the MLDZ and influenced the recrystallization of monazite.

The localization of garnets in shear bands in the NRFZ is of particular interest as it suggests the channeling of fluids in shear zones as a factor in their genesis. Despite the apparent restriction of garnet growth to regions of elevated strain in the NCGB, there is a non-systematic variability among geochemical compositions. Though likely influenced by the same fluid presence, dominantly the pulse catalyzing monazite recrystallization at c. 2.44 Ga, there is no discernible trend observed in the geochemistry of abundant fabric forming minerals of the southeastern arm. It is difficult to draw equivocal conclusions about the geochemistry of garnet and fabric forming minerals without knowledge of the whole rock chemistry. However, the ambiguity of the results leads me to caution the use of geochemical

signatures as a vector to distinguish a metamorphic from a hydrothermal genesis of these minerals. It is possible that the background metamorphic signature, in the North Caribou greenstone belt, is too high to make use of these geochemical data.

10. Conclusions

- The shear zones of the North Caribou greenstone belt record a protracted history of tectonism that spans over 400 million years, and discrete events are broadly correlatative with the dominant terrane accretions, consistent with a horizontal evolution of the Superior craton.
- Though difficult to distinguish between a metamorphic and hydrothermal signature on the basis of garnet, chlorite, and mica geochemistry, both the recrystallization of monazite at low temperatures and the restriction of garnet growth to local manifestations of high-strain necessitate late-stage transportation of fluids in crustal-scale shear zones of the NCGB.
- There is a predominance of shear zones in the southeastern arm in contrast with the observations of Breaks et al. (2001) in the northwest, and the latest pulse of tectonic activity (c. 2.44 Ga) was accompanied by an influx of fluids and focused primarily in the Markop Lake deformation zone.
- Additional P-T analyses should be done with chlorite, micas, and garnet to further demonstrate their importance as metamorphic and alteration minerals in regions of high strain.

REFERENCES

Anderson, J.L., Smith, D.R., 1995. The effects of temperature and f_{O2} on the Al-in-hornblende barometer. American Mineralogist 80, 549–559.

Andrews, A.J., Hugon, H., Durocher, W.E., Corfu, F., Lavigne, M.J., 1986. The anatomy of a gold-bearing greenstone belt; Red Lake, northwestern Ontario, Canada. In: Macdonald, A.J. (Ed.), Gold '86; An International Symposium on the Geology of Gold Deposits. 28 September to 1 October 1986, Toronto, Vol. X, pp. 3–22.

Ayers, J.C., Loflin, M., Miller, C.F., Barton, M.D., Coath, C.D., 2006. In situ oxygen isotope analysis of monazite as a monitor of fluid infiltration during contact metamorphism: Birch Creek Pluton aureole, White Mountains, eastern California. Geology 34, 653–656.

Biczok, J., Hollings, P., Klipfel, P., Heaman, L., Maas, R., Hamilton, M., Kamo, S., Friedman, R., 2012. Geochronology of the North Caribou greenstone belt, Superior Province of Canada: implications for tectonic history and gold mineralization in the Musselwhite Mine. Precambrian Research 192-195, 209–230.

Bingen, B., Austreheim, H., Whitehouse, M., 2001. Ilmenite as a potential source for zirconium during high-grade metamorphism? Textural evidence from the Caledonides of Western Norway and implications for zircon geochronology. Journal of Petrology 42, 355–375.

Böhm, C.O., Heaman, L.M., Creaser, R.A., Corkery, M.T., 2000. Discovery of pre-3.5 Ga exotic crust at the northwestern Superior Province margin, Manitoba. Geology 28, 75–78.

Böhm, C.O., Heaman, L.M., Stern, R.A., Corkery M.T., Creaser, R.A., 2003. Nature of Assean Lake ancient crust, Manitoba: a combined SHRIMP-ID-TIMS U-Pb geochronology and Sm-Nd isotope study. Precambrian Research 126, 55–94.

Breaks, F.W., Bartlett, J.R., deKemp, E.A., 1985. Opapimiskan Lake project: Precambrian and economic geology of the North Caribou Lake greenstone belt, Eyapamikama Lake area, northwestern Ontario, District of Kenora, Patricia Portion. Ontario Geological Survey, Miscellaneous Paper 126, pp. 268–276.

Breaks, F.W., Bartlett, J.R., 1991. Geology of the Eyapamikama Lake area. Ontario Geological Survey, Open File Report 5972, 132 p.

Breaks, F.W., Bartlett, J.R., deKemp, E.A., Osmani, I.A., 1991. Geology of the Doubtful-Akow Lakes area, District of Kenora. Ontario Geological Survey, Open File Report 5795, 131 p.

Breaks, F.W., Osmani, I.A., deKemp, E.A., 2001. Geology of the North Caribou Lake area, northwestern Ontario. Ontario Geological Survey, Open File Report 6023, 80 p.

Card, K.D., 1990. A review of the Superior Province of the Canadian Shield, a product of Archean accretion. Precambrian Research 48, 99–156.

Card, K.D., Ciesielski, A., 1986. Subdivisions of the Superior Province of the Canadian Shield. Geoscience Canada 13, 5–13.

Carter, N.L., Tsenn, M.C., 1987. Flow properties of continental lithosphere. Tectonophysics 136, 1–26.

Chardon, D., Choukroune, P., Jayananda, M., 1996. Strain patterns, décollement and incipient sagducted greenstone terrains in the Archaean Dharwar craton (south India). Journal of Structural Geology 18, 991–1004.

Chardon, D., Choukroune, P., Jayananda, M., 1998. Sinking of the Dharwar Basin (South India): implications for Archaean tectonics. Precambrian Research 91, 15–39.

Chardon, D., Pencat, J.-J., Jayananda, M., Choukroune, P., Fanning, C.M., 2002. Archean granite-greenstone tectonics at Kolar (South India): interplay of diapirism and bulk inhomogeneous contraction during juvenile magmatic accretion. Tectonics 27, 1016–1032, doi: 10.1029/2001TC901032.

Cherniak, D.J., Watson, E.B., 2001. Pb diffusion in zircon. Chemical Geology 172, 5–24.

Chi, G., Liu, Y., Dubé, B., 2009. Relationship between CO_2-dominated fluids, hydrothermal alterations and gold mineralization in the Red Lake greenstone belt, Canada. Applied Geochemistry 24, 504–516.

Choukroune, P., Ludden, J.N., Chardon, D., Calvert, A.J., Bouhallier, H., 1997. Archean crustal growth and tectonic processes: a comparison of the Superior Province, Canada and the Dharwar Craton, India. In: Burg, J.-P., Ford, M. (Eds.), Orogeny Through Time, Geological Society, London, Special Publications 121, 63–98.

Cocherie, A., Legender, O., Peucat., J.J., Kouamelan, A.N., 1998. Geochronology of polygenetic monazites constrained by in situ electron microprobe Th-U-total lead determination: Implications for lead behaviour in monazite. Geochimica et Cosmochimica Acta 61, 2475–2497.

Corfu, F., Stott, G.M., Breaks, F.W., 1995. U-Pb geochronology and evolution of the English River subprovince, an Archean low P - high T metasedimentary belt in the Superior Province. Tectonics 14, 1220–1233.

Corfu, F., Hanschar, J.M., Hoskin, P.W.O., Kinny, P., 2003. Atlas of zircon textures. In: Hanchar, J.M., Hoskin, P.W.O. (Eds.), Zircon. Reviews in Mineralogy and Geochemistry, pp. 469–500.

Corkery, M.T., Cameron, H.D.M., Lin, S., Skulski, T., Whalen, J.B., Stern, R.A., 2000. Geological investigations in the Knee Lake belt (Parts of NTS 53L). In: Report of Activities 2000. Manitoba Industry, Trade and Mines, Manitoba Geological Survey, pp. 129–136.

Davis, D.W., Stott, G.M., 2001. Geochronology of several greenstone belts in the Sachigo Subprovince, northwestern Ontario, #18 Project Unit 89-7. In: Summary of Field Work and Other Activities 2001. Ontario Geological Survey, Open File Report 6070, pp. 18–1 to 18–13.

Degeling, H., Eggins, S., Ellis, D.J., 2001. Zr budgets for metamorphic reactions, and the formation of zircon from garnet breakdown. Mineralogical Magazine 65, 749–758.

deKemp, E.A., 1987. Stratigraphy, provenance, and geochronology of Archean supracrustal rocks of western Eyapamikama Lake area, Northwestern Ontario. Unpublished M.Sc. thesis, Carleton University, 98 p.

Dubé, B., Williamson, K., McNicoll, V., Malo, M., Skuilski, T., Twomey, T., Sanborn-Barrie, M., 2004. Timing of gold mineralization at Red Lake, northwestern Ontario, Canada: new constraints from U-Pb geochronology at the Goldcorp high-grade zone, Red Lake mine and the Madsen mine. Economic Geology and the Bulletin of the Society of Economic Geologists 99, 1611–1641.

Duff, J., Hattori, K., Schneider, D., Cossette, E., Jackson, S., Biczok, J., 2012. Using garnet to record mineralization in a BIF hosted orogenic Au deposit. Goldschmidt Geochemistry Conference, Montreal, Canada.

Easton, R.M., 2000. Metamorphism of the Canadian Shield, Ontario, Canada; I, The Superior Province. In: Tectonometamorphic studies in the Canadian Shield (Part II). The Canadian Mineralogist 38, part 2, pp. 287–317.

François, C., Philippot, P., Rey. P., 2012. Formation and exhumation mechanisms of high-grade rocks: sagduction and subduction processes during the Archean. Geophysical Research Abstracts 14, EGU2012–5136.

Fraser, G., Ellis, D., Eggins, S., 1997. Zirconium abundance in granulite-facies minerals, with implications for zircon geochronology in high-grade rocks. Geology 25, 607–610.

Franz, G., Andrehs, G., Rhede, D., 1996. Crystal chemistry of monazite and xenotime from Saxthuringian-Moldanubian metapelites, NE Bavaria, Germany. European Journal of Mineralogy 8, 1097–1118.

Froese, E., Gasparinni, E., 1975. Metamorphic zones in the Snow Lake area, Manitoba. The Canadian Mineralogist 13, 162–167.

Frost, H.J., Ashby, M.F., 1982. Deformation Mechanism Maps: The plascitic and creep of metals and ceramics, Pergamon Press, New York, 166 p.

Fyon, J.A., Breaks, F.W., Heather, K.B., Jackson, S.L., Muir, T.L., Stott, G.M., Thurston P.C., 1992. Metallogeny of metallic mineral deposits in the Superior Province of Ontario. In: Thurston, P.C., Williams, H.R., Sutcliffe, R.H., Stott, G.M. (Eds.), Geology of Ontario, Special Volume 4, Part 2. Ontario Geological Survey, pp. 1091–1174.

Gaides, F., Krenn, E., De Capitani, C., Abart, R., 2008. Coupling forward modeling of garnet growth with monazite geochronology: an application to the Rappold Complex (Australopine crystalline basement). Journal of Metamorphic Geology 26, 775–793.

Goodwin, A.M., Smith, I.E.M., 1980. Chemical discontinuities in Archaean metavolcanic terrains and the development of Archaean crust. Precambrian Research 10, 301–311.

Gorman, B.E., Pearce, T.H., Birkette, T.C., 1978. On the structure of Archean greenstone belts. Precambrian Research 6, 23–41.

Hall, R.S., Rigg, D.M., 1986. Geology of the west anticline zone, Musselwhite prospect, Opapimiskan Lake, Ontario, Canada. In: Macdonald, A.J. (Ed.), Gold ’86: An International Symposium on the Geology of Gold Deposits, Proceedings Volume, pp. 124–136.

Harley, S.L., Kelly, N.M., Möller, A., 2007. Zircon behaviour and the thermal histories of mountain chains. Elements 3, 25–30.

Harlov, D.E., Wirth, R., Hetherington, C.J., 2011. Fluid-mediated partial alteration in monazite: the role of coupled dissolution–reprecipitation in element redistribution and mass transfer. Contributions to Mineralogy and Petrology 162, 329–348.

Harris, L. B., Godin, L., Yakymchuk, C., 2012. Regional shortening followed by channel flow induced collapse: a new mechanism for “dome and keel” geometries in Neoarchean granite-greenstone terrains. Precambrian Research, *in press*, doi: 10.1016/j.precamres.2012.04.022.

Hay, D.C., Dempster, T.J., Lee, M.R., Brown, D.J., 2010. Anatomy of a low temperature zircon outgrowth. Contributions to Mineralogy and Petrology 159, 81–92, doi: 10.1007/s/00410-009-0417-2.

Heaman, L.M., Böhm, Ch.O., Machado, N., Krogh, T.E., Weber, W., Corkery, M.T., 2011. The Pikwitonei Granulite Domain, Manitoba: a giant Neoarchean high-grade terrane in the northwest Superior Province. Canadian Journal of Earth Science 48, 205–245.

Heaman, L.M., 1997. Global mafic magmatism at 2.45 Ga: remnants of an ancient large igneous province? Geology 25, 299–302.

Holland, T., Blundy, J. 1994. Non-ideal interactions in calcic amphiboles and their bearing on amphibole-plagioclase thermometry. Contributions to Mineralogy and Petrology 116, 433–447.

Hollings, P., Wyman, D.A., Kerrich, R., 1999. Komatiite - basalt - rhyolite volcanic associations in Northern Superior Province greenstone belts: Significance of plume-arc interaction in the generation of the proto continental Superior Province. Lithos 46, 137–161.

Hollings, P., Kerrich, R., 2000. An Archean arc basalt-Nb-enriched basalt-adakite association: the 2.7 Ga Confederation assemblage of the Birch-Uchi greenstone belt, Superior Province. Contributions to Mineralogy and Petrology 139, 208–226.

Hollings, P., Stott, G., Wyman, D., 2000. Trace elemental geochemistry of the Meen-Dempster greenstone belt, Uchi subprovince. Canadian Journal of Earth Sciences 37, 1021–1038.

Hollings, P., 2002. Archean Nb-enriched basalts in the Northern Superior Province. Lithos 64, 1–14.

Hoschek, G., 1969. The stability of staurolite and chloritoid and their significance in metamorphism of pelitic rocks. Contributions to Mineralogy and Petrology 22, 208–232.

Hoskin, P.W.O., Black, L.P., 2000. Metamorphic zircon formation by solid-state recrystallization of protolith igneous zircon. Journal of Metamorphic Geology 18, 423–439.

Hrabi, B., Cruden, A.R., 2006. Structure of the Archean English River subprovince: implications for the tectonic evolution of the western Superior Province, Canada. Canadian Journal of Earth Sciences 43, 947–966.

Ingebristen, S., Sanford, W., 1998. Groundwater in geologic processes. Cambridge University Press, Cambridge, 341 p.

Isaac, C., 2008. Stable isotope (N, O, H) geochemistry, petrology and compositions of biotite of the Musselwhite Mine, Ontario: implications for mineralization. Unpublished M.Sc. thesis, Lakehead University, 136 p.

Kingsbury, J.A., Miller, C.F., Wooden, J.L., Harrison, T.M., 1993. Monazite paragenesis and U-Pb systematics in rocks of the eastern Mojave Desert, California, U.S.A.: implications for thermochronometry. Chemical Geology 110, 147–167.

Kohn, M.J., Malloy, M.A., 2004. Formation of monazite via prograde metamorphic reactions among common silicates: implications for age determinations. Geochimica et Cosmochimica Acta 68, 101–113, doi: 10.1016/S0016-7037(03)00258-8.

Krohe, A., Wawrzenitz, N., 2000. Domainal variations of U-Pb monazite ages and Rb-Sr whole- rock dates in polymetamorphic paragneisses (KTB Drill Core, Germany): influence of strain and deformation mechanisms on isotope systems. Journal of Metamorphic Geology 18, 271–291.

Langford, F.F., Morin, J.A., 1976. The development of the Superior Province of northwestern Ontario by merging island arcs. American Journal of Science 276, 1023–1034.

Lanzirotti, A., Hanson, G.N., 1996. Geochronology and geochemistry of multiple generations of monazite from the Wepawaug Schist, Connecticut, USA: implications for monazite stability in metamorphic rocks. Contributions to Mineralogy and Petrology 125, 332–340.

Lin, S., 2005. Synchronous vertical and horizontal tectonism in the Neoarchean: kinematic evidence from a synclinal keel in the northwestern Superior craton, Canada. Precambrian Research 139, 181–194.

Lin, S., Davis, D.W., Rotenberg, E., Corkery, M.T., Bailes, A.H., 2006. Geological evolution of the northwestern Superior Province: clues from geology, kinematics and geochronology in the Gods Lake Narrows area, Oxford-Stull terrane, Manitoba. Canadian Journal of Earth Sciences 43, 749–765.

Maurice, C., David, J., O'Neil, J., Francis, D., 2009. Age and tectonic implications of Paleoproterozoic mafic dyke swarms for the origin of 2.2 Ga enriched lithosphere beneath the Ungava Peninsula, Canada. Precambrian Research 174, 163–180.

McLelland, J.M., Chiarenzelli, J., 1990. Isotopic constraints on emplacement age of anorthosititc rocks of the Marcy massif, Adriondack Mts, New York. Journal of Geology 98, 19–41.

Möller, A., O'Brien, P.J., Kennedy, A., Kröner, A., 2003. Linking growth episodes of zircon and metamorphic textures to zircon chemistry: an example from the ultrahigh-temperature granulites of Rogaland (SW Norway). In: Vance D., Müller W., Villa I.M. (Eds.), Geochronology: Linking the Isotopic Record with Petrology and Textures. Geological Society of London Special Publication 220, pp. 65–81.

Newton, R.C., Smith, J.V., Windley, B.F., 1980. Carbonic metamorphism, granulites and crustal growth. Nature 288, 45–50.

Newton, R.C., 1990. Fluids and shear zones in the deep crust. Tectonophysics 182, 21–37.

Ontario Geological Survey, 1992. Tectonic assemblages of Ontario, northern sheet. Ontario Geological Survey, Map P. 2575, scale 1: 1 000 000.

Osmani, I.A., Stott, G.M., 1988. Regional scale shear zones in Sachigo Subprovince and their economic significance. In: Summary of Field Work and Other Activities 1988. Ontario Geological Survey Miscellaneous Paper 141, pp. 53–67.

Otto, A., 2002. Ore forming processes in the BIF-hosted gold deposit Musselwhite Mine, Ontario, Canada. Unpublished M.Sc. thesis, Freiberg University of Mining and Technology, 160 p.

Overstreet, W.C., 1967. The geologic occurrence of monazite. U.S. Geological Survey Professional Paper 530, 1–327.

Pan, Y., Heaman, L.M., Breaks, F.W., 1999. Thermo-tectonic evolution of the Umfreville-Conifer Lake granulite zone and the English River-Winnipeg River boundary zone: preliminary U-Pb geochronological results. In: Harrap, R.M., Helmstaedt, H.H. (Eds.), Western Superior Transect 5th Annual Workshop. Lithoprobe Secretariat, The University of British Columbia, Vancouver, B.C., Lithoprobe Report 70, pp. 104–108.

Parks, J., Lin S., Davis, D.W., Corkery, M.T., 2006. New High precision U-Pb ages for the Island Lake greenstone belt, northwestern Superior Province: implications for regional stratigraphy and the extent of the North Caribou terrane. Canadian Journal of Earth Sciences 43, 789–803.

Parmenter, A.C., Lin, S., Corkery, M.T., 2006. Structural evolution of the Cross Lake greenstone belt in the northwestern Superior Province, Manitoba: implications for relationship between vertical and horizontal tectonism. Canadian Journal of Earth Siences 43, 767–787.

Parra, T., Vidal, O., Agard, P., 2002. A thermodynamic model for Fe-Mg dioctahedral K white micas using data from phase-equilbrium experiments and natural pelitic assemblages. Contributions to Minearlogy and Petrology 143, 706–732, doi: 10.1007/s00410-002-0373-6.

Parrish, R.R., 1990. U–Pb dating of monazite and its application to geological problems Canadian Journal of Earth Sciences 27, 1435–1450.

Pervical, J.A., Mortensen, J.K., Stern, R.A., Card, K.D., Bégin, N.J., 1992. Giant granulite terranes of northeastern Superior Province: the Ashunipi complex and Minto block. Canadian Jouirnal of Earth Sciences 29, 2287–2308.

Percival, J.A., Stern, R.A., Mortensen, J.K., Card, K.D., Bégin, N.J., 1994. Minto block Superior Province: missing link in deciphering tectonic assembly of the craton at 2.7 Ga. Geology 22, 839–842.

Percival, J.A., Sandborn-Barrie, M., Skulski, T. Stott, G.M., Helmstaedt, H., White, D.J., 2006. Tectonic evolution of the western Superior Province from NATMAP and Lithoprobe studies. Canadian Journal of Earth Sciences 43, 1085–1117.

Piroshco, D.W., 1986. Structural geology and gold mineralization of the Eyapamikama Lake area of the North Caribou Lake greenstone belt, District of Kenora (Patricia Portion). Ontario Geological Survey, Miscellaneous Paper 132, 379–385.

Poitrasson, F., Chenery, S., Bland, D.J., 1996. Contrasted monazite hydrothermal alteration mechanisms and their geochemical implications. Earth and Planetary Science Letters 145, 79–96.

Pyle, J.M., Spear, F.S., 2003. Four generations of accessory-phase growth in low-pressure migmatites from SW New Hampshire. American Mineralogist 88, 338–351.

Rubatto, D., Williams, I.S., Buick, I.S., 2001. Zircon and monazite response to prograde metamorphism in the Reynolds Range, central Australia. Contributions to Mineralogy and Petrology 140, 458–468.

Sage, R.P., Breaks, F.W., 1982. Geology of the Cat Lake-Pickle Lake area, districts of Kenora and thunder Bay. Ontario Geological Survey, Geological Report 207, 238 p.

Sanborn-Barrie, M., Skulski, T., Parker, J.R., 2001. Three hundred million years of tectonic history recorded by the Red Lake greenstone belt, Ontario. In: Geological Survey of Canada, Current Research 2001–C19.

Sanborn-Barrie, M., Rogers, N., Skulski, T., Parker, J.R., McNicoll, V., Devaney, J., 2004. Geology and tectonostratigraphic assemblages, east Uchi, Red Lake and Birch-Uchi belts, Ontario. Geological Survey of Canada, Open File 4255; Ontario Geological Survey, Map P.3446, scale 1:250 000.

Schaltegger, U., 2007. Hydrothermal zircon. Elements 3, 51–79, doi:10.2113/gselements.3.1.51.

Scharer, U., Corfu, F., Demaiffe, D., 1997. U-Pb and Lu-Hf isotopes in baddeleyite and zircon megacrysts from the Mbuji-Mayi kimberlite: constraints on the subcontinental mantle. Chemical Geology 143, 1–16.

Schmitz, M.D., Bowring, S.A., 2000. The significance of U-Pb dates in lower crustal xenoliths from the southwestern margin of the Kaapvaal craton, southern Africa. Chemical Geology 172, 59–76.

Scoates, J.S., Chaimberlain, K.R., 1997. Orogenic to post-orogenic origin for the 1.76 Ga Horse Creek anorthosite complex, Woming, USA. Journal of Geology 105, 331–343.

Selverstone, J., Morteani, G., Staude, J.-M., 1991. Fluid channelling during ductile shearing: transformation of granodiorite into aluminous schist in the Tauern Window, Eastern Alps. Journal of Metamorphic Geology 9, 419–431.

Seydoux-Guillaume, A.M., Paquette, J.L., Wiedenbeck, M., 2002. Experimental resetting of the U-Th-Pb system in monazite. Chemical Geology 191, 165–181.

Skulski, T., Corkery, M.T., Stone, D., Whalen, J.B., Stern, R.A., 2000. Geological and geochronological investigations in the Stull Lake - Edmund Lake greenstone belt and granitoid rocks of the northwestern Superior Province. In: Report of Activities 2000. Manitoba Industry, Trade and Mines, Manitoba Geological Survey, pp. 117–128.

Smith, H.A., Barreiro, B., 1990. Monazite U-Pb dating of staurolite grade metamorphism in pelitic schists. Contributions to Mineralogy and Petrology 105, 602–615.

Spry, P.G., Heimann, A., Messerly, J.D., Houk, R.S., 2007. Discrimination of metamorphic and metasomatic processes at the Broken Hill Pb-Zn-Ag deposit, Australia: rare earth element signatures of garnet-rich rocks. Economic Geology 102, 471–494.

Storey, C.D., Prior, D.J., 2005. Plastic Deformation and Recrystallization of Garnet: A Mechanism to Facilitate Diffusion Creep. Journal of Petrology 46, 2593–2613, doi:10.1093/petrology/egi067.

Stott, G.M., 1997. The Superior Province, Canada. In: deWit, M.J., Ashwal, L.D. (Eds.), The tectonic evolution of greenstone belts. Oxford University Press, pp. 480–507.

Stott, G.M., Corkery, T., Leclair, A., Boily, M., Percival, J., 2007. A revised terrane map for the Superior Province as interpreted from aeromagnetic data. Institute on Lake Superior Geology Proceedings, 53rd Annual Meeting, Lusten, MN, v. 53, part 1, pp. 74–75.

Stott, G.M., Josey, S.D., 2009. Proterozoic mafic (diabase) dikes and other post-Archean intrusions of northwestern Ontario, north of latitude 49°30'. Ontario Geological Survey. Preliminary Map P. 3606, scale 1:1 000 000.

Stott, G.M., Biczok, J., 2010. North Caribou greenstone belt: gold and its possible relation to the North Caribou pluton emplacement - a belt wide contact strain aureole? In: Ayer, J.A., Easton, R.M., Beakhouse, G.P., Stott, G.M., Kelly, R.I., Debicki, E.J., Parker, J.R., Brown, T. (Eds.), Summary of Field Work and Other Activities 2010. Ontario Geological Survey, Open File Report 6260, pp. 22-1 to 22-12.

Stott, G.M., Corkerty, M.T., Percival, J.A., Simard, M., Goutier, J., 2010. A revised terrane subdivision of the Superior Province. In: Ayer, J.A., Easton, R.M., Beakhouse, G.P., Stott, G.M., Kelly, R.I., Debicki, E.J., Parker, J.R., Brown, T. (Eds.), Summary of Field Work and Other Activities 2010. Ontario Geological Survey, Open File Report 6260, pp. 20-1 to 20-10.

Syme, E.C., Corkery, M.T., Bailes, A.H., Lin, S., Skulski, T., Stern, R.A., 1999. Towards a new tectonostratigraphy for the Knee Lake Greenstone Belt, Sachigo Subprovince, Manitoba. In: Harrap, R.M., Helmstaedt, H.H. (Eds.), Western Superior Transect 5th Annual workshop. Lithoprobe Secretariat, The University of British Columbia, Vancouver, B.C., Lithoprobe report 70, pp. 124–131.

Thurston, P.C., Chivers, K.M., 1990. Secular variation in greenstone sequence development emphasizing Superior Province, Canada. Precambrian Research 46, 21–58.

Thurston, P.C., Osmani, I.A., Stone, D., 1991. Northwestern Superior Province: review and terrane analysis. In: Thurston, P.C., Williams, H.R., Stucliffe, R.H., Stott, G.M. (Eds.), Geology of Ontario, Special Volume 4, Part 1. Ontario Geological Survey, pp. 80–142.

Tichomirowa, M., Whitehouse, M.J., Nasdala, L., 2005. Resorption, growth, solid state recrystallization, and annealing of granulite facies zircon - a case study from the Central Erzgebirge, Bohemian Massif. Lithos 82, 25–50.

Tomlinson, K.Y., Stevenson, R.K., Hughes, D.J., Hall, R., Thurston, P., Henry, P., 1998. The Red Lake greenstone belt, Superior Province: evidence of plume related magmatism at 3 Ga and evidence of an older enriched source. Precambrian Research 89, 59–76.

van Emden, B., Thornber, M.R., Graham, J., Lincoln, F.J., 1997. The incorporation of actinides in monazite and xenotime from placer deposits in western Australia. Canadian Mineralogist 35, 95–104.

Van Kranendonk, M.J., Collins, W.J., Hickman, A., Pawley, M.J., 2004. Critical tests of vertical versus horizontal tectonic models for the Archean East Pilbara Granite-Greenstone Terrane, Pilbara Craton, Western Australia. Precambrian Research 131, 173–211.

Van Lankvelt, A., Schneider, D.A., Hattori, K., Biczok, J., 2012. Anatomy of a Mesoarchean batholith, Institute on Lake Superior Geology Conference, Thunder Bay, Canada, pp. 91.

Vavra, G., Gebauer, D., Schmid, R., Compston, W., 1996. Multiple zircon growth and recrystallization during polyphase Late Carboniferous to Triassic metamorphism in granulites of the Ivrea Zone (Southern Alps): an ion microprobe (SHRIMP) study. Contributions to Mineralogy and Petrology 122, 337–358.

Vidal, O., Parra, T., Trotet, F., 2001. A thermodynamic model for Fe-Mg aluminous chlorite using data from phase equilibrium experiments and natural pelitic assemblages in the 100-600°C, 1-25 kbar range. American Journal of Science 6, 557–592.

Walshe, J.L., 1986. A six-component chlorite solid solution model and the conditions of chlorite formation in hydrothermal and geothermal systems. Economic Geology 81, 681–703.

Watson, E.B., Vicenzi, E.P., Rapp, R.P., 1989. Inclusion/host relations involving accessory minerals in high-grade metamorphic and anatectic rocks. Contributions to Mineralogy and Petrology 101, 220–231.

Watson, E.B., Cherniak, D.J., Hanchar, J.M., Harrison, T.M., Wark D.A., 1997. The incorporation of Pb into zircon. Chemical Geology 141, 19–31.

Watt, G.R., Harley, S.L., 1993. Accessory phase controls on the geochemistry of crustal melts and restites produced during water-undersaturated partial melting. Contributions to Mineralogy and Petrology 11, 550–566.

Wawrzenitz N., Krohe, A., Rhede, D., Romer, R.L., 2012. Dating rock deformation with monazite: the impact of dissolution precipitation creep. Lithos 134-135, 52–74.

Weinberg, R.F., Hodkiewicz, P., Groves, D.I., 2004. What controls gold distribution in the Archean? Geology 32, 545–548.

White, D.J., Musacchio, G., Helmstaedt, H., Harrap, R.M., Thurston, P.C., van der Velden, A., Hall, K., 2003. Images of a lower-crustal oceanic slab: direct evidence for tectonic accretion in the Archean western Superior province. Geology 31, 997–1000.

Williams, H.R., 1990. Subprovince accretion tectonics in the south-central Superior Province. Canadian Journal of Earth Sciences 27, 570–581.

Williams, I.S., Buick, I.S., Cartwright, I., 1996. An extended episode of early Mesoproterozoic fluid flow in the Reynolds Range, central Australia. Journal of Metamorphic Geology 14, 29–47.

Williams, M.L, Jercinovic, M.J., Terry, M.P., 1999. Age mapping and dating of monazite on the electron microprobe: Deconvoluting multistage tectonic histories. Geology 27, 1023–1026.

Williams, M.L., Jercinovic, M.J., Hetherington, C.J., 2007. Microprobe monazite geochronology: understanding geologic processes by integrating composition and chronology. Annual Review of Earth and Planetary Science 35, 137–175.

Williams, M.L., Jercinovic, M.J., Harlov, D.E., Budzyn, B., Hetherington, C.J., 2011. Resetting monazite ages during fluid-related alteration. Chemical Geology 283, 218–225.

Wing, B.A., Ferry, J.M., Harrison T.M., 2003. Prograde destruction and formation of monazite and allanite during contact and regional metamorphism of pelites: petrology and geochronology. Contributions to Mineralogy and Petrology 145, 228–50.

Wu, Y., Zheng, Y., 2004. Genesis of zircon and its constraints on interpretation of U-Pb age. Chinese Science Bulletin 49, 1554–1569.

Young, M.D., McNicoll, V., Helmstaedt, H., Skulski, T., Percival, J.A., 2006. Pickle Lake revisited: new structural, geochronological and geochemical constraints on greenstone belt assembly, western Superior Province, Canada. Canadian Journal of Earth Sciences 43, 821–847.

Zhu, X.K., O'Nions, R.K., Belshaw, N.S., Givv, A.J., 1997. Significance of *in-situ* SIMS chronometry of zoned monazite from the Lewisian granulites, northwest Scotland. Chemical Geology 135, 35–53.

Zhu, X.K., O'Nions, R.K., 1999a. Zonation of monazite in metamorphic rocks and its implications for high temperature thermochronology; a case study from the Lewisian terrain. Earth and Planetary Science Letters 171, 209–220.

Zhu, X.K., O'Nions, R.K., 1999b. Monazite chemical composition; some implications for monazite geochronology. Contributions to Mineralogy and Petrology 137, 351–363.

APPENDIX 1

Sample descriptions

SAMPLES

Throughout detailed petrography and microstructural analysis special attention was given to those bearing quartz affected by dynamic recrystallization or dissolution precipitation creep, an abundance of fabric-forming minerals and/or amphibolite facies index minerals, occurring within or in proximity to zones of high strain. Samples were carefully selected for *in situ* geochronological and geochemical analyses to investigate the relative timing of regional deformation events and any associated hydrothermal activity and fluid flux in the NCGB. **Table 1** provides a sample summary including type, location, minerals analyzed, apparent metamorphic grade and mineral assemblages, as well as degree of strain and habit of fabric.

NCTK10-8

A sample of biotite schist situated within the projected termination of the Markop Lake deformation zone near the contact with the granitoids to the southeast (**Fig. 1B**), thought to be of sedimentary origin, based on unpublished geochemistry of a similar sample <100 m away (pers. comm. A. Van Lankvelt, 2012). Foliated intensely through segregation of biotite from microlithons of quartz and feldspars (dominantly of the potassic variety), this sample is marked by a crenulation that dissipates in surrounding samples marked by increased levels of strain. Titanite, apatite, and zircon are accessories along with opaque minerals most likely to be ilmenite ± magnetite. Most of the zircons are euhedral prismatic, oscillatory zoning is common, and a small core is observed in certain grains (**Fig. 7B,E**). The c-axis of the zircons is often in the plane of the fabric and roughly perpendicular to a lineation defined by preferential orientation of the blocky biotite in this sample, chosen for U-Pb dating of zircon as representative of elevated strain in the Markop Lake deformation zone.

NCTK10-12 & NCTK10-15

These samples consist of highly deformed metasediments (two-mica schist and mica schist) from within the MLDZ (**Fig. 1B**) that contain both coarse-grained quartz in ribbons and dynamically recrystallized finer-grained quartz. Plagioclase is full of inclusions and likely porphyroblastic, white mica is aligned in the foliation and chlorite appears to have formed on the retrograde path replacing local biotite (very minimal in NCTK10-15). White mica is dominant in both of these samples and segregated by grain size as coarse- and fine-grained varieties grade into and out of one another throughout. Good kinematic indicators are present in the outcrop from which NCTK10-12 was collected (**Fig. 2B**). Sigmoidal quartz sweats ± deformed veinlets indicate dextral displacement and primary bedding features are evidently transposed. Sample NCTK10-15 bears calcite that I interpret to be remnant diagenetic calcite. These samples were chosen for geochemistry of abundant phyllosilicate minerals that form the fabric in this high strain region of the North Caribou greenstone belt.

NCTK10-16A&B

NCTK10-16A is a staurolite-chloritoid-chlorite schist situated within the MLDZ, not too far from the samples discussed previously, and marked by tight mesoscopic folds that plunge 35° to the ENE. The limbs and hinge zones of the folds are host to quartz sweats associated with poikiolitic garnet that I collected for geochemical anlaysis (NCTK10-16B, **Fig. 1B**, **15B**). One garnet in the thin section is at least 5 mm in diameter and full of inclusions of mostly quartz. This sample is peppered with fine-grained chlorite that defines a fairly heterogeneous foliation through a matrix of mostly fine-grained quartz, and chloritoid and staurolite prophyroblasts occur locally (**Fig. 3B**). Cumulates of randomly oriented coarse-grained white mica are potential pseudomorphs after staurolite. Opaque minerals are accessory phases in

this sample, selected for geochemistry of garnet associated with deformation events in the Markop Lake deformation zone.

NCTK10-19

This sample is an albite schist situated within the MLDZ (**Fig. 1B**), characterized by a weak SC-fabric, and sigmoidal strain shadows cast by albite porphyroblasts indicate dextral kinematics. Quartz is abundant and dynamically recrystallized through grain bulging migration and subgrain rotation. Apatite, rutile, monazite, and opaque minerals (ilmenite ± ilmenite) are present as accessories alongside altered plagioclase feldspar, potassium feldspar, local coarse-grained white mica, and fine-grained pervasive biotite. A bearer of monazite, this sample presents potential for dating deformation in the Markop Lake deformation zone and was chosen for U-Th-total Pb age determination. Monazites are 40-70 μm-long, have diffuse boundaries, and are surrounded by a combination of allanite and clay minerals. The thin section contains a group of three that align together parallel to the foliation bundles of biotite and white mica and sparsely peppered blocky biotite throughout the matrix and is found at the boundary between a plagioclase matrix and a foliation sub-parallel quartz ribbon.

NCTK10-20A

This sample is a highly strained schist situated within the MLDZ at the contact with amphibolite (**Fig 1B**). Intensely foliatied through the alignment of white mica and chlorite segregating quartz and plagioclase feldspar into microlithons, this sample was chosen to investigate the phyllosilicates defining the deformation-induced fabric in this high-strain zone.

NCTK10-24

This sample is a biotite-tonalite gneiss from just north of the MLDZ in the Schade Lake gneiss complex (**Fig. 1B**). Gneissic banding is observed from the thin-section scale to the

outcrop-scale through segregation of biotite-rich from biotite-poor fabrics. Where biotite is abundant, microlithons of quartz and sericite-altered plagioclase are finer-grained and segregated by discontinuous foliation planes. Pyroxene is present as well as titanite and zircon is available for U-Pb dating of this granitoid sample at the northern margin of the southeastern arm of the North Caribou greenstone belt. The zircons are mostly subhedral (e.g. **Fig. 7I**), often display weak oscillatory zoning, and though commonly in contact with biotite, a preferred orientation is less evident in this least deformed of all samples analyzed for U-Pb geochronology.

NCTK10-26A&B

NCTK10-26A is situated just north of the main strand of the MLDZ (**Fig. 1B**) and constitutes a garnet-biotite schistose granule to cobble conglomerate that has experienced increased levels of strain, evidenced in 3:1 length to width flattening of cobbles (**Fig. 3C**), and garnet zone metamorphism. Coarse-grained biotite is aligned in continuous foliation planes and there is a distinct compositional segregation between more Si-rich minerals and phyllosilicates. The matrix is dominantly plagioclase feldspar and accessory phases consist of monazite, ilmenite, ± magnetite. Monazite grains are abundant, most of which are fabric-elongate, range in size from 25 x 20 μm to 80 x 50 μm, and found either at the boundary between albite grains in the matrix or surrounded by clay minerals, and sometimes in contact with or proximity to fabric-forming biotite ± chlorite. Grains in the matrix are fairly euhedral and free of inclusions. Sample NCTK10-26B is from a pods filled with coarse-grained minerals that appear to have crystallized from a hydrothermal fluid, broadly undeformed and somewhat controlled by the more porous matrix surrounding abundant flattened cobbles. Euhedral garnet grains range in size from 500 μm to >5 mm and are contained mostly within nests of randomly oriented

coarse-grained biotite (**Fig. 15C,D**).This sample was chosen for U-Th-total Pb dating of monazite as well as geochemistry of garnet.

NCTK10-38

A sample of biotite schist is highly deformed and situated in the region of the ALFZ that parallels the eastern contact of the ELS with the NRV north of Opapimiskan Lake (**Fig. 1B**). The level of strain is indicated by dynamically recrystallized quartz isolated with albite in microlithons through segregation by penetrative SC-fabric defined by biotite and chlorite. The thin section contains three small foliation-elongate monazite grains that reside either at the boundary between quartz and albite or in contact with biotite ± ilmenite and was chosen for geochronological investigation of the Akow Lake fault zone.

NCTK10-44A

This sample is an andalusite-staurolite schist situated 4 km to the north of NCTK10-38 in the ALFZ (**Fig. 1B**). On the outcrop scale, porphyroblastic staurolite and andalusite are localized in tightly folded bands that crosscut bedding and/or axial-planar foliation. Andalusite is poikiloblastic, containing many small inclusions of quartz, and locally books of biotite and euhedral staurolite as well. Biotite is the dominant phyllosilicate mineral in this sample, followed by white mica and both define the foliation that for the most part wraps around poikiloblasts (**Fig. 3A**). Chlorite is very minor and slightly replacing biotite in the foliation, and rare fibrolite wraps around euhedral matrix-bound staurolite poikiloblasts. Coarser-grained quartz is strained has sutured grain boundaries, and isolated amongst finer-grained quartz and plagioclase feldspars in the matrix. Accessory minerals in this sample include zircon, monazite, tourmaline, and opaque minerals such as ilmenite ± magnetite. Zircons are dominantly euhedral and oscillatory-zoned zircon and where the c-axis is not perpendicular to

the direction of principal strain, it is often fractured and slightly displaced in the plane of foliation (**Fig. 7A,D**). Monazites are 30-40 μm in size, most are found in the matrix of plagioclase ± quartz, often in contact with (and more rarely embedded in) fabric forming micas (biotite ± muscovite or chlorite; e.g. **Fig. 10C,D**), and one is an inclusion in poikiloblastic andalusite (**Fig. 10A,B**). This sample was selected for geochronology of zircon and monazite and is representative of amphibolite facies metamorphism within a crustal-scale deformation zone.

NCTK10-51A

This sample consists of a high-strain biotite schist from the ELS at the eastern extremity of the belt in the NCTSZ (**Fig. 1B**). Alignment of blocky biotite is a pervasive feature and long sinuous dextral bundles of biotite, chlorite, and muscovite weave between dynamically recrystallized microlithons of quartz and plagioclase feldspar among sweats of recovered quartz. Magnetite and ilmenite and monazite are accessory phases in this sample. Small (~20 μm) monazite grains are situated at the junction between plagioclase grains and somewhat elongate in the direction of foliation and in contact with biotite. This sample was selected for monazite dating and geochemistry of chlorite and fabric forming micas because it represents deformation in the North Caribou-Totogan shear zone at the most eastern extremity of the NCGB.

NCTK10-63

This sample of proto-mylonitic trondhjemite is banded through strain-induced segregation of mm-scale layers of biotite and mafic minerals from plagioclase-rich microlithons and situated in the Neawagank Lake fault (**Fig. 1B**). Biotite is locally replaced by chlorite and aligned with hornblende and orthopyroxene in an anastomosing foliation that locally wraps around heavily

altered poikiloblastic potassium feldspar and forms augen-shaped pods of alteration. This sample was chosen for zircon dating of a highly deformed granitoid sample from the eastern termination of the North Caribou greenstone belt. Zircons are found in the matrix with a locally observed fabric-parallel orientation and where a few are euhedral prismatic, most are subhedral with slightly rounded edges. A common feature of these zircons is a weakly zoned core with a distinctly more strongly zoned and complex rim (**Fig. 7H**).

NCTK10-74

This sample is a biotite schist situated northwest of the Markop Lake deformation zone, closer to Opapimiskan Lake (**Fig. 1B**), is fine-grained, foliated, and bears dynamically recrystallized quartz. Some plagioclase is partially altered by sericite and white mica is dominant in foliation planes although sometimes found at angles oblique to the foliation. Biotite is also present in the foliation but is finer-grained and undergone some retrograde alteration by chlorite. This sample is situated close to the contact with metavolcanics and as such is of interest in terms of the geochemistry of fabric forming micas and chlorites.

NCTK10-75 & NCTK10-76

These samples are two-mica schists from the North Caribou-Totogan shear zone (**Fig. 1B**) and similar in terms of mineralogy and fabric, however NCTK10-76 bears monazite and NCTK10-75 does not. Both samples are marked by anastomosing foliation planes defined by sinuous bundles of white mica, biotite, and chlorite and also have more blocky micas segregating quartz and sericite-altered plagioclase into fairly evenly spaced finer-grained microlithons and less commonly coarser-grained quartz ribbons. Zircon, and opaque minerals are accessory phases in both samples. The subhedral to slightly rounded prismatic zircons in NCTK10-76 are mostly found in association with fabric forming minerals, often with their c-

axis in the plane of foliation. While the zircons are most commonly oscillatory zoned, some also display a patchy sector zoning (**Fig. 7G**) and others a small distinct core. Certain monazite grains in this same two-mica schist are small (~20 μm) with fairly smooth grain boundaries, and some are bigger (~40 x 30 μm to >100 μm) with resorbed boundaries. One large monazite grain is oriented perpendicular to the fabric and completely immersed in a bundle of biotite and muscovite. Representative of deformation style in the NCTSZ, these samples were both chosen for geochemistry of fabric forming phyllosilicates, and sample NCTSZ-76 is ideal to compare the age of zircon with the age of monazite in such a high-strain region as it is also situated proximal to the Markop Lake deformation zone.

NCB11-24 & NCB11-28

These two garnet-bearing samples, biotite schist and hornblende schist, are part of the ELS and situated near North Rim fault zone at the regional contact with the NRV in the northwestern arm of the NCGB (**Fig. 1B**). The rocks are highly deformed and lithological contrasts and bedding planes are an obvious focal point for strain localization. In the biotite-schist (NCB11-24) the fabric-elongate subhedral garnet grains are fractured and have been displaced along slip planes. Commonly accompanied by aggregates of smaller euhedral crystals and locally bearing some inclusion trails, the garnets appear to have grown preferentially and been brittly deformed and boudinaged in response to the same stresses that formed the penetrative foliaiton (**Fig. 15E**). The grains and/or fragments range in size from 1 to 3 mm. Very fine-grained biotite aligns in the matrix of equally fine-grained quartz but is a bit coarser-grained and occurrs at random orientations, sometimes with needle-like blue-green amphibole, in regions surrounding garnet blasts. The same amphibole, similar to the coarser-grained biotite, occurs with no preferred orientation surrounding, and between some,

fragmented garnet blasts. Bundles of sericite locally radiate from the fragments of garnet, commonly in proximity to carbonate-altered domains within the shear band. In the hornblende schist (NCB11-28), the garnet is euhedral, relatively inclusion-free, and shows no preferential alignment. It is situated among abundant, potentially hydrothermal, coarse-grained biotite and dark green amphibole within a fabric-parallel dilation crack. These samples were chosen for geochemistry of garnet that has an affinity for deformation features in the host rock.

NCB11-33

This sample of cordierite schist of the ELS is situated in the contact metamorphic aureole at the southern border of the western arm with the North Caribou Lake batholith (**Fig. 1B**). Both granitic and aplitic mafic dikes cut through the metasedimentary rocks in the outcrop and mm- to cm-scale cordierite nodules resist weathering in proximal surfaces of the host rock. Retrograde chlorite alteration is concentrated in pseudomorphs of the fabric-elongate (2-3 mm x 5 mm) cordierite poikiloblasts (**Fig. 3C**). The matrix is fine-grained and foliated through weak alignment of fibrous chlorite and blocky biotite in planes that anastomose through variably recrystallized quartz grains and ribbons, as well as around the occasional albite poikiloblast. This sample was chosen for U-Pb geochronology of zircon because of its evident cordierite-grade contact metamorphism that appears to be somewhat syn-tectonic. Zircons in this sample are mostly asymmetrical and subhedral, although a euhedral prismatic variety is present dominantly in the coarser-size fraction ~45-80 μm. Oscillatory zoning is prevalent (e.g. **Fig. 7C**), but sometimes patchy or faint, and sector zoning is also present, but to a much lesser extent (e.g. **Fig. 7F**).

NCB11-34

This sample is a meta-granule conglomerate near the contact of the ELS with the SRV on the southern shore of Eyapamikama Lake (**Fig. 1B**). The strain is localized along bedding planes and zones of lithological contrast in very coarse-grained and thick-bedded metasediments. Much finer grains in the matrix are found in tightly spaced microlithons segregated by pervasive foliation planes dominated by fine-grained micas that wrap around granules of albite ± quartz to form a heterogeneous fabric. Ribbon quartz is highly strained and partially dynamically recrystallized. This sample bears abundant zircon and lesser monazite as well as allanite and a non-monazite phase that is rich in Ce. This sample was chosen as it is the only sample from the northwestern arm that contained any trace of monazite and I wanted to obtain a monazite age in this region. The monazite grains are 50-60 μm long and only 10 μm wide, often kinked but roughly parallel to the very fine-grained foliation, and they have convoluted edges and sieve textures.

E591 479

This sample comprises schist peppered with round to ellipsoid euhedral garnet porphyroblasts within an ultra-fine-grained siliceous matrix bearing abundant phyllosilicate minerals. The long axes of garnets roughly parallel foliation and garnets present in strain shadows are oriented more randomly with respect to principal strain. The foliation wraps around some garnet grains, on occasion with a sigmoidal shape as shown in **Fig. 15A**. Situated in the NRV at the northern bend of the NCGB (**Fig. 1B**), this high-strain sample contains local ribbons or sweats of coarser-grained quartz that has partially recrystallized through grain-boundary migration and formation of small subgrains, abundant fine-grained chlorite, and minor

amounts of biotite. This sample was chosen for geochemical analysis of garnet to represent a potentially syn-tectonic porphyroblastic garnet growth.

APPENDIX 2

U-Pb methodology

METHODS

In situ LA-ICP-MS U-Pb geochronology was undertaken for investigation of zircon grains ranging in size from 25 to 100 μm in highly strained rocks to constrain the tectonic evolution of the NCGB. Since the abundance of zircon in any rock thin section was inadequate to achieve statistically reliable U-Pb ages, five to six thick sections of each sample containing zircon were cut at spaced intervals through the rock to improve the number of targets for geochronology. The sections were mounted onto glass using Canadian Balsam and polished to ~100 μm in the facilities at the University of Ottawa (Ottawa, Canada). The JEOL 6610LV Scanning Electron Microscope (SEM) at the University of Ottawa was used to map the locations of the zircon in the sections and to identify any zonation patterns in or rim overgrowths on the zircon grains. I used the Resonetics M-50-LR 193 nm ArF Excimer laser ablation system coupled to an Agilent 7700x quadrupole inductively coupled mass spectrometer (ICP-MS) at the University of New Brunswick (UNB, Fredericton, Canada). The Zeiss AxioImager and AxioVision software available at UNB enabled programming of spot locations on zircon grains and thin section mapping prior to laser ablation. For all samples except one, the laser was operated at a repetition rate of 4.5 Hz, with a lateral spot size of 24 μm, and pulse energy of 120 mJ. The spot size was reduced to the minimum, 17 μm, and the repetition rate increased to 5 Hz for a sample of protomylonitic trondhjemite from the Neawagank Lake fault in order to better target potential cores and rims. Elemental fractionation and mass bias effects were corrected simultaneously by bracketing sample analyses with analyses of standards of known composition and maintaining constant analytical conditions throughout. Two reference materials were analyzed: 91500 zircon (1065 Ma, Wiedenbeck et al., 1995) and NIST 610 glass (Pearce et al., 1997) under the same

conditions as the unknowns. The time-resolved signal was carefully inspected to detect U-Pb isotope heterogeneities within the ablated volume and only homogeneous intervals of at least 5 s were considered. Data reduction was carried out using the Iolite software package (Paton et al., 2011) in which the baseline is subtracted from the input channels and the resulting intensities are used to calculate raw isotope ratios and ages. Iolite's U-Pb geochronology data reduction scheme (DRS, Paton et al., 2010) then performs a down-hole fractionation correction, followed by a drift correction, reference material normalization, and uncertainty propagation. VizualAge (Petrus and Kamber, 2012) DRS applies a $^{207}Pb/^{206}Pb$ age calculation, discordance calculation, a common lead correction (using Andersen's routine and the conventional ^{204}Pb correction) to the data. VizualAge has the ability to display an active Concordia diagram, which makes it possible to visualize the average and uncertainty of an Iolite integration in real time as it is being adjusted. For each analytical run the error associated with the reproducibility of the external reference standard 91500 zircon (calculated on the basis of 12 to 15 determinations and reduced with VizualAge to an MSWD between 0.9 and 2.0 for the concordant age of all standard analyses) was propagated to the error associated with the single analyses using the equation reported in Paton et al. (2010). A secondary zircon standard, TEMORA zircon (416 Ma, Black et al., 2003), is routinely analyzed to test the internal accuracy of the method.

REFERENCES

Black, L.P., Kamo, S.L., Allen, C.M., Aleinikoff, J.N., Davis, D.W., Korsch, R.J., and Foudoulis, C. 2003. TEMORA 1: a new zircon standard for Phanerozoic U-Pb geochronology. Chemical Geology 200, 155–170.

Paton, C., Woodhead, J.D., Hellstrom, J.C., Hergt, J.M., Greig, A., Maas R., 2010. Improved laser ablation U-Pb zircon geochronology through robust downhole fractionation correction, Geochemistry Geophysics Geosystems 11, Q0AA06, doi: 10.1029/1009GC002618.

Paton, C., Hellstrom, J., Bence, P., Woodhead, J., Hergt, J., 2011. Iolite: Freeware for the visualisation and processing of mass spectrometric data. Journal of Analytical Atomic Spectrometry 26, 2508–2518, doi: 10.1039/c1ja10172b.

Petrus, J.A., Kamber, B.S., 2012. VizualAge: A novel approach to laser ablation ICP-MS U-Pb geochronology data reduction. Geostandards and Geoanalytical Research, doi: 10.1111/j.1751-908X.2012.00158.x.

Pearce, N.J.G., Perkins, W.T., Westgate, J.A., Gorton, M.P., Jackson, S.E., Neal, C.R., Cheney, S.P., 1997. New data for National Institute of Standards and Technology 610 and 612 glass reference materials: Geostandards Newsletter 21, 115–144.

Wiedenbeck, M., Alle, P., Corfu, F., Griffin, W.L., Meier, M., Oberli, F., Von Quadt, A., Roddick, J.C., Spiegel, W., 1995. Three natural zircon standards for U-Th-Pb, Lu-Hf, trace elements and REE analyses. Geostandardard Newsletter 19, 1–23.

Table A2 LA-ICP-MS U-Pb data for zircon in metasedimentary and metagranitoid rocks of the NCGB, NW Ontario

			Isotopic ratios							Ages (Ma)					
	Th/U	$^{206*}Pb/^{204*}Pb$	$^{207*}Pb/^{206*}Pb$	2 σ	$^{207*}Pb/^{235}U$	2 σ	$^{206*}Pb/^{238}U$	2 σ	Err. Corr.	$^{207*}Pb/^{206*}Pb$	1 σ	$^{207*}Pb/^{235}U$	1 σ	$^{206*}Pb/^{238}U$	1 σ
NCTK10-8 ***Bt schist*** *NAD27, zone 15: 689866E, 5820991N*															
8-1-z21	*0.53*	*3840*	*0.2040*	*0.0018*	*15.7300*	*0.2600*	*0.5573*	*0.0095*	*0.4903*	*2861*	*18*	*2859*	*16*	*2663*	*100*
8-1-z28	*0.46*	*4300*	*0.2051*	*0.0013*	*15.8300*	*0.2700*	*0.5586*	*0.0096*	*0.7845*	*2867*	*13*	*2866*	*17*	*3072*	*110*
8-1-z11	*0.59*	*2520*	*0.2056*	*0.0017*	*15.8200*	*0.2900*	*0.5582*	*0.0100*	*0.5739*	*2870*	*15*	*2865*	*18*	*2239*	*100*
8-1-z4b	*0.97*	*9400*	*0.2064*	*0.0009*	*15.8700*	*0.2700*	*0.5609*	*0.0097*	*0.9136*	*2877*	*8*	*2868*	*16*	*2882*	*100*
8-1-z8	*0.64*	*3110*	*0.2068*	*0.0029*	*15.7800*	*0.3000*	*0.5563*	*0.0077*	*0.7906*	*2879*	*19*	*2865*	*19*	*2695*	*96*
8-1-z22	*0.51*	*2800*	*0.2074*	*0.0019*	*15.8600*	*0.2200*	*0.5583*	*0.0080*	*0.5238*	*2884*	*17*	*2870*	*13*	*2635*	*110*
8-1-z26<	*0.76*	*4040*	*0.2006*	*0.0021*	*14.4400*	*0.6000*	*0.5187*	*0.0190*	*0.8620*	*2831*	*19*	*2778*	*49*	*2460*	*150*
8-1-z7a<	*0.39*	*3150*	*0.2023*	*0.0029*	*15.6100*	*0.3400*	*0.5560*	*0.0099*	*0.6790*	*2846*	*26*	*2853*	*21*	*3095*	*120*
8-1-z23a<	*0.53*	*3810*	*0.2025*	*0.0013*	*15.6100*	*0.3800*	*0.5570*	*0.0140*	*0.9259*	*2846*	*13*	*2851*	*25*	*2910*	*120*
8-1-z13c<	*0.48*	*4290*	*0.2032*	*0.0013*	*13.4100*	*0.3400*	*0.4790*	*0.0110*	*0.9205*	*2851*	*18*	*2707*	*23*	*2389*	*140*
8-1-z7b<	*0.48*	*5260*	*0.2034*	*0.0021*	*15.7700*	*0.3500*	*0.5571*	*0.0110*	*0.7591*	*2855*	*15*	*2860*	*21*	*2929*	*120*
8-1-z17<	*0.42*	*2760*	*0.2036*	*0.0029*	*15.6900*	*0.4500*	*0.5580*	*0.0130*	*0.8507*	*2856*	*25*	*2852*	*27*	*2999*	*120*
8-1-z4a<	*0.48*	*2900*	*0.2042*	*0.0019*	*15.6800*	*0.4300*	*0.5535*	*0.0150*	*0.3234*	*2859*	*17*	*2857*	*29*	*3102*	*150*
8-1-z1c<	*0.75*	*2520*	*0.2046*	*0.0018*	*13.3100*	*0.3400*	*0.4719*	*0.0110*	*0.9275*	*2862*	*14*	*2704*	*23*	*1978*	*87*
8-1-z15<	*0.42*	*3530*	*0.2046*	*0.0021*	*15.6000*	*0.3300*	*0.5560*	*0.0110*	*0.7993*	*2865*	*21*	*2853*	*21*	*3419*	*130*
8-1-z5b<	*0.33*	*2690*	*0.2051*	*0.0028*	*14.5700*	*0.3700*	*0.5100*	*0.0130*	*0.8564*	*2868*	*23*	*2791*	*24*	*2522*	*110*
8-1-z14<	*0.60*	*3420*	*0.2048*	*0.0016*	*14.9900*	*0.2400*	*0.5316*	*0.0079*	*0.8080*	*2868*	*13*	*2814*	*15*	*2615*	*98*
8-1-z9<	*0.41*	*3770*	*0.2050*	*0.0025*	*16.6100*	*0.3000*	*0.5910*	*0.0093*	*0.8450*	*2868*	*22*	*2911*	*18*	*3233*	*120*
8-1-z1b<	*0.42*	*2160*	*0.2060*	*0.0019*	*15.7100*	*0.5000*	*0.5570*	*0.0180*	*0.8891*	*2873*	*18*	*2857*	*32*	*2330*	*170*
8-1-z5c<	*0.70*	*2680*	*0.2060*	*0.0024*	*13.6900*	*0.3000*	*0.4858*	*0.0100*	*0.7979*	*2873*	*18*	*2729*	*21*	*1917*	*80*
8-1-z13b<	*0.48*	*3720*	*0.2061*	*0.0011*	*15.7200*	*0.3600*	*0.5560*	*0.0130*	*0.9651*	*2875*	*8*	*2858*	*21*	*2932*	*120*
8-1-z5a<	*0.49*	*3270*	*0.2057*	*0.0021*	*15.4600*	*0.2800*	*0.5487*	*0.0084*	*0.5675*	*2877*	*19*	*2845*	*17*	*2851*	*110*
8-1-z10<	*0.54*	*2640*	*0.2070*	*0.0017*	*16.0300*	*0.3100*	*0.5624*	*0.0110*	*0.5678*	*2881*	*17*	*2878*	*18*	*2866*	*110*
8-1-z1a<	*0.54*	*2040*	*0.2087*	*0.0019*	*14.8300*	*0.2200*	*0.5153*	*0.0071*	*0.6171*	*2895*	*15*	*2804*	*15*	*2709*	*100*
8-1-z12>	0.54	3020	0.1761	0.0030	7.2800	0.2800	0.3012	0.0089	0.8933	2614	33	2152	43	1674	72
8-1-z2>	0.56	4470	0.1793	0.0023	7.8900	0.3800	0.3169	0.0110	0.9215	2646	15	2217	37	1426	97
8-1-z16>	1.01	6240	0.1824	0.0028	7.5500	0.3700	0.3015	0.0120	0.8565	2672	30	2175	39	1466	79
8-1-z1d>	0.42	4300	0.1871	0.0025	9.8500	0.3800	0.3797	0.0120	0.7698	2715	26	2419	31	2231	100
8-1-z20>	0.89	4750	0.1882	0.0018	9.0500	0.2400	0.3514	0.0075	0.8449	2731	15	2342	23	1526	64
8-1-z23b>	0.65	5060	0.1932	0.0011	9.6300	0.2900	0.3622	0.0110	0.9522	2770	9	2399	25	1804	110
8-1-z24b>	0.71	6130	0.1978	0.0026	11.5300	0.5100	0.4210	0.0160	0.9515	2806	23	2565	44	2076	97
8-1-z18>	0.91	7400	0.1977	0.0027	12.4800	0.5700	0.4550	0.0160	0.9181	2808	25	2632	41	2291	160
8-1-z6>	0.62	4480	0.2015	0.0023	12.6000	0.4400	0.4560	0.0140	0.9238	2836	23	2648	33	2171	91
8-1-z13a>	0.60	2580	0.2023	0.0016	10.8800	0.3000	0.3890	0.0110	0.9571	2844	13	2516	27	1662	89

Table A2 LA-ICP-MS U-Pb data for zircon in metasedimentary and metagranitoid rocks of the NCGB, NW Ontario

			Isotopic ratios							Ages (Ma)					
	Th/U	$^{206*}Pb/^{204*}Pb$	$^{207*}Pb/^{206*}Pb$	2 σ	$^{207*}Pb/^{235}U$	2 σ	$^{206*}Pb/^{238}U$	2 σ	Err. Corr.	$^{207*}Pb/^{206*}Pb$	1 σ	$^{207*}Pb/^{235}U$	1 σ	$^{206*}Pb/^{238}U$	1 σ
8-1-zfp3b*	0.04	177	0.1762	0.0038	11.0300	0.3000	0.4519	0.0099	0.4832	2616	37	2522	25	8810	880
8-1-zfp3a*	0.04	183	0.1794	0.0034	11.9100	0.2500	0.4806	0.0085	0.3796	2658	30	2598	21	6690	700
8-1-zfp1c*	0.03	192	0.1750	0.0026	11.0000	0.2300	0.4574	0.0080	0.4595	2603	26	2521	20	8480	780
8-1-zfp4b*	0.09	192	0.1770	0.0031	11.4400	0.3000	0.4715	0.0093	0.6220	2620	30	2562	23	4960	430
8-1-zfp3c*	0.03	192	0.1757	0.0034	11.4400	0.2700	0.4697	0.0088	0.3918	2612	32	2559	22	7890	790
8-1-zfp3d*	0.06	198	0.1798	0.0039	11.9700	0.3100	0.4788	0.0092	0.6029	2650	36	2604	24	9640	710
8-1-z3b*	0.09	196	0.1845	0.0065	12.5800	1.2000	0.4990	0.0300	0.5787	2697	62	2654	69	8110	510
8-1-zfp5b*	0.04	200	0.1759	0.0033	10.9800	0.3400	0.4560	0.0110	0.3896	2622	34	2519	28	6710	880
8-1-zfp4a*	0.16	208	0.1817	0.0039	12.0400	0.2800	0.4837	0.0087	0.2708	2663	35	2605	22	7230	890
8-1-zfp5a*	0.04	217	0.1798	0.0040	12.3900	0.9100	0.4950	0.0260	0.8282	2655	43	2628	58	8400	###
8-1-z27*	0.08	246	0.1778	0.0046	11.5700	0.4100	0.4723	0.0120	0.3453	2624	47	2567	30	5580	690
8-1-zfp7*	0.07	256	0.1761	0.0061	11.6000	0.5500	0.4784	0.0260	0.5072	2610	49	2569	49	6880	670
8-1-zfp6*	0.03	284	0.1745	0.0043	11.7400	0.3900	0.4800	0.0120	0.4668	2597	36	2581	29	13200	1100
8-1-zfp3e*	0.75	281	0.1963	0.0055	15.2400	0.8500	0.5580	0.0320	0.7781	2793	44	2833	53	6210	750
8-1-zfp1a*	0.26	309	0.1864	0.0027	15.5200	0.4500	0.6080	0.0160	0.8346	2708	25	2846	29	8640	830
8-1-zfp2*	0.20	358	0.1735	0.0029	11.0700	0.2400	0.4642	0.0071	0.4113	2588	28	2534	20	3590	320
8-1-zfp1b*	0.24	369	0.1878	0.0037	13.3100	1.9000	0.5190	0.0640	0.8928	2725	36	2696	95	7900	650
8-1-z24a*	0.61	1530	0.2120	0.0160	14.0300	1.5000	0.4960	0.0150	0.4661	2916	40	2755	75	2210	550
NCTK10-24A ***Bt-tonalite gneiss***† *NAD27, zone 15: 694245E, 5824386N*															
24-2-z19c	*0.16*	*4070*	*0.1974*	*0.0049*	*14.4700*	*0.4600*	*0.5250*	*0.0130*	*0.9063*	*2804*	*15*	*2780*	*33*	*2721*	*55*
24-2-z13	*0.40*	*3150*	*0.2049*	*0.0055*	*15.8000*	*0.6600*	*0.5610*	*0.0150*	*0.7483*	*2864*	*20*	*2863*	*36*	*2869*	*63*
24-2-z26	*0.41*	*2650*	*0.2059*	*0.0052*	*15.7900*	*0.4300*	*0.5604*	*0.0092*	*0.8579*	*2873*	*11*	*2864*	*26*	*2867*	*38*
24-2-z27	*0.29*	*1680*	*0.2062*	*0.0053*	*15.3000*	*0.3600*	*0.5382*	*0.0059*	*0.6201*	*2875*	*15*	*2833*	*23*	*2775*	*25*
24-2-z24c	*0.44*	*2610*	*0.2072*	*0.0052*	*16.2600*	*0.5000*	*0.5644*	*0.0130*	*0.6649*	*2882*	*27*	*2895*	*32*	*2884*	*53*
24-2-z17c	*0.29*	*1100*	*0.2069*	*0.0055*	*16.3800*	*0.6900*	*0.5660*	*0.0190*	*0.8565*	*2883*	*19*	*2890*	*41*	*2885*	*77*
24-2-z15c	*0.26*	*2310*	*0.2075*	*0.0058*	*14.7500*	*0.5700*	*0.5220*	*0.0170*	*0.8217*	*2885*	*24*	*2803*	*41*	*2708*	*78*
24-2-z17r	*0.40*	*1790*	*0.2077*	*0.0054*	*15.1800*	*0.3800*	*0.5265*	*0.0058*	*0.7487*	*2886*	*17*	*2825*	*24*	*2726*	*25*
24-2-z18	*0.21*	*3260*	*0.2082*	*0.0055*	*17.1000*	*0.4500*	*0.5889*	*0.0075*	*0.7735*	*2890*	*20*	*2939*	*25*	*2984*	*31*
24-2-z29c<	0.34	1140	0.1914	0.0051	10.0700	0.4000	0.3790	0.0120	0.8178	2750	42	2436	44	2072	60
24-2-z1<	0.38	1650	0.1988	0.0140	9.4800	0.5800	0.3480	0.0170	0.9853	2816	17	2377	55	1920	82
24-2-z7<	0.25	3540	0.2010	0.0049	13.6200	0.6400	0.4890	0.0170	0.9911	2835	8	2717	41	2558	73
24-2-z23<	0.23	1680	0.2059	0.0053	10.4600	0.3000	0.3740	0.0076	0.8098	2871	27	2479	26	2048	35
24-2-z15r<	0.50	3790	0.2062	0.0052	13.1300	0.4000	0.4561	0.0097	0.9455	2877	14	2686	28	2420	42
24-2-z12<	0.33	2280	0.2069	0.0051	13.9400	0.3400	0.4902	0.0045	0.8728	2884	21	2744	24	2571	20
24-2-z21c<	0.41	1790	0.2073	0.0055	11.3700	0.3900	0.3961	0.0090	0.8592	2885	19	2551	32	2154	41

Table A2 LA-ICP-MS U-Pb data for zircon in metasedimentary and metagranitoid rocks of the NCGB, NW Ontario

			Isotopic ratios							Ages (Ma)					
	Th/U	$^{206*}Pb/^{204*}Pb$	$^{207*}Pb/^{206*}Pb$	2 σ	$^{207*}Pb/^{235}U$	2 σ	$^{206*}Pb/^{238}U$	2 σ	Err. Corr.	$^{207*}Pb/^{206*}Pb$	1 σ	$^{207*}Pb/^{235}U$	1 σ	$^{206*}Pb/^{238}U$	1 σ
24-2-z6<	0.46	4240	0.2083	0.0051	14.2400	0.3700	0.4992	0.0067	0.9271	2892	11	2768	25	2609	29
24-1-z2<	0.24	1120	0.2124	0.0026	14.0000	0.3600	0.4746	0.0087	0.7768	2927	19	2752	23	2502	38
24-2-z8<	0.59	623	0.2165	0.0054	11.8200	0.3400	0.3955	0.0075	0.9242	2954	12	2588	27	2147	35
24-2-z16>	0.17	2090	0.1795	0.0045	7.5800	0.4700	0.3081	0.0160	0.9370	2647	20	2180	47	1730	73
24-2-z25c>	0.21	2880	0.1815	0.0048	7.3300	0.4600	0.2900	0.0140	0.9766	2665	18	2135	47	1637	66
24-2-z19r>	0.12	5290	0.1819	0.0047	11.5000	0.3500	0.4680	0.0095	0.8232	2669	24	2568	31	2473	43
24-2-z29r>	0.08	2580	0.1902	0.0052	11.6100	0.3600	0.4384	0.0072	0.8445	2742	22	2571	29	2342	32
24-2-z2>	0.23	956	0.1966	0.0049	7.3200	0.3600	0.2700	0.0130	0.9861	2798	12	2151	51	1537	68
24-2-z11>	0.41	1140	0.2077	0.0053	8.4900	0.2700	0.2944	0.0081	0.9034	2891	15	2285	29	1663	40
24-2-z4>	0.23	1020	0.2095	0.0064	3.6000	0.1800	0.1238	0.0076	0.9899	2902	12	1563	36	752	43
24-2-z24r>	0.22	1210	0.1815	0.0055	6.3100	0.6200	0.2470	0.0190	0.9611	2667	15	2013	60	1420	86
24-2-z25r>	0.12	3040	0.1839	0.0048	7.2400	0.4600	0.2850	0.0150	0.9695	2692	18	2140	56	1611	74
24-2-z3>	0.41	1077	0.1879	0.0047	5.6100	0.1700	0.2185	0.0047	0.9183	2723	18	1915	27	1273	25
24-2-z21r>	0.11	656	0.1878	0.0048	8.7800	0.3500	0.3350	0.0100	0.9562	2722	20	2308	41	1861	51
24-2-z20r^	0.06	2380	0.1857	0.0053	6.5000	0.9100	0.2553	0.0260	0.9019	2704	19	2045	79	1466	120
24-2-z20c^	0.04	2440	0.1971	0.0087	14.3500	2.5000	0.5250	0.0420	0.9249	2802	17	2772	95	2720	160
24-1-z19^	0.33	322	0.2178	0.0059	15.4700	0.8500	0.5120	0.0200	0.7325	2962	45	2841	52	2662	87
24-1-z22^	0.13	470	0.2244	0.0021	18.4300	1.0000	0.6020	0.0300	0.9314	3013	15	3010	54	3040	120
24-1-z6r*	0.21	5710	0.1372	0.0012	3.9680	0.1000	0.2099	0.0044	0.8622	2191	16	1627	21	1228	23
24-1-z1*	0.16	4530	0.1465	0.0018	4.4200	0.2300	0.2171	0.0088	0.9732	2304	21	1714	44	1266	47
24-1-z12*	0.09	1540	0.1486	0.0017	4.9100	0.1600	0.2401	0.0054	0.8561	2329	19	1806	26	1387	28
24-1-z14b*	0.16	1980	0.1576	0.0014	5.3200	0.2300	0.2472	0.0094	0.9632	2429	15	1870	37	1421	48
24-1-z6c*	0.22	5970	0.1618	0.0012	5.9500	0.1900	0.2661	0.0059	0.9372	2475	13	1967	27	1521	30
24-1-z24c*	0.50	4520	0.1618	0.0012	5.9700	0.1800	0.2700	0.0065	0.9478	2474	13	1973	27	1540	33
24-1-z6r*	0.15	10900	0.1667	0.0008	6.7340	0.1400	0.2920	0.0041	0.9101	2524	8	2077	19	1651	20
24-1-z23*	0.19	3370	0.1691	0.0018	6.6700	0.1900	0.2909	0.0071	0.9439	2551	19	2068	25	1645	35
24-1-z24r*	0.32	2370	0.1741	0.0027	6.2200	0.2300	0.2618	0.0059	0.9213	2593	27	2005	32	1498	30
24-1-z20*	0.08	707	0.1770	0.0015	4.7000	0.2100	0.1935	0.0066	0.9783	2625	14	1770	35	1140	36
24-1-z18*	0.15	664	0.1795	0.0023	8.1300	0.3700	0.3220	0.0120	0.9353	2647	21	2252	40	1798	56
24-1-z10*	0.08	1370	0.1802	0.0013	7.2800	0.2700	0.2945	0.0099	0.9816	2654	12	2146	33	1661	49
24-1-z16*	0.10	4910	0.1805	0.0014	9.1500	0.3100	0.3666	0.0092	0.9600	2657	13	2355	32	2011	43
24-1-z9*	0.08	922	0.1832	0.0011	7.1400	0.2000	0.2841	0.0062	0.9704	2682	10	2127	24	1611	31
24-1-z21*	0.15	2130	0.1859	0.0013	8.4600	0.1900	0.3322	0.0053	0.8730	2706	11	2280	20	1849	26
24-1-z14a*	0.17	1750	0.1871	0.0013	7.7500	0.2800	0.3000	0.0110	0.9755	2716	11	2195	34	1689	54
24-1-z11*	0.32	974	0.1906	0.0024	9.3300	0.3000	0.3549	0.0076	0.8727	2746	21	2367	29	1957	36

Table A2 LA-ICP-MS U-Pb data for zircon in metasedimentary and metagranitoid rocks of the NCGB, NW Ontario

			Isotopic ratios							Ages (Ma)					
	Th/U	**^{206*}Pb/^{204*}Pb**	**^{207*}Pb/^{206*}Pb**	**2 σ**	**^{207*}Pb/^{235}U**	**2 σ**	**^{206*}Pb/^{238}U**	**2 σ**	**Err. Corr.**	**^{207*}Pb/^{206*}Pb**	**1 σ**	**^{207*}Pb/^{235}U**	**1 σ**	**^{206*}Pb/^{238}U**	**1 σ**
24-1-z7*	0.20	1910	0.1932	0.0020	12.2600	0.3000	0.4597	0.0070	0.8242	2769	17	2624	23	2438	31
24-1-z15r*	0.21	1390	0.1991	0.0036	15.1700	0.5600	0.5520	0.0160	0.8393	2824	27	2820	35	2830	68
24-1-z4c*	0.15	1680	0.2054	0.0018	12.5500	0.3500	0.4430	0.0110	0.8994	2869	14	2644	27	2362	51
24-1-z4r*	0.29	1640	0.2055	0.0021	16.2400	0.6900	0.5680	0.0190	0.9786	2870	17	2886	44	2895	80
24-1-z17*	0.27	1000	0.2067	0.0027	15.8300	0.4400	0.5508	0.0110	0.7451	2879	21	2871	24	2828	46
24-1-z8r*	0.24	1700	0.2073	0.0013	12.7900	0.3600	0.4464	0.0110	0.9546	2884	10	2661	27	2377	48
24-1-z5*	0.30	1920	0.2074	0.0018	16.2200	0.4700	0.5630	0.0150	0.9249	2885	14	2888	28	2891	61
24-1-z8c*	0.24	1260	0.2098	0.0018	13.4000	0.3500	0.4609	0.0082	0.8654	2903	14	2707	24	2448	35
NCB11-33 ***Crd schist*** *NAD27, zone 15: 657319E, 5867427N*															
33-1-z5	*0.47*	*3060*	*0.1947*	*0.0035*	*11.3800*	*0.5200*	*0.4200*	*0.0160*	*0.9808*	*2784*	*14*	*2543*	*43*	*2258*	*75*
33-2-z24	*0.51*	*1850*	*0.1961*	*0.0055*	*9.3700*	*0.4400*	*0.3510*	*0.0130*	*0.9511*	*2793*	*20*	*2376*	*46*	*1936*	*65*
33-3-z5	*0.44*	*2860*	*0.1978*	*0.0038*	*12.9500*	*0.3400*	*0.4670*	*0.0097*	*0.9463*	*2808*	*16*	*2646*	*71*	*2439*	*130*
33-2-z19a	*0.39*	*2440*	*0.2018*	*0.0051*	*11.5800*	*0.4000*	*0.4165*	*0.0100*	*0.9471*	*2840*	*11*	*2571*	*33*	*2242*	*47*
33-1-z26	*0.46*	*2020*	*0.2025*	*0.0037*	*13.1300*	*0.6700*	*0.4750*	*0.0200*	*0.9807*	*2846*	*13*	*2686*	*49*	*2510*	*88*
33-1-z1	*0.36*	*2840*	*0.2028*	*0.0039*	*12.3200*	*0.4500*	*0.4410*	*0.0140*	*0.9207*	*2847*	*18*	*2625*	*35*	*2353*	*63*
33-2-z32	*0.64*	*5600*	*0.2030*	*0.0052*	*15.3600*	*0.5600*	*0.5478*	*0.0160*	*0.7804*	*2850*	*13*	*2837*	*40*	*2816*	*68*
33-1-z28	*0.65*	*2600*	*0.2029*	*0.0038*	*16.3500*	*0.3600*	*0.5817*	*0.0120*	*0.5968*	*2851*	*16*	*2897*	*22*	*2958*	*50*
33-2-z20a	*0.36*	*2780*	*0.2038*	*0.0053*	*16.3600*	*0.4700*	*0.5828*	*0.0083*	*0.6161*	*2856*	*13*	*2897*	*28*	*2960*	*34*
33-2-z12	*0.54*	*2870*	*0.2039*	*0.0054*	*13.3400*	*0.7300*	*0.4770*	*0.0240*	*0.9782*	*2857*	*16*	*2699*	*64*	*2513*	*110*
33-2-z19b	*0.46*	*3880*	*0.2040*	*0.0052*	*16.9800*	*0.4900*	*0.6064*	*0.0096*	*0.8810*	*2858*	*10*	*2933*	*28*	*3055*	*39*
33-1-z30	*0.54*	*4290*	*0.2040*	*0.0034*	*14.9900*	*0.3400*	*0.5304*	*0.0110*	*0.8763*	*2858*	*10*	*2814*	*22*	*2743*	*46*
33-2-z20b	*0.40*	*2940*	*0.2039*	*0.0052*	*15.4000*	*0.5100*	*0.5490*	*0.0130*	*0.9441*	*2859*	*10*	*2838*	*33*	*2819*	*54*
33-1-z17	*0.43*	*3320*	*0.2043*	*0.0035*	*16.1800*	*0.3600*	*0.5722*	*0.0110*	*0.7752*	*2860*	*12*	*2887*	*21*	*2917*	*46*
33-1-z23	*0.57*	*4100*	*0.2060*	*0.0036*	*16.2000*	*0.3900*	*0.5690*	*0.0120*	*0.8314*	*2874*	*12*	*2887*	*23*	*2903*	*49*
33-3-z3b	*0.20*	*5400*	*0.2014*	*0.0050*	*13.0900*	*0.3200*	*0.4558*	*0.0110*	*0.8205*	*2837*	*23*	*2736*	*64*	*2625*	*110*
33-3-z3a	*0.27*	*2210*	*0.2055*	*0.0052*	*13.0800*	*0.3100*	*0.4617*	*0.0096*	*0.8870*	*2869*	*24*	*2558*	*82*	*2175*	*180*
33-3-z12	*0.35*	*1890*	*0.2182*	*0.0018*	*12.5800*	*0.7100*	*0.4600*	*0.0270*	*0.9313*	*2966*	*13*	*2956*	*15*	*2942*	*36*
33-3-z9	*0.28*	*2600*	*0.2175*	*0.0034*	*13.6600*	*0.5600*	*0.4901*	*0.0220*	*0.8588*	*2966*	*50*	*2745*	*38*	*2458*	*70*
33-3-z11	*0.29*	*3520*	*0.2128*	*0.0024*	*12.6000*	*0.6900*	*0.4570*	*0.0220*	*0.9791*	*2925*	*21*	*2949*	*51*	*2956*	*120*
33-2-z17/	*0.42*	*1800*	*0.2081*	*0.0074*	*11.4100*	*0.7000*	*0.3990*	*0.0140*	*0.9880*	*2881*	*39*	*2542*	*46*	*2162*	*63*
33-2-z5/	*0.28*	*1730*	*0.2126*	*0.0057*	*12.5300*	*0.4400*	*0.4272*	*0.0100*	*0.8922*	*2924*	*19*	*2650*	*34*	*2291*	*48*
33-2-z36/	*1.09*	*2540*	*0.2117*	*0.0053*	*12.5600*	*0.4400*	*0.4288*	*0.0110*	*0.9382*	*2919*	*9*	*2647*	*32*	*2300*	*50*
33-2-z27/	*0.55*	*2860*	*0.2155*	*0.0055*	*13.2400*	*0.4600*	*0.4430*	*0.0110*	*0.9680*	*2949*	*10*	*2693*	*32*	*2362*	*48*
33-3-z6a/	*0.35*	*3480*	*0.2023*	*0.0019*	*13.3600*	*0.4100*	*0.4530*	*0.0120*	*0.8892*	*2847*	*12*	*2726*	*34*	*2570*	*61*
33-3-z6b/	*0.80*	*1830*	*0.2018*	*0.0053*	*13.9600*	*0.4900*	*0.4650*	*0.0150*	*0.4059*	*2839*	*36*	*2688*	*49*	*2469*	*68*

Table A2 LA-ICP-MS U-Pb data for zircon in metasedimentary and metagranitoid rocks of the NCGB, NW Ontario

			Isotopic ratios							Ages (Ma)					
	Th/U	$^{206*}Pb/^{204*}Pb$	$^{207*}Pb/^{206*}Pb$	2 σ	$^{207*}Pb/^{235}U$	2 σ	$^{206*}Pb/^{238}U$	2 σ	Err. Corr.	$^{207*}Pb/^{206*}Pb$	1 σ	$^{207*}Pb/^{235}U$	1 σ	$^{206*}Pb/^{238}U$	1 σ
33-1-z24/	*0.40*	*2240*	*0.2179*	*0.0037*	*14.7000*	*0.3700*	*0.4881*	*0.0110*	*0.8962*	*2964*	*11*	*2799*	*23*	*2566*	*49*
33-3-z2/	*0.55*	*2110*	*0.2170*	*0.0260*	*15.2200*	*0.2600*	*0.5245*	*0.0073*	*0.8163*	*2963*	*29*	*2693*	*130*	*2331*	*140*
33-1-z29/	*0.32*	*2070*	*0.2114*	*0.0040*	*16.7400*	*0.7500*	*0.5690*	*0.0210*	*0.9674*	*2920*	*17*	*2908*	*45*	*2895*	*87*
33-2-z4/	*0.43*	*1800*	*0.2187*	*0.0058*	*15.6700*	*0.5800*	*0.5259*	*0.0150*	*0.6246*	*2970*	*18*	*2856*	*41*	*2724*	*66*
33-1-z18/	*0.25*	*3120*	*0.2181*	*0.0040*	*16.0400*	*0.6000*	*0.5320*	*0.0180*	*0.9557*	*2966*	*14*	*2872*	*36*	*2746*	*77*
33-1-z11/	*0.54*	*6200*	*0.2109*	*0.0045*	*15.9600*	*0.7900*	*0.5460*	*0.0220*	*0.9659*	*2911*	*16*	*2883*	*50*	*2802*	*90*
33-1-z25/	*0.68*	*2420*	*0.2173*	*0.0038*	*16.5100*	*0.4000*	*0.5486*	*0.0120*	*0.8686*	*2960*	*13*	*2908*	*23*	*2818*	*49*
33-2-z30b/	*0.42*	*2160*	*0.2198*	*0.0056*	*17.4300*	*0.5400*	*0.5718*	*0.0110*	*0.7593*	*2979*	*11*	*2958*	*32*	*2915*	*46*
33-3-z1/	*0.38*	*2410*	*0.2146*	*0.0150*	*17.3700*	*0.2600*	*0.5785*	*0.0088*	*0.8370*	*2940*	*11*	*2647*	*160*	*2286*	*250*
33-2-z8/	*0.22*	*3470*	*0.2176*	*0.0055*	*17.4100*	*0.5300*	*0.5820*	*0.0098*	*0.9117*	*2964*	*11*	*2956*	*30*	*2956*	*40*
33-1-z9/	*0.48*	*2520*	*0.2172*	*0.0038*	*17.5300*	*0.4800*	*0.5850*	*0.0140*	*0.9229*	*2960*	*10*	*2962*	*26*	*2969*	*58*
33-2-z3^	0.51	3410	0.2212	0.0057	16.0200	0.5800	0.5210	0.0140	0.9114	2989	16	2876	37	2703	61
33-2-z9*	0.55	1520	0.2097	0.0058	10.5900	0.7300	0.3638	0.0220	0.5958	2901	23	2486	52	1999	96
33-1-z31*	0.54	1010	0.2184	0.0042	10.7000	0.4000	0.3528	0.0140	0.9288	2967	18	2494	32	1947	65
33-3-z10*	0.85	1580	0.2048	0.0025	6.7200	0.6000	0.2350	0.0210	0.9877	2863	20	2040	79	1350	110
33-3-z7*	0.35	650	0.2740	0.0210	8.7500	0.5100	0.3366	0.0110	0.7526	3116	99	3450	210	3850	390
33-2-z28*	0.49	870	0.2105	0.0056	12.0100	0.4000	0.4160	0.0091	0.8717	2908	20	2603	30	2239	41
33-1-z12*	0.44	1010	0.2019	0.0037	10.6600	0.2900	0.3851	0.0089	0.9072	2843	16	2494	24	2099	42
33-2-z34*	0.60	1055	0.2027	0.0054	11.7200	0.4200	0.4196	0.0099	0.9084	2853	16	2578	33	2257	44
33-2-z30a*	0.23	1150	0.2024	0.0053	10.6100	0.5000	0.3799	0.0150	0.7488	2845	20	2488	38	2075	67
33-3-z4*	0.78	1360	0.1988	0.0470	17.4200	0.3300	0.5864	0.0084	0.7499	2815	37	2444	240	2044	260
33-2-z23*	0.80	1480	0.2089	0.0067	11.9300	0.5400	0.4160	0.0200	0.9451	2896	14	2606	45	2248	92
33-1-z15*	0.31	1420	0.2086	0.0038	11.8200	0.3100	0.4136	0.0100	0.8590	2894	14	2594	26	2230	49
33-2-z7*	0.85	1620	0.2057	0.0054	12.5000	0.4900	0.4440	0.0130	0.9279	2871	13	2636	36	2362	58
33-2-z37*	0.57	1460	0.2244	0.0058	18.2700	0.7000	0.5933	0.0170	0.4593	3012	22	3004	42	3002	71
33-1-z13*	0.22	1520	0.2169	0.0037	15.0300	0.3400	0.5021	0.0110	0.8625	2958	10	2816	21	2622	45
33-1-z21*	0.51	1680	0.2042	0.0040	11.6500	0.3900	0.4080	0.0150	0.9215	2858	20	2576	33	2209	68
NCTK10-44A ***And-st schist*** *NAD83, zone 15: 670289E, 5850342N*															
44-1-z2	*0.38*	*6660*	*0.1983*	*0.0047*	*12.5200*	*0.4500*	*0.4520*	*0.0140*	*0.9759*	*2813*	*11*	*2638*	*35*	*2398*	*65*
44-2-z19	*0.44*	*2530*	*0.1994*	*0.0013*	*12.5300*	*0.1900*	*0.4562*	*0.0110*	*0.9321*	*2822*	*11*	*2644*	*14*	*2422*	*46*
44-2-z12	*0.71*	*4060*	*0.1992*	*0.0022*	*13.7000*	*0.2700*	*0.5009*	*0.0130*	*0.8061*	*2822*	*20*	*2728*	*18*	*2617*	*55*
44-3-z28	*0.43*	*2000*	*0.1997*	*0.0060*	*10.8900*	*0.2800*	*0.3912*	*0.0072*	*0.6852*	*2824*	*21*	*2511*	*24*	*2131*	*33*
44-3-z29	*0.29*	*2430*	*0.1996*	*0.0063*	*10.1400*	*0.5400*	*0.3720*	*0.0200*	*0.9665*	*2825*	*25*	*2446*	*54*	*2034*	*95*
44-2-z18	*0.47*	*2550*	*0.2003*	*0.0012*	*14.3600*	*0.2400*	*0.5188*	*0.0130*	*0.8966*	*2828*	*14*	*2773*	*17*	*2693*	*58*
44-3-z35	*0.31*	*2890*	*0.2020*	*0.0062*	*13.8200*	*0.4500*	*0.5030*	*0.0190*	*0.8848*	*2841*	*24*	*2735*	*30*	*2586*	*60*

Table A2 LA-ICP-MS U-Pb data for zircon in metasedimentary and metagranitoid rocks of the NCGB, NW Ontario

			Isotopic ratios							Ages (Ma)					
	Th/U	$^{206*}Pb/^{204*}Pb$	$^{207*}Pb/^{206*}Pb$	2 σ	$^{207*}Pb/^{235}U$	2 σ	$^{206*}Pb/^{238}U$	2 σ	Err. Corr.	$^{207*}Pb/^{206*}Pb$	1 σ	$^{207*}Pb/^{235}U$	1 σ	$^{206*}Pb/^{238}U$	1 σ
44-2-z26	*0.34*	*4540*	*0.2025*	*0.0020*	*15.4300*	*0.5000*	*0.5540*	*0.0190*	*0.9254*	*2845*	*23*	*2840*	*35*	*2838*	*84*
44-2-z1	*0.35*	*1820*	*0.2031*	*0.0031*	*15.2800*	*0.4900*	*0.5390*	*0.0200*	*0.6790*	*2848*	*35*	*2830*	*35*	*2778*	*87*
44-3-z15	*0.38*	*3470*	*0.2028*	*0.0058*	*14.4300*	*0.3400*	*0.5159*	*0.0092*	*0.7680*	*2848*	*15*	*2778*	*22*	*2681*	*39*
44-3-z10	*0.53*	*3670*	*0.2024*	*0.0060*	*14.7200*	*0.3800*	*0.5197*	*0.0094*	*0.7951*	*2848*	*18*	*2795*	*25*	*2697*	*40*
44-2-z16	*0.48*	*6400*	*0.2026*	*0.0032*	*13.4400*	*0.8000*	*0.4839*	*0.0200*	*0.8707*	*2849*	*17*	*2709*	*40*	*2543*	*82*
44-1-z16	*0.41*	*3090*	*0.2027*	*0.0056*	*12.8200*	*0.6200*	*0.4570*	*0.0180*	*0.8959*	*2849*	*25*	*2667*	*50*	*2435*	*80*
44-3-z1	*0.32*	*2790*	*0.2027*	*0.0061*	*15.5500*	*0.5400*	*0.5540*	*0.0150*	*0.9239*	*2850*	*20*	*2845*	*34*	*2839*	*64*
44-3-z32	*0.40*	*5170*	*0.2032*	*0.0063*	*13.9900*	*0.7200*	*0.5010*	*0.0230*	*0.9433*	*2850*	*24*	*2744*	*51*	*2612*	*96*
44-3-z34	*0.44*	*4500*	*0.2036*	*0.0057*	*12.3000*	*0.8600*	*0.4410*	*0.0300*	*0.9725*	*2857*	*11*	*2622*	*69*	*2370*	*130*
44-1-z8	*0.40*	*4200*	*0.2040*	*0.0048*	*11.2200*	*0.1800*	*0.4058*	*0.0064*	*0.5275*	*2858*	*13*	*2541*	*16*	*2196*	*29*
44-2-z31	*0.50*	*4670*	*0.2042*	*0.0020*	*14.5700*	*0.2500*	*0.5209*	*0.0130*	*0.8613*	*2858*	*16*	*2785*	*16*	*2702*	*53*
44-1-z13	*0.32*	*2050*	*0.2038*	*0.0060*	*10.4900*	*0.6300*	*0.3727*	*0.0190*	*0.6084*	*2859*	*34*	*2475*	*72*	*2041*	*96*
44-1-z9	*0.41*	*3440*	*0.2050*	*0.0048*	*14.4700*	*0.2700*	*0.5105*	*0.0089*	*0.8796*	*2866*	*13*	*2782*	*18*	*2658*	*38*
44-1-z7	*0.42*	*2430*	*0.2053*	*0.0049*	*15.9500*	*0.3600*	*0.5617*	*0.0110*	*0.8591*	*2868*	*17*	*2872*	*23*	*2873*	*44*
44-2-z47b	*0.38*	*2990*	*0.2054*	*0.0023*	*13.4100*	*0.3300*	*0.4738*	*0.0130*	*0.8780*	*2873*	*18*	*2708*	*23*	*2498*	*55*
44-3-z36	*0.37*	*4170*	*0.2052*	*0.0068*	*10.8700*	*0.3500*	*0.3884*	*0.0100*	*0.7706*	*2873*	*28*	*2517*	*33*	*2124*	*45*
44-1-z17	*0.50*	*2490*	*0.2066*	*0.0058*	*14.1800*	*0.3200*	*0.4936*	*0.0077*	*0.5867*	*2879*	*25*	*2760*	*20*	*2586*	*33*
44-1-z18	*0.50*	*1910*	*0.2065*	*0.0057*	*13.5700*	*0.3800*	*0.4790*	*0.0110*	*0.6833*	*2879*	*43*	*2715*	*27*	*2519*	*46*
44-2-z47a	*0.43*	*4690*	*0.2064*	*0.0026*	*12.2200*	*0.3800*	*0.4320*	*0.0150*	*0.9015*	*2879*	*20*	*2620*	*29*	*2319*	*65*
44-1-z11a	*0.30*	*4460*	*0.2074*	*0.0059*	*14.8400*	*0.4100*	*0.5230*	*0.0130*	*0.6545*	*2882*	*34*	*2802*	*27*	*2709*	*57*
44-2-z42	*0.41*	*2920*	*0.2071*	*0.0035*	*12.3700*	*0.2300*	*0.4288*	*0.0100*	*0.5160*	*2884*	*27*	*2631*	*18*	*2300*	*46*
44-1-z11b	*0.46*	*2530*	*0.2077*	*0.0052*	*15.3300*	*0.3300*	*0.5343*	*0.0089*	*0.8347*	*2888*	*17*	*2834*	*21*	*2759*	*38*
44-3-z7^	0.43	3890	0.1915	0.0053	10.5900	0.2900	0.3968	0.0092	0.9532	2755	10	2486	26	2153	43
44-2-z38^	0.26	3470	0.1938	0.0026	9.3000	0.4100	0.3530	0.0160	0.9383	2775	22	2365	41	1943	76
44-2-z29^	0.28	4680	0.1942	0.0019	11.3800	0.3500	0.4230	0.0140	0.9134	2777	18	2556	30	2273	67
44-2-z14^	0.52	1920	0.1943	0.0025	10.6200	0.2100	0.3966	0.0093	0.8912	2779	10	2492	14	2153	43
44-2-z13^	0.73	2290	0.1959	0.0023	13.4600	0.2800	0.4949	0.0120	0.7850	2793	19	2712	20	2590	52
44-1-z12^	0.45	4800	0.1987	0.0054	10.6400	0.4200	0.3960	0.0150	0.9234	2817	22	2498	38	2156	71
44-3-z19^	0.26	2040	0.2170	0.0066	16.8600	0.5100	0.5680	0.0130	0.7822	2957	21	2925	29	2898	52
44-2-z36^	0.42	4000	0.2183	0.0023	16.2000	0.2700	0.5420	0.0120	0.7897	2967	17	2887	17	2791	51
44-3-z8^	0.28	4250	0.2206	0.0080	15.4000	0.5200	0.5083	0.0100	0.4945	2986	38	2837	32	2648	44
44-3-z2*	0.30	930	0.2060	0.0120	14.8000	0.8700	0.5170	0.0270	0.6712	2865	82	2815	48	2720	130
44-2-z25*	0.41	1050	0.2011	0.0490	12.7400	24.0000	0.4630	0.2400	0.9244	2835	17	2660	320	2452	650
44-3-z18*	0.31	1110	0.2009	0.0062	11.9100	0.4800	0.4280	0.0170	0.9179	2837	24	2590	40	2303	76
44-3-z13*	0.38	1070	0.2126	0.0083	12.4700	0.4700	0.4285	0.0100	0.7150	2920	45	2637	35	2298	46

Table A2 LA-ICP-MS U-Pb data for zircon in metasedimentary and metagranitoid rocks of the NCGB, NW Ontario

			Isotopic ratios							Ages (Ma)					
	Th/U	$^{206*}Pb/^{204*}Pb$	$^{207*}Pb/^{206*}Pb$	2 σ	$^{207*}Pb/^{235}U$	2 σ	$^{206*}Pb/^{238}U$	2 σ	Err. Corr.	$^{207*}Pb/^{206*}Pb$	1 σ	$^{207*}Pb/^{235}U$	1 σ	$^{206*}Pb/^{238}U$	1 σ
44-3-z14*	0.31	1290	0.2050	0.0059	17.1700	0.3900	0.6047	0.0100	0.5461	2865	16	2945	21	3048	41
44-1-z4*	0.55	1420	0.2039	0.0049	10.1600	0.2900	0.3637	0.0100	0.8992	2857	13	2446	28	1998	50
44-3-z33*	0.26	1590	0.2032	0.0060	10.7400	0.6700	0.3860	0.0250	0.9791	2851	18	2485	59	2100	120
44-2-z20*	0.28	1460	0.1844	0.0080	8.2200	2.0000	0.3240	0.0510	0.9821	2691	23	2260	120	1810	210
44-2-z34*	0.18	1660	0.1987	0.0029	12.0000	1.0000	0.4400	0.0320	0.9441	2814	20	2598	59	2345	130
44-2-z23*	0.47	1780	0.1979	0.0070	12.6800	1.2000	0.4630	0.0280	0.8770	2808	17	2655	74	2452	120
44-2-z8*	0.32	5700	0.1907	0.0061	7.0600	1.1000	0.2670	0.0290	0.9855	2751	18	2112	96	1525	130
44-2-z46*	0.32	2910	0.1952	0.0051	8.0700	0.9900	0.3010	0.0250	0.9744	2785	28	2227	81	1693	120
44-3-z22*	0.31	1940	0.1980	0.0058	9.0000	0.3000	0.3261	0.0091	0.9039	2808	17	2341	29	1824	46
44-2-z4*	0.25	2870	0.1944	0.0250	13.0400	6.2000	0.4870	0.0900	0.9305	2779	14	2680	200	2556	310
44-2-z45*	0.39	6500	0.2041	0.0100	13.5000	2.9000	0.4825	0.0610	0.5785	2856	31	2714	120	2537	230
NCTK10-63 ***Protomylonitic trondhjemite***† *NAD83, zone 16: 308451E, 5816070N*															
63-3-z25r	*0.41*	*3580*	*0.1874*	*0.0031*	*9.4900*	*0.5500*	*0.3720*	*0.0170*	*0.9145*	*2717*	*20*	*2393*	*56*	*2043*	*76*
63-2-z5c	*0.58*	*1880*	*0.1880*	*0.0038*	*9.9100*	*0.4400*	*0.3790*	*0.0120*	*0.9257*	*2724*	*20*	*2430*	*46*	*2068*	*59*
63-3-z21c	*0.13*	*2010*	*0.1926*	*0.0027*	*9.6300*	*0.6000*	*0.3660*	*0.0200*	*0.9823*	*2764*	*10*	*2401*	*57*	*2034*	*97*
63-2-z11r	*0.47*	*3110*	*0.1935*	*0.0025*	*10.9300*	*0.3400*	*0.4114*	*0.0110*	*0.8123*	*2771*	*12*	*2515*	*29*	*2220*	*51*
63-1-z14c	*0.41*	*5440*	*0.1966*	*0.0042*	*13.5900*	*0.4400*	*0.5040*	*0.0140*	*0.6043*	*2792*	*30*	*2718*	*31*	*2628*	*61*
63-2-z2c	*0.71*	*1960*	*0.1963*	*0.0025*	*10.9400*	*0.4200*	*0.4116*	*0.0140*	*0.7413*	*2795*	*20*	*2518*	*41*	*2222*	*68*
63-2-z15	*0.36*	*1930*	*0.1983*	*0.0043*	*11.5500*	*0.5200*	*0.4240*	*0.0160*	*0.9269*	*2806*	*42*	*2553*	*46*	*2291*	*77*
63-3-z20r	*0.16*	*2040*	*0.1974*	*0.0036*	*10.4600*	*0.6400*	*0.3890*	*0.0190*	*0.9650*	*2807*	*20*	*2471*	*62*	*2116*	*90*
63-2-z4c	*0.80*	*5600*	*0.1982*	*0.0030*	*11.2700*	*0.4400*	*0.4120*	*0.0140*	*0.9135*	*2810*	*28*	*2542*	*43*	*2220*	*68*
63-3-z19r	*0.38*	*1950*	*0.1992*	*0.0030*	*13.4900*	*0.7100*	*0.4950*	*0.0230*	*0.8973*	*2821*	*14*	*2713*	*50*	*2590*	*97*
63-3-z13c	*0.80*	*3940*	*0.1993*	*0.0029*	*10.9500*	*0.6100*	*0.3998*	*0.0190*	*0.9413*	*2822*	*13*	*2519*	*49*	*2166*	*86*
63-3-z8	*0.34*	*3500*	*0.2001*	*0.0029*	*11.5800*	*0.6000*	*0.4200*	*0.0180*	*0.9577*	*2827*	*16*	*2566*	*52*	*2257*	*80*
63-3-z16r	*0.35*	*2880*	*0.2021*	*0.0034*	*13.8000*	*0.7500*	*0.5058*	*0.0210*	*0.7872*	*2842*	*21*	*2734*	*51*	*2638*	*89*
63-3-z12c	*0.38*	*5380*	*0.2023*	*0.0032*	*15.9900*	*0.8100*	*0.5732*	*0.0240*	*0.7557*	*2846*	*18*	*2874*	*48*	*2919*	*97*
63-3-z14	*0.32*	*2600*	*0.2024*	*0.0031*	*13.5500*	*0.7300*	*0.4900*	*0.0220*	*0.9198*	*2846*	*15*	*2718*	*52*	*2568*	*97*
63-2-z6c	*0.24*	*4640*	*0.2028*	*0.0035*	*12.5800*	*0.5400*	*0.4520*	*0.0170*	*0.7565*	*2846*	*24*	*2646*	*40*	*2401*	*77*
63-3-z15c	*0.50*	*4100*	*0.2027*	*0.0029*	*13.0600*	*0.7500*	*0.4750*	*0.0250*	*0.9650*	*2849*	*13*	*2681*	*56*	*2498*	*110*
63-2-z4r	*0.39*	*3490*	*0.2031*	*0.0031*	*11.4000*	*0.3400*	*0.4097*	*0.0110*	*0.7600*	*2850*	*19*	*2555*	*28*	*2213*	*51*
63-2-z2r	*0.12*	*2040*	*0.2026*	*0.0027*	*11.9200*	*0.4400*	*0.4360*	*0.0140*	*0.9541*	*2851*	*18*	*2602*	*39*	*2333*	*64*
63-2-z1r	*0.43*	*3510*	*0.2033*	*0.0028*	*14.0700*	*0.3800*	*0.5054*	*0.0110*	*0.6861*	*2852*	*15*	*2754*	*26*	*2636*	*48*
63-2-z16r	*0.58*	*5070*	*0.2036*	*0.0038*	*13.9400*	*0.4400*	*0.4939*	*0.0120*	*0.6630*	*2855*	*26*	*2745*	*30*	*2586*	*53*
63-3-z20c	*0.57*	*3260*	*0.2032*	*0.0033*	*15.2400*	*0.7900*	*0.5520*	*0.0240*	*0.8772*	*2856*	*22*	*2829*	*54*	*2834*	*100*
63-3-z13r	*0.40*	*2610*	*0.2038*	*0.0029*	*14.2900*	*0.6900*	*0.5130*	*0.0200*	*0.7724*	*2856*	*11*	*2769*	*46*	*2669*	*88*

Table A2 LA-ICP-MS U-Pb data for zircon in metasedimentary and metagranitoid rocks of the NCGB, NW Ontario

			Isotopic ratios							Ages (Ma)					
	Th/U	$^{206*}Pb/^{204*}Pb$	$^{207*}Pb/^{206*}Pb$	2 σ	$^{207*}Pb/^{235}U$	2 σ	$^{206*}Pb/^{238}U$	2 σ	Err. Corr.	$^{207*}Pb/^{206*}Pb$	1 σ	$^{207*}Pb/^{235}U$	1 σ	$^{206*}Pb/^{238}U$	1 σ
63-2-z3r	*0.43*	*3800*	*0.2047*	*0.0033*	*13.1900*	*0.7600*	*0.4633*	*0.0220*	*0.8835*	*2864*	*20*	*2693*	*52*	*2454*	*95*
63-2-z5r	*0.35*	*2550*	*0.2062*	*0.0036*	*13.4700*	*0.4500*	*0.4780*	*0.0120*	*0.6865*	*2879*	*39*	*2712*	*32*	*2529*	*54*
63-3-z12r^	0.19	2290	0.1672	0.0028	11.5100	0.6900	0.4960	0.0270	0.9861	2529	20	2581	74	2590	130
63-2-z17c^	0.20	13400	0.1781	0.0039	10.1300	0.5700	0.4100	0.0190	0.9300	2634	19	2443	66	2210	93
63-3-z16c^	0.20	7000	0.1791	0.0039	11.2800	0.7500	0.4540	0.0250	0.9311	2643	30	2552	62	2405	110
63-2-z7^	0.10	3360	0.1797	0.0053	9.2500	0.3500	0.3780	0.0140	0.8929	2655	27	2364	35	2080	66
63-2-z9c^	0.23	16700	0.1815	0.0034	9.0000	0.5800	0.3560	0.0200	0.9420	2665	25	2334	54	1959	91
63-3-z7^	0.55	3460	0.1834	0.0032	8.6900	0.5000	0.3391	0.0160	0.9438	2686	19	2301	51	1880	75
*63-3-z29r^*	*0.52*	*5190*	*0.1920*	*0.0032*	*14.8600*	*0.9600*	*0.5570*	*0.0290*	*0.9640*	*2758*	*16*	*2806*	*67*	*2849*	*120*
*63-2-z10r^*	*0.26*	*2060*	*0.2038*	*0.0028*	*11.1600*	*0.3400*	*0.3949*	*0.0099*	*0.6582*	*2859*	*17*	*2536*	*30*	*2145*	*46*
*63-2-z10c^*	*0.30*	*2070*	*0.2044*	*0.0026*	*12.4400*	*0.4600*	*0.4360*	*0.0170*	*0.9593*	*2861*	*13*	*2635*	*34*	*2332*	*74*
63-3-z6c^	0.19	2300	0.2099	0.0039	13.4300	0.7800	0.4650	0.0240	0.7379	2903	26	2713	64	2460	110
63-2-z1c^	0.96	3320	0.2107	0.0036	11.5100	0.5900	0.3901	0.0250	0.9171	2910	14	2565	42	2123	110
63-2-z9r^	0.32	2860	0.2157	0.0039	13.3200	0.5100	0.4520	0.0150	0.8019	2946	31	2699	40	2403	67
63-3-z31r*	0.14	230	0.2580	0.0220	27.6000	3.8000	0.7070	0.0880	0.8123	3170	##	3290	150	3450	330
63-3-z23a*	0.04	470	0.1872	0.0081	7.1700	0.4900	0.2880	0.0180	0.8738	2702	66	2118	60	1626	92
63-3-z29r2*	0.23	470	0.2740	0.0280	27.4000	4.3000	0.6080	0.0770	0.7171	3140	##	3180	170	2960	290
63-3-z18c*	0.11	510	0.2460	0.0190	28.7000	7.0000	0.7300	0.1100	0.9799	2966	61	3210	190	3420	350
63-3-z27r*	0.24	560	0.2290	0.0130	19.2000	2.4000	0.5800	0.0350	0.8894	3006	78	2994	100	2930	140
63-1-z4*	0.46	690	0.1947	0.0038	7.1400	0.6400	0.2603	0.0230	0.6396	2779	37	2127	66	1491	110
63-2-z14*	0.29	631	0.2034	0.0059	12.2700	0.5000	0.4420	0.0150	0.6119	2854	46	2624	39	2355	69
63-3-z24*	0.51	830	0.1952	0.0044	5.5000	0.5000	0.2120	0.0170	0.9299	2781	31	1914	81	1229	90
63-3-z15r*	0.25	830	0.2117	0.0320	12.4000	3.2000	0.4210	0.0440	0.9715	2916	37	2620	140	2250	180
63-3-z10*	0.53	930	0.1949	0.0044	7.4000	0.6700	0.2700	0.0200	0.9802	2783	17	2138	76	1548	100
63-3-z26r*	0.42	1030	0.1965	0.0027	11.1300	0.5800	0.4080	0.0180	0.9501	2798	12	2534	49	2204	81
63-3-z22*	0.55	1140	0.1838	0.0032	7.1300	0.5100	0.2820	0.0190	0.9478	2685	21	2114	65	1591	95
63-3-z26c*	0.12	1180	0.2021	0.0031	15.2600	0.9000	0.5499	0.0280	0.7616	2842	20	2830	67	2824	130
63-3-z28*	0.54	1360	0.1759	0.0067	6.1900	0.5000	0.2600	0.0200	0.8332	2615	59	1983	72	1480	100
63-3-z30c*	0.62	1280	0.2044	0.0033	14.7900	0.7500	0.5143	0.0210	0.8431	2860	17	2803	47	2674	91
63-3-z30c*	0.62	1280	0.2044	0.0033	14.7900	0.7500	0.5143	0.0210	0.8431	2860	17	2803	47	2674	91
63-3-z11r*	0.34	1420	0.1916	0.0032	6.9100	0.3700	0.2594	0.0120	0.9520	2755	15	2103	45	1486	60
63-3-z6r*	0.08	1430	0.1889	0.0066	9.3800	1.7000	0.3570	0.0410	0.8598	2738	37	2373	110	1968	180
63-2-z13*	0.30	1600	0.2014	0.0041	8.4200	0.3700	0.3101	0.0110	0.8506	2832	29	2292	36	1754	53
63-3-z12r*	0.60	1530	0.2049	0.0047	15.7200	0.9800	0.5533	0.0260	0.8529	2865	22	2859	67	2838	110
63-3-z23c*	0.11	2000	0.1654	0.0045	4.9700	0.5800	0.2200	0.0220	0.9894	2519	41	1780	100	1270	110

Table A2 LA-ICP-MS U-Pb data for zircon in metasedimentary and metagranitoid rocks of the NCGB, NW Ontario

			Isotopic ratios							Ages (Ma)					
	Th/U	$^{206*}Pb/^{204*}Pb$	$^{207*}Pb/^{206*}Pb$	2 σ	$^{207*}Pb/^{235}U$	2 σ	$^{206*}Pb/^{238}U$	2 σ	Err. Corr.	$^{207*}Pb/^{206*}Pb$	1 σ	$^{207*}Pb/^{235}U$	1 σ	$^{206*}Pb/^{238}U$	1 σ
63-3-z23b*	0.22	2380	0.1845	0.0035	7.8000	0.6000	0.3100	0.0200	0.9742	2691	24	2204	71	1730	98
63-3-z11c*	0.13	2280	0.1761	0.0028	6.2900	0.3700	0.2580	0.0130	0.9489	2616	20	2013	52	1477	66
63-1-z1*	0.65	7260	0.1528	0.0026	4.3210	0.2600	0.2015	0.0097	0.9230	2377	14	1696	47	1183	51
63-3-z27c*	0.65	7240	0.1531	0.0038	4.3310	0.9500	0.2015	0.0300	0.9162	2380	14	1698	76	1183	130
63-3-z6r*	0.45	2490	0.2039	0.0044	13.7900	1.0000	0.4940	0.0300	0.6421	2854	38	2735	58	2585	120
63-3-z9*	0.15	4900	0.1852	0.0045	12.5400	1.1000	0.4910	0.0400	0.9077	2697	25	2648	98	2580	180
63-3-z32*	0.70	2010	0.2016	0.0058	12.7100	2.2000	0.4490	0.0600	0.6138	2850	40	2657	110	2386	240
NCTK10-76 ***2-mca schist*** *NAD27, zone 15: 702814E, 5821125N*															
76-2-z15	*0.07*	*6100*	*0.1951*	*0.0027*	*11.7900*	*0.3600*	*0.4210*	*0.0120*	*0.9854*	*2787*	*14*	*2580*	*35*	*2259*	*56*
76-1-uns2	*0.55*	*3160*	*0.1978*	*0.0030*	*14.0900*	*0.1400*	*0.5136*	*0.0097*	*0.7869*	*2808*	*12*	*2755*	*10*	*2671*	*43*
76-2-z16	*0.21*	*1930*	*0.1983*	*0.0027*	*13.7000*	*0.3100*	*0.4878*	*0.0110*	*0.8062*	*2812*	*14*	*2729*	*22*	*2561*	*50*
76-2-z8b	*0.75*	*2290*	*0.1998*	*0.0047*	*15.6600*	*0.3300*	*0.5590*	*0.0110*	*0.8662*	*2822*	*25*	*2852*	*29*	*2860*	*51*
76-1-z4	*0.09*	*3200*	*0.1998*	*0.0035*	*13.3100*	*0.3500*	*0.4819*	*0.0130*	*0.8244*	*2824*	*15*	*2701*	*25*	*2535*	*56*
76-2-z8a	*0.54*	*3260*	*0.2009*	*0.0031*	*12.0300*	*0.3600*	*0.4394*	*0.0140*	*0.8158*	*2830*	*22*	*2609*	*30*	*2353*	*64*
76-2-z14a	*0.56*	*2030*	*0.2015*	*0.0027*	*10.7900*	*0.2700*	*0.3817*	*0.0100*	*0.8901*	*2838*	*17*	*2505*	*23*	*2091*	*47*
76-2-z13	*0.45*	*3170*	*0.2020*	*0.0026*	*14.0000*	*0.3400*	*0.5112*	*0.0120*	*0.7718*	*2842*	*14*	*2751*	*23*	*2661*	*52*
76-3-z11b	*0.22*	*4760*	*0.2026*	*0.0035*	*13.6400*	*0.2900*	*0.4899*	*0.0067*	*0.5740*	*2845*	*20*	*2726*	*21*	*2573*	*29*
76-3-z7	*0.57*	*2660*	*0.2034*	*0.0050*	*13.1600*	*0.6300*	*0.4733*	*0.0180*	*0.7891*	*2851*	*22*	*2689*	*38*	*2497*	*77*
76-3-z22a	*0.60*	*3080*	*0.2033*	*0.0033*	*14.6000*	*0.3200*	*0.5213*	*0.0092*	*0.8992*	*2851*	*17*	*2788*	*21*	*2703*	*39*
76-1-z11	*0.35*	*4640*	*0.2037*	*0.0041*	*15.7300*	*0.2600*	*0.5583*	*0.0140*	*0.2844*	*2852*	*36*	*2863*	*16*	*2859*	*60*
76-1-z8	*0.31*	*2430*	*0.2031*	*0.0032*	*16.0500*	*0.2500*	*0.5721*	*0.0120*	*0.7866*	*2853*	*16*	*2883*	*15*	*2921*	*51*
76-1-z1	*0.46*	*3750*	*0.2043*	*0.0034*	*12.7100*	*0.3600*	*0.4510*	*0.0160*	*0.9291*	*2862*	*16*	*2662*	*27*	*2402*	*69*
76-2-z5c	*0.35*	*2300*	*0.2049*	*0.0030*	*15.5500*	*0.4700*	*0.5493*	*0.0140*	*0.7710*	*2865*	*14*	*2848*	*29*	*2821*	*56*
76-3-z16	*0.50*	*1750*	*0.2039*	*0.0033*	*14.0400*	*0.3100*	*0.5040*	*0.0085*	*0.7631*	*2866*	*17*	*2756*	*21*	*2630*	*37*
76-2-z5b	*0.76*	*4620*	*0.2050*	*0.0021*	*16.0300*	*0.3300*	*0.5679*	*0.0130*	*0.7847*	*2867*	*11*	*2882*	*20*	*2898*	*51*
76-3-z6	*0.63*	*2280*	*0.2054*	*0.0055*	*13.1200*	*0.5900*	*0.4560*	*0.0120*	*0.6905*	*2868*	*28*	*2693*	*39*	*2422*	*55*
76-2-z1b	*0.43*	*2640*	*0.2061*	*0.0047*	*13.8400*	*0.4600*	*0.4859*	*0.0150*	*0.6714*	*2871*	*29*	*2736*	*33*	*2551*	*62*
76-2-z12	*0.45*	*2740*	*0.2057*	*0.0023*	*14.2400*	*0.3200*	*0.4845*	*0.0100*	*0.6036*	*2871*	*19*	*2767*	*22*	*2547*	*45*
76-1-z7	*0.59*	*2880*	*0.2059*	*0.0033*	*13.4600*	*0.2200*	*0.4735*	*0.0110*	*0.8399*	*2873*	*13*	*2711*	*16*	*2498*	*47*
76-2-z1c	*0.39*	*2980*	*0.2057*	*0.0034*	*15.9800*	*0.4400*	*0.5631*	*0.0130*	*0.5871*	*2873*	*25*	*2875*	*27*	*2878*	*54*
76-3-z11a	*0.30*	*4960*	*0.2061*	*0.0033*	*15.8600*	*0.3500*	*0.5609*	*0.0086*	*0.7547*	*2874*	*17*	*2867*	*21*	*2874*	*35*
76-2-z11b	*0.58*	*3410*	*0.2065*	*0.0038*	*14.2000*	*0.3900*	*0.5029*	*0.0120*	*0.7558*	*2875*	*26*	*2763*	*28*	*2630*	*52*
76-1-z12	*0.38*	*3670*	*0.2067*	*0.0038*	*13.2000*	*0.5300*	*0.4645*	*0.0200*	*0.8869*	*2880*	*13*	*2693*	*29*	*2459*	*84*
76-1-z10a	*0.35*	*3760*	*0.2069*	*0.0033*	*15.1600*	*0.2500*	*0.5318*	*0.0120*	*0.8608*	*2881*	*13*	*2825*	*16*	*2748*	*51*
76-3-z10b	*0.32*	*3140*	*0.2073*	*0.0034*	*15.8800*	*0.5300*	*0.5597*	*0.0160*	*0.7246*	*2882*	*26*	*2868*	*37*	*2865*	*67*

Table A2 LA-ICP-MS U-Pb data for zircon in metasedimentary and metagranitoid rocks of the NCGB, NW Ontario

			Isotopic ratios							Ages (Ma)					
	Th/U	$^{206*}Pb/^{204*}Pb$	$^{207*}Pb/^{206*}Pb$	2 σ	$^{207*}Pb/^{235}U$	2 σ	$^{206*}Pb/^{238}U$	2 σ	Err. Corr.	$^{207*}Pb/^{206*}Pb$	1 σ	$^{207*}Pb/^{235}U$	1 σ	$^{206*}Pb/^{238}U$	1 σ
76-2-z1a	*0.30*	*2180*	*0.2074*	*0.0042*	*14.2300*	*0.4400*	*0.4990*	*0.0150*	*0.8189*	*2883*	*19*	*2765*	*28*	*2616*	*64*
76-1-z6	*0.54*	*1990*	*0.2079*	*0.0034*	*16.9400*	*0.1800*	*0.5885*	*0.0110*	*0.4626*	*2888*	*15*	*2931*	*10*	*2983*	*45*
76-1-z9a	*0.33*	*1990*	*0.2079*	*0.0036*	*13.0200*	*0.3400*	*0.4513*	*0.0140*	*0.8097*	*2891*	*23*	*2679*	*24*	*2400*	*60*
76-2-z7^	0.20	5200	0.1852	0.0054	9.9100	0.3900	0.3880	0.0120	0.8375	2694	36	2430	39	2111	58
76-2-z5a^	0.39	5120	0.1865	0.0021	11.7900	0.2600	0.4520	0.0099	0.8670	2710	20	2586	21	2403	45
76-2-z3^	0.56	4580	0.1917	0.0055	12.3100	0.4200	0.4714	0.0140	0.5429	2750	45	2631	35	2488	59
76-2-z14b^	0.79	6600	0.1930	0.0020	10.5100	0.4400	0.3880	0.0140	0.9831	2767	11	2478	39	2112	67
76-1-z5a^	0.20	2280	0.1938	0.0033	12.5000	0.2700	0.4659	0.0130	0.8830	2773	18	2646	21	2464	52
76-3-z20^	0.52	4250	0.1948	0.0031	11.1100	0.2700	0.4140	0.0069	0.7915	2782	18	2534	22	2233	31
76-2-z10a^	0.51	2580	0.2115	0.0067	15.5100	0.5500	0.5313	0.0120	0.2610	2904	45	2841	34	2746	52
76-1-z10b^	0.40	*3900*	0.2099	0.0032	16.0800	0.5800	0.5641	0.0220	0.6123	2912	26	2881	44	2883	97
76-3-z19^	0.66	2100	0.2117	0.0037	15.2100	0.3200	0.5187	0.0073	0.8146	2916	20	2826	20	2692	31
76-3-z14a*	0.82	167	0.2620	0.0067	15.6800	0.6900	0.4380	0.0210	0.9332	3258	13	2854	49	2341	100
76-3-z3*	0.74	1520	0.1938	0.0031	8.4400	0.3900	0.3200	0.0150	0.9475	2772	21	2272	46	1785	74
76-3-z17*	0.68	1100	0.2055	0.0048	9.6300	0.3300	0.3464	0.0120	0.4130	2860	69	2396	32	1916	57
76-1-z3*	0.58	1570	0.1875	0.0160	6.7300	2.2000	0.2540	0.0380	0.9658	2714	43	2046	110	1451	150
76-3-z14b*	1.48	589	0.2110	0.0062	8.5700	0.7000	0.2904	0.0240	0.6776	2912	32	2308	130	1643	130
76-1-z9b*	1.95	1220	0.2142	0.0039	6.5100	0.3400	0.2206	0.0120	0.8793	2935	31	2053	41	1284	61
76-2-z11c*	1.51	739	0.2078	0.0056	5.3900	0.2000	0.1860	0.0068	0.9599	2889	29	1865	36	1116	38
76-3-z22b*	2.07	400	0.2302	0.0032	5.7000	0.3100	0.1780	0.0085	0.9778	3054	43	1880	18	1060	36
76-3-z5*	1.65	110	0.2618	0.0068	7.3000	0.7800	0.2140	0.0220	0.9854	3252	52	2080	120	1220	130
76-3-z9*	1.01	114	0.2190	0.0270	1.6800	0.4200	0.0539	0.0140	0.8401	2980	##	990	120	338	84
76-3-z10a*	0.92	229	0.2433	0.0042	3.7600	0.4900	0.1132	0.0140	0.9791	3141	27	1575	75	690	81
76-3-z13*	0.54	394	0.2290	0.0041	16.6200	0.4400	0.5332	0.0094	0.8045	3042	21	2910	25	2753	39
76-3-z12b*	2.22	662	0.2189	0.0037	16.3200	0.5500	0.5410	0.0160	0.8155	2976	19	2900	36	2786	69
76-2-z9b*	0.93	760	0.2041	0.0042	12.4700	0.3700	0.4475	0.0120	0.6944	2858	28	2649	28	2382	54
76-3-z12a*	1.14	815	0.2121	0.0038	13.4300	0.4100	0.4553	0.0086	0.4597	2921	17	2710	27	2419	38
76-1-z2*	0.49	1100	0.1957	0.0160	13.1000	9.3000	0.4833	0.1700	0.2875	2798	39	2685	220	2541	520
76-3-z15*	0.87	1070	0.2062	0.0030	10.8600	0.2600	0.3814	0.0078	0.9132	2875	15	2510	22	2082	36
76-2-z4*	0.48	1160	0.1870	0.0075	9.8300	0.4600	0.3910	0.0110	0.6691	2707	63	2414	43	2126	51
76-2-z11a*	0.46	1340	0.2062	0.0039	11.7400	0.3600	0.4180	0.0130	0.8572	2874	23	2580	28	2250	60
76-3-z21*	0.61	1410	0.2082	0.0037	12.5000	0.3400	0.4370	0.0110	0.8251	2890	18	2640	25	2351	48
76-2-z2a*	1.34	1280	0.2077	0.0040	13.6900	0.6800	0.4900	0.0210	0.8987	2884	27	2731	46	2562	91
76-2-z9a*	0.54	1430	0.2010	0.0051	10.9900	0.4100	0.3950	0.0110	0.7583	2827	35	2514	34	2144	52
76-2-z2b*	0.23	1450	0.1991	0.0029	13.4900	0.3200	0.4924	0.0110	0.7720	2817	18	2713	23	2580	48

Table A2 LA-ICP-MS U-Pb data for zircon in metasedimentary and metagranitoid rocks of the NCGB, NW Ontario

			Isotopic ratios							Ages (Ma)					
	Th/U	$^{206*}Pb/^{204*}Pb$	$^{207*}Pb/^{206*}Pb$	2 σ	$^{207*}Pb/^{235}U$	2 σ	$^{206*}Pb/^{238}U$	2 σ	Err. Corr.	$^{207*}Pb/^{206*}Pb$	1 σ	$^{207*}Pb/^{235}U$	1 σ	$^{206*}Pb/^{238}U$	1 σ
76-3-z18*	0.21	1560	0.2094	0.0032	15.1300	0.8100	0.5330	0.0290	0.9314	2900	20	2821	67	2749	130
76-1-z5b*	0.51	1540	0.2101	0.0035	15.7900	0.2400	0.5425	0.0140	0.7573	2905	17	2862	14	2797	58
76-2-z10b*	0.72	1610	0.2151	0.0053	16.9400	0.5400	0.5470	0.0130	0.7015	2944	31	2934	32	2816	54
76-3-z1*	0.14	4280	0.1927	0.0150	11.9100	5.6000	0.4489	0.1100	0.8092	2765	17	2596	180	2390	360
76-3-z8*	0.83	2270	0.1975	0.0043	12.2400	4.7000	0.4500	0.1600	0.7235	2811	32	2621	150	2396	450

[*] Refers to radiogenic Pb (corrected from common Pb).

Italics denote results applied to obtain upper intercept age or Concordia age.

> Denotes results omitted from NCTK10-8 at >12% discordance, and from NCTK10-24 at >30% discordance.

< Denotes results applied to upper intercept in NCTK10-8 at <12% discordance, or that push the MSWD to 10.9 in NCTK10-24 at >8%.

* Denotes results omitted with $^{207}Pb/^{204}Pb$ <350.

^ Denotes results omitted from metasediment samples, final % discordance >30.

[†] c: core, r: rim.

/ Denotes results applied to older age population in NCB11-33.

APPENDIX 3

U-Th-total Pb methodology

METHODS

I used the Cameca SX-100 electron microprobe at New Mexico Institute of Mining and Technology (NMT, Socorro, USA) to obtain *in situ* U-Th-total Pb ages for <100-μm anhedral resorbed to euhedral monazite grains that exhibit clear microstructural relationships with fabric elements (cf. Williams et al., 1999). The two-part EMPA portion of the investigation involved high-resolution compositional mapping to identify intracrystalline age domains and quantitative chemical analyses of Y, Th, U, and Pb. Monazite grains were identified through manual scanning of rock thin sections noting high Ce-peaks, in addition to using energy dispersion spectra (EDS). Images were collected using high sample current (>200 nA) and small step sizes (~0.5 μm), while rastering the electron beam with the stage fixed (50 ms per pixel resolution of 512 x 512 pixels). Elemental maps were analyzed for distinct chemical domains to identify compositional zones that are likely consequent of monazite re(?)-crystallization. This step is important to determine optimal spot placement and ensure analysis of resolvable age domains; analytical protocol was carried out following Williams and Jercinovic (2002). Matrix corrections were made using the PAP method of Pouchou and Pichoir (1984, 1985). Quantitative trace-element analysis was done using a beam current of 150-200 nA at 15 kV accelerating voltage with a counting time of 700-900 s. To determine the appropriate background levels for Th, Y, Pb, and U the data were processed in BKGII (BackgroundII), a program developed by M. Jercinovic that performs a regression analysis to determine background concentrations. Once concentrations of U, Th, and Pb were obtained, the age equation of Montel et al. (1996) was solved by iteration based on calculated Pb.

REFERENCES

Montel, J.-M., Foret, S., Veschambre, M., Nicollet, C., Provost, A., 1996. Electron microprobe dating of monazite. Chemical Geology 131, 37–53.

Pouchou L., Pichoir, F., 1984. A new model for quantitative X-ray micro-analysis. Part I: application to the analysis of homogeneous samples. La Recherche Aérospatiale 3, 13–38.

Pouchou J.L., Pichoir, F., 1985. "PAP" (phi-ro-z) procedure for improved quantitative microanalysis. In: Armstrong, J.T. (Ed.), Microbeam Analysis. San Francisco Press, San Francisco, pp. 104–106.

Williams, M.L, Jercinovic, M.J., Terry, M.P., 1999. Age mapping and dating of monazite on the electron microprobe: Deconvoluting multistage tectonic histories. Geology 27, 1023–1026.

Williams, M.L., Jercinovic, M.J., 2002. Microprobe monazite geochronology: Putting absolute time into microstructural analysis. Journal of Structural Geology 24, 1013–1028.

Table A3 EMPA U-Th-total Pb data[a] for monazite in metasedimentary rocks of the NCGB, NW Ontario

	Y	Th	U	Pb	Age	Std. Err.
NCTK10-19 ***Ab schist*** *NAD27, zone 15: 692153E, 5821302N*						
19-2-1*	12140	5120	2100	1200	1978	50
19-2-2*	7290	6520	1390	960	1780	50
19-2-3*	8580	6440	1600	1110	1921	50
19-2-4*	8260	7420	1700	1540	2324	50
19-3-5	3050	30320	860	3860	2427	50
19-3-6	3010	28150	960	3610	2399	50
19-3-7	3340	29230	960	3720	2392	50
19-3-8	3340	33760	1030	4330	2427	50
19-3-9	3420	25970	1010	3310	2350	50
19-4-10	4270	42710	1400	5920	2584	50
19-4-11	5110	47020	1590	6260	2484	50
19-4-12	2460	30690	760	3860	2429	50
19-4-13	4600	36960	1130	4650	2384	50
19-4-14	4480	33930	860	4240	2410	50
19-5-15	3510	39130	1020	5260	2570	50
19-5-16*	5420	40720	1290	5910	2703	50
19-5-17	4990	28420	1080	3840	2484	50
19-5-18	3130	29510	960	3820	2431	50
19-5-19	2690	15750	500	1920	2307	50
19-5-20	2680	13850	580	1690	2238	50
NCTK10-26A ***Gt-bt schistose conglomerate*** *NAD27, zone 15: 694428E, 5823783N*						
26A-1-1	11750	92160	2660	12380	2488	50
26A-1-2*	12560	98930	2690	13530	2600	50
26A-1-3	12090	112240	2820	15170	2591	50
26A-1-4	13300	52820	3750	8050	2509	50
26A-1-5	14380	44540	4660	7320	2457	50
26A-1-6	14470	62500	4500	9710	2545	50
26A-1-7	14510	49040	4890	7970	2462	50
26A-3-8	11060	29090	2490	4340	2369	50
26A-3-9	11340	35040	2520	5150	2425	50
26A-3-10	11730	44220	2910	6540	2479	50
26A-5-11	10290	22200	2420	3620	2415	50
26A-5-12	10660	37950	2630	5660	2474	50
26A-5-13	10770	23130	2620	3670	2335	50
26A-7-14	10560	15770	2930	2860	2245	50
26A-7-15	10510	16900	2900	3090	2324	50
26A-7-16	10750	15290	3110	2970	2302	50
26A-8-17	12100	35080	3530	5450	2363	50
26A-8-18	11440	17480	3720	3650	2403	50
26A-8-19	10140	22930	2480	3770	2437	50
26A-8-20	11010	5910	3460	1990	2202	50
26A-8-21	11140	15390	3830	3470	2407	50
26A-9-22	10230	29700	2870	4660	2407	50
26A-9-23	10800	16620	2940	3330	2483	50
26A-10-24	11800	39650	3230	5990	2421	50
26A-10-25*	6400	43600	80	3910	1915	50
26A-10-26	12100	47370	3160	7100	2502	50
26A-10-27	11680	33210	2660	5000	2423	50
26A-10-28	10680	28240	2350	4210	2382	50
26A-11-29	12860	45120	3370	6900	2492	50
26A-11-30	13890	43300	4170	7190	2530	50
26A-11-31	11270	59430	2510	8060	2460	50

Table A3 EMPA U-Th-total Pb data[a] for monazite in metasedimentary rocks of the NCGB, NW Ontario

	Y	Th	U	Pb	Age	Std. Err.
NCTK10-38 *Bt schist* *NAD 83, Zone 15: 673555E, 5843971N*						
38-1-1	9600	28600	2110	4210	2416	50
38-1-2	9970	20700	2490	3750	2572	50
38-1-3	11140	18260	3560	3920	2539	50
38-1-4	10280	17670	3100	3690	2576	50
38-2-5	11420	18300	2530	3400	2524	50
38-2-6	11400	27850	2740	4740	2570	50
38-2-7	10390	44240	2540	6710	2596	50
38-3-8	9760	44640	1270	5520	2363	50
38-3-9	9820	40190	2230	5560	2407	50
38-3-10	9730	32740	2140	4710	2423	50
38-3-11	10660	32750	2800	5380	2576	50
38-1-12	9720	39340	2750	5770	2434	50
38-2-13	11320	17490	2480	3150	2440	50
38-?-14	10440	29910	2680	4790	2494	50
NCTK10-44A *And-st schist* *NAD 83, zone 15: 670289E, 5850342N*						
44A-1-1	10700	30120	3550	5450	2584	50
44A-1-2	10740	40460	3380	6050	2386	50
44A-1-3	12080	41650	3590	6300	2394	50
44A-1-4	11730	33610	3420	5950	2636	50
44A-2-5	12590	72340	3800	9840	2391	50
44A-2-6	10710	34660	2920	5660	2572	50
44A-2-7	11890	56560	3120	7660	2363	50
44A-3-8	11890	45650	3280	7220	2586	50
44A-3-9	11460	44190	3240	7110	2614	50
44A-3-10*	10760	41930	2990	6970	2703	50
44A-3-11	11380	51910	3060	7160	2376	50
44A-3-12	12850	71390	3550	9010	2254	50
44A-3-13	12040	70850	3250	9080	2312	50
44A-4-14	10760	68170	3120	8630	2287	50
44A-4-15	12110	65620	3580	8780	2342	50
44A-5-16	12320	116680	3570	14090	2296	50
44A-5-17	12370	51210	3070	7960	2633	50
44A-6-18	11390	106870	3390	12970	2298	50
44A-6-19	11720	73630	2770	8770	2218	50
44A-6-20	11490	90030	2910	10650	2241	50
44A-1-21	11290	40490	3420	6530	2543	50
44A-1-22	11240	33560	3210	5660	2568	50
44A-1-23	11340	36860	3090	5870	2519	50
44A-1-24	11020	29980	3000	4960	2498	50
44A-3-25	11670	56920	3100	8500	2583	50
44A-3-26	12030	55660	3350	8460	2580	50
44A-4-27	10850	56940	2950	8370	2568	50
44A-5-28	11520	108800	3240	14960	2591	50
44A-5-29	12590	60540	2880	8750	2562	50
44A-5-30	12070	84860	3090	12140	2628	50
NCTK10-51A *Bt schist* *NAD83, zone 16: 312525E, 5819101N*						
51-1-1	11190	24620	5250	5900	2685	50
51-1-2	9560	15960	2510	3170	2563	50
51-2-3	9280	15290	2000	2820	2550	50
51-2-4*	6750	28520	2450	4010	2246	50
51-2-5	10380	46210	4670	7670	2499	50
51-2-6	9770	42430	4180	7160	2551	50

Table A3 EMPA U-Th-total Pb data[a] for monazite in metasedimentary rocks of the NCGB, NW Ontario

	Y	Th	U	Pb	Age	Std. Err.
51-3-7	11540	15490	2310	2990	2546	50
51-3-8	9000	29830	4170	5670	2564	50
51-4-9	8450	26720	3700	5160	2605	50
NCTK10-76 ***Two-mica schist*** *NAD27, zone 15: 702814E, 5821125N*						
76-1-1*	9230	43540	730	6740	3016	50
76-1-2	9500	40660	840	5490	2628	50
76-1-3	9770	44380	690	5230	2360	50
76-1-4	12210	57650	5010	8960	2447	50
76-1-5*	11970	71020	110	9710	2851	50
76-1-6	10960	75330	230	9910	2735	50
76-1-7	18130	73960	2530	9570	2399	50
76-2-8	12930	86230	960	11070	2595	50
76-2-9	9270	63170	880	7810	2481	50
76-2-10	10070	54340	1330	7560	2569	50
76-2-11*	19360	72020	3230	11830	2891	50
76-2-12	10920	86390	1870	12300	2748	50
76-3-13	8030	35830	750	4530	2472	50
76-3-14	10470	53550	190	6940	2692	50
76-3-15	12420	77560	2690	10770	2573	50
76-3-16	10430	132560	990	14940	2329	50
76-4-17	11440	57490	1800	8420	2728	50
76-4-18	10610	52680	1610	7820	2768	50
76-4-19	9370	7610	2590	2280	2638	50
76-5-20	12620	59560	6010	11020	2741	50
NCB11-34 ***Meta-granule conglomerate*** *NAD 27, zone 15: 649138E, 5867125N*						
B34-1-1	5500	26910	950	3420	2370	50
B34-2-2	4250	9770	670	1390	2377	50
B34-2-3	3650	6590	790	970	2154	50
B34-2-4*	3590	9340	390	1280	2486	50
B34-2-5	4130	5370	700	820	2170	50
B34-3-6	3340	14090	790	1900	2348	50
B34-3-7	3710	6270	620	900	2215	50
B34-3-8	3180	14190	570	1790	2318	50
B34-6-9	3560	12280	600	1590	2312	50
B34-6-10	19110	8080	0	830	2193	50
B34-6-11	3620	10210	630	1390	2330	50
B34-6-12	4570	3860	810	740	2250	50

Spot name follows the convention x-y-z;
where x = sample number, y = grain number, and z = spot number.

[a] Elemental data in ppm; age and error in Ma.

* Denotes samples that were not used for determination of age populations.

* Denotes samples that were not used for determination of age populations.

APPENDIX 4

Geochemical analysis of garnet

METHODS

Garnets in two samples were analyzed *in situ* through EMPA with a Cameca SX-100 operated by the Bureau of Geology and Mineral Resources, New Mexico Institute of Mining & Technology (Socorro, USA). The probe is equipped with high-speed, backscatter electron detectors and 3 wavelength dispersive (WD) spectrometers, each outfitted with multiple analyzing crystals, for precise quantitative analysis of a wide range of elemental abundances. Polished thin sections were prepared and treated with a conductive carbon coating to prevent charging during electron bombardment. During analysis, heating of a tungsten filament held at negative potential produced and accelerated electrons toward the sample. A series of magnetic electron lenses focused and concentrated a 15kV, 10nA electron beam to a minimum resolution of 1 μm. Garnets in three additional samples, were analyzed *in situ* at the University of Ottawa (Ottawa, Canada) using the JEOL JXA-8230 SuperProbe which operates in a similar fashion, but with an accelerating voltage of 20 kV and beam current of 20 nA to focus and concentrate the electron beam to a minimum of 1 μm.

Two X-ray maps of Fe, Mg, Mn, Ca, and Y in garnets from the alteration pod in schistose cobble conglomerate (Fig. 15F-K) were produced using both the wavelength dispersive spectrometer (WDS) as well as the energy dispersive spectrometer (EDS) of the JEOL JXA-8230 SuperProbe at the University of Ottawa (Ottawa, Canada). An accelerating voltage of 20 kv and a beam current of 200 nA combined with a spot size of 1 μm to produce one 400 x 400 pixel and one 500 x 500 pixel map each with a 20 μm pixel size and 200 ms dwell time on each pixel.

The garnets from all five samples were also analyzed *in situ* for trace element concentrations using a Photon-Machines Analyte 193 μm ArF excimer laser ablation system

coupled to an Agilent 7700x quadrupole ICP-MS at the Geological Survey of Canada (Ottawa, Canada). Using calcium (^{43}Ca) as an internal standard, with CaO concentrations varying between 2.5 and 5 wt% (as determined from EMPA for each sample), both the cores and rims of garnets were ablated for 60 s, following a 45 s background collection, at a repetition rate of 15 Hz, 40% energy, and a spot size of 52 μm. Two external standards of USGS basaltic glass were analyzed with a spot size of 43 μm, GSD-1G (Guillong et al., 2005, Jochum et al., 2005) twice and BCR-2G (Jochum et al., 2005) once approximately every 20 unknown analyses. A time-resolved plot of signal for each element was integrated and concentrations computed using an on-line data reduction program called GLITTER! (Van Achterberg et al., 2001).

REFERENCES

Guillong, M., Hametner, K., Reusser, E., Wilson, S.A., Günther, D., 2005. Preliminary characterisation of new glass reference materials (GSA-1G, GSC-1G, GSD-1G and GSE-1G) by laser ablation-inductively coupled plasma-mass spectrometry using 193 nm, 213 nm and 266 nm wavelengths. Geostandards and Geoanalytical Research 29, 315–331.

Jochum, K.P., Willbold, M., Raczek, I., Stoll, B., Herwig, K., 2005. Chemical characterization of the USGS reference glasses GSA-1G, GSC-1G, GSE-1G, BCR-2G, BHVO-2G and BIR-1G using EPMA, ID-TIMS, ID-ICP-MS and LA-ICP-MS. Geostandards and Geoanalytical Research 29, 285–302.

Van Achterberg, E., Ryan, C.G., Jackson, S.E., Griffin, W.L., 2001. Data reduction software for LA-ICP-MS In: Appendix, Mineralogical Association of Canada Short Course Series 29, pp. 239–243.

Table A4a EMPA major element geochemistry data for garnet in highly deformed rocks of the NCGB, NW Ontario

	core[a]	mean[b]	rim[c]	core	mean	rim	core	mean	rim
NCTK10-26B ***Grt-bt schistose conglomerate*** *NAD27, zone 15: 694428E, 5823783N*									
Wt %	Grt 1, n: 15			Grt 2, n: 10			Grt 3, n: 15		
SiO_2	36.92	36.51	36.81	36.63	36.55	36.49	36.69	36.60	36.77
TiO_2	0.08	0.05	0.04	0.09	0.05	0.02	0.02	0.06	0.03
Al_2O_3	20.96	20.95	21.00	21.30	21.06	20.82	21.07	21.01	21.10
FeO_T	30.64	31.17	31.69	31.25	31.42	31.72	28.79	29.86	31.55
MnO	6.71	5.86	6.98	5.54	5.60	6.55	8.97	7.43	5.96
MgO	3.60	3.72	2.82	4.17	3.87	2.97	3.33	3.60	3.38
CaO	1.69	1.56	0.98	1.18	1.25	0.99	1.23	1.29	1.25
Cr_2O_3	0.14	0.14	0.16	0.01	0.03	0.13	0.00	0.03	0.06
Total	100.73	99.96	100.48	100.15	99.83	99.69	100.11	99.87	100.09
Number of atoms in formulae (oxygen basis 12)									
Si	2.960	2.949	2.971	2.943	2.952	2.968	2.963	2.959	2.966
Ti	0.005	0.003	0.002	0.005	0.003	0.001	0.001	0.003	0.002
Al	1.980	1.994	1.998	2.017	2.005	1.995	2.005	2.001	2.006
Fe	2.054	2.106	2.139	2.100	2.122	2.157	1.944	2.018	2.128
Mn	0.455	0.400	0.477	0.377	0.383	0.451	0.613	0.509	0.407
Mg	0.430	0.448	0.340	0.499	0.466	0.360	0.401	0.434	0.406
Ca	0.146	0.135	0.084	0.101	0.108	0.086	0.106	0.111	0.108
Cr	0.010	0.010	0.012	0.000	0.002	0.009	0.000	0.002	0.004
Wt %	Grt 4, n: 20			Grt 5, n: 20			Grt 6, n: 19		
SiO_2	36.65	36.59	37.06	36.57	36.58	37.09	36.81	36.58	36.56
TiO_2	0.03	0.08	0.03	0.05	0.07	0.03	0.06	0.06	0.01
Al_2O_3	20.12	20.66	21.02	20.46	20.74	20.78	20.76	20.69	20.96
FeO_T	25.49	28.89	31.68	29.05	29.65	32.30	29.30	29.60	31.72
MnO	11.11	8.60	5.99	8.72	7.76	6.40	8.99	7.98	6.63
MgO	2.48	3.20	3.16	2.89	3.28	3.05	3.22	3.28	2.87
CaO	2.97	1.57	1.21	1.81	1.75	1.06	1.30	1.49	1.06
Cr_2O_3	0.69	0.31	0.10	0.26	0.26	0.47	0.36	0.39	0.23
Total	99.53	99.88	100.23	99.81	100.08	101.18	100.80	100.07	100.03
Number of atoms in formulae (oxygen basis 12)									
Si	2.983	2.964	2.985	2.972	2.958	2.973	2.961	2.959	2.964
Ti	0.002	0.005	0.002	0.003	0.004	0.002	0.004	0.004	0.001
Al	1.930	1.972	1.995	1.959	1.976	1.963	1.968	1.972	2.002
Fe	1.735	1.957	2.133	1.974	2.004	2.165	1.971	2.002	2.150
Mn	0.766	0.591	0.408	0.600	0.532	0.434	0.612	0.547	0.455
Mg	0.301	0.386	0.379	0.350	0.396	0.364	0.386	0.395	0.347
Ca	0.259	0.136	0.105	0.157	0.152	0.091	0.112	0.129	0.092
Cr	0.050	0.022	0.007	0.019	0.018	0.033	0.025	0.028	0.017
	min[d]	**mean**	**max[e]**						
End member composition[†]									
%Prp	9.8%	13.4%	16.8%						
%Sps	10.6%	16.3%	25.3%						
%Grs	2.8%	4.2%	8.5%						
%Alm	56.7%	66.0%	73.1%						

Table A4a EMPA major element geochemistry data for garnet in highly deformed rocks of the NCGB, NW Ontario

	core[a]	**mean**[b]	**rim**[c]	**core**	**mean**	**rim**
NCTK10-16B *Chl schist* *NAD27, zone 15: 690904E, 5821552N*						
Wt %	Tr 1, n: 15			Tr 2, n: 15		
SiO_2	36.32	36.24	36.41	36.03	36.08	35.85
TiO_2	0.01	0.05	0.07	0.06	0.05	0.04
Al_2O_3	20.36	20.38	20.36	20.56	20.52	20.53
FeO_T	37.82	37.96	37.40	37.84	38.05	38.53
MnO	2.61	2.44	2.42	2.65	2.43	2.31
MgO	0.93	0.91	0.67	0.93	0.89	0.84
CaO	1.92	1.99	2.64	1.89	1.96	1.88
Cr_2O_3	0.00	0.00	0.00	0.00	0.00	0.00
Total	99.97	99.97	99.98	99.97	99.98	99.97
Number of atoms in formulae (oxygen basis 12)						
Si	2.987	2.479	2.449	2.431	2.431	2.414
Ti	0.001	0.003	0.004	0.003	0.003	0.002
Al	1.973	1.642	1.614	1.635	1.630	1.629
Fe	2.600	2.170	2.104	2.135	2.144	2.170
Mn	0.182	2.035	2.131	2.162	2.172	2.198
Mg	0.114	0.194	0.265	0.190	0.197	0.189
Ca	0.169	0.175	0.174	0.192	0.175	0.166
Cr	0.00	0.00	0.00	0.00	0.00	0.00
	min[d]	**mean**	**max**[e]			
End member composition[†]						
%Prp	3.7%	7.3%	9.9%			
%Sps	4.7%	5.2%	5.8%			
%Grs	5.5%	6.6%	7.3%			
%Alm	78.5%	80.9%	82.0%			

Table A4a EMPA major element geochemistry data for garnet in highly deformed rocks of the NCGB, NW Ontario

	core[a]	**mean**[b]	**rim**[c]	**core**	**mean**	**rim**	**core**	**mean**	**rim**
E591 479 ***Grt schist*** *NAD83, zone 15: 664565E, 5867407N*									
Wt %	Grt 1, n: 14			Grt 2, n: 25			Grt 4, n: 26		
SiO_2	37.08	37.15	37.02	37.94	37.33	37.17	37.34	37.33	39.04
TiO_2	0.01	0.02	0.00	0.02	0.02	-0.01	0.02	0.06	0.01
Al_2O_3	21.33	21.61	21.37	20.97	21.38	21.64	21.22	v	19.86
FeO_T	29.35	30.12	32.25	30.69	31.09	32.12	30.20	30.34	32.76
MnO	4.41	3.18	3.04	2.14	2.11	2.40	3.56	2.86	3.23
MgO	4.82	5.12	4.07	5.75	5.77	5.01	5.00	5.07	4.61
CaO	3.11	2.82	2.08	2.22	2.34	2.00	2.93	3.06	1.95
Cr_2O_3	NA[f]	NA	NA	NA	NA	NA	NA	NA	NA
Total	100.12	100.00	99.82	99.73	100.06	100.38	99.82	99.82	99.82
Number of atoms in formulae (oxygen basis 12)									
Si	2.953	2.951	2.969	3.007	2.959	2.951	2.966	2.959	3.076
Ti	0.001	0.001	0.000	0.001	0.001	-0.001	0.001	0.004	0.000
Al	2.001	2.023	2.020	1.959	1.997	2.025	1.987	2.009	1.844
Fe	1.954	2.001	2.163	2.034	2.060	2.132	2.006	2.011	2.159
Mn	0.298	0.214	0.207	0.144	0.142	0.161	0.239	0.192	0.215
Mg	0.572	0.607	0.486	0.679	0.682	0.593	0.592	0.599	0.541
Ca	0.265	0.240	0.178	0.188	0.199	0.170	0.249	0.260	0.165
Cr	NA	NA	NA	NA	NA	NA	NA	NA	NA
Wt %	Grt 5, n: 26								
SiO_2	37.55	37.37	37.66						
TiO_2	0.02	0.02	0.02						
Al_2O_3	21.32	21.39	21.68						
FeO_T	30.08	30.19	32.12						
MnO	3.61	3.44	2.49						
MgO	5.29	5.25	5.00						
CaO	2.47	2.61	2.16						
Cr_2O_3	NA	NA	NA						
Total	99.82	99.82	99.82						
Number of atoms in formulae (oxygen basis 12)									
Si	2.972	2.962	2.967						
Ti	0.001	0.001	0.001						
Al	1.988	1.998	2.012						
Fe	1.990	2.001	2.115						
Mn	0.242	0.231	0.166						
Mg	0.624	0.620	0.587						
Ca	0.209	0.222	0.182						
Cr	NA	NA	NA						
	min[d]	**mean**	**max**[e]						
End member composition[†]									
%Prp	13.8%	20.5%	23.0%						
%Sps	4.4%	6.3%	11.3%						
%Grs	5.3%	7.4%	10.4%						
%Alm	60.8%	65.8%	73.0%						

Table A4a EMPA major element geochemistry data for garnet in highly deformed rocks of the NCGB, NW Ontario

	core[a]	**mean**[b]	**rim**[c]	**core**	**mean**	**rim**	**core**	**mean**	**rim**
NCB11-24 ***Grt-bt schist*** *NAD27, zone 15: 646720E, 5871092N*									
Wt %	Grt 1, n: 30			Grt 2, n: 27			Grt 3, n: 30		
SiO_2	34.89	36.37	40.90	35.60	36.30	36.50	36.10	36.27	36.50
TiO_2	0.01	0.06	0.13	0.00	0.05	0.12	0.02	0.07	0.14
Al_2O_3	18.91	20.92	21.11	20.81	21.16	21.32	20.90	21.12	21.31
FeO_T	31.91	33.58	35.83	30.61	33.00	34.35	35.32	36.27	37.50
MnO	1.88	2.75	3.25	1.82	2.69	3.59	1.03	1.32	2.19
MgO	1.65	2.01	3.19	1.62	2.08	2.57	1.59	2.14	2.34
CaO	1.98	4.00	5.83	3.11	4.25	6.25	2.25	2.51	2.96
Cr_2O_3	NA[f]	NA	NA	NA	NA	NA	NA	NA	NA
Total	98.24	99.71	100.17	98.68	99.55	100.03	99.18	99.73	100.34
Number of atoms in formulae (oxygen basis 12)									
Si	2.883	2.958	3.256	2.936	2.950	2.960	2.942	2.954	2.965
Ti	0.001	0.004	0.008	0.000	0.003	0.007	0.001	0.004	0.008
Al	1.774	2.005	2.048	2.014	2.027	2.041	2.006	2.027	2.043
Fe	2.160	2.284	2.466	2.080	2.243	2.331	2.423	2.470	2.550
Mn	0.129	0.190	0.225	0.125	0.186	0.247	0.071	0.091	0.152
Mg	0.199	0.244	0.393	0.196	0.252	0.310	0.194	0.259	0.284
Ca	0.169	0.349	0.506	0.275	0.370	0.544	0.196	0.219	0.260
Cr	NA	NA	NA	NA	NA	NA	NA	NA	NA
	min[d]	**mean**	**max**[e]						
End member composition[†]									
%Prp	6.4%	8.2%	12.5%						
%Sps	2.3%	5.1%	8.1%						
%Grs	6.0%	10.2%	17.8%						
%Alm	68.3%	76.5%	83.9%						

Table A4a EMPA major element geochemistry data for garnet in highly deformed rocks of the NCGB, NW Ontario

	core[a]	**mean**[b]	**rim**[c]
NCB11-28 *Hbl schist* *NAD27, zone 15: 638553E, 5871489N*			
Wt %		Grt 1, n: 20	
SiO_2	36.817	36.90	37.195
TiO_2	0.117	0.07	0.023
Al_2O_3	20.846	20.85	20.784
FeO_T	29.387	29.58	28.832
MnO	6.906	6.14	6.08
MgO	2.25	2.47	2.619
CaO	3.672	3.87	4.367
Cr_2O_3	NA[f]	NA	NA
Total	99.998	99.90	99.924
Number of atoms in formulae (oxygen basis 12)			
Si	2.97761	2.981	2.99471
Ti	0.00712	0.004	0.00139
Al	1.98688	1.985	1.9721
Fe	1.98737	1.998	1.9411
Mn	0.47303	0.420	0.41458
Mg	0.27129	0.297	0.31436
Ca	0.31816	0.334	0.37668
Cr	NA	NA	NA
	min[d]	**mean**	**max**[e]
End member composition[†]			
%Prp	8.9%	9.7%	10.7%
%Sps	12.4%	13.8%	15.5%
%Grs	10.1%	11.0%	12.4%
%Alm	63.7%	65.5%	66.1%

[a] Values from the single spot at the core of the garnet.
[b] Average of values from the core to the rim of the garnet.
[c] Values from the single spot at the rim of the garnet.
[d] Minimum value.
[e] Maximum value.
[f] NA: not applicable, garnet was not analyzed for chromium.
[†] Calculated as follows:
%Prp = Mg/(Mg+Fe+Mn+Ca)
%Sps = Mn/(Mg+Fe+Mn+Ca)
%Grs = Ca/(Mg+Fe+Mn+Ca)
%Alm = Fe/(Mg+Fe+Mn+Ca)

Table A4b LA-ICP-MS trace element data (ppm) for garnet in highly deformed rocks of the NCGB, NW Ontario

NCTK10-26B ***Grt-bt schistose conglomerate*** *NAD27, zone 15: 694428E, 5823783N*

ppm[a]	**4COR**	**4RIM**	**5COR**	**5RIM**	**5RIM**	**7RIM**	**7RIM**	**7COR**	**6COR**	**6RIM**
La	0.030	BDL	BDL	BDL	BDL	BDL	BDL	BDL	BDL	BDL
Ce	0.032	0.006	0.008	BDL	0.010	0.011	0.011	0.005	0.004	BDL
Pr	0.065	0.051	0.089	BDL	0.072	0.080	0.045	0.104	0.045	0.068
Nd	0.439	0.383	0.590	0.038	0.524	0.501	0.343	0.670	0.191	0.169
Sm	10.36	8.99	11.39	1.43	9.77	11.70	9.67	13.53	6.90	7.04
Eu	13.97	13.60	17.09	2.28	15.69	17.97	14.35	18.80	10.78	9.95
Gd	60.20	28.89	38.53	24.07	33.92	34.21	29.16	50.63	72.46	53.52
Tb	94.38	29.16	51.43	63.89	45.64	32.78	23.12	45.37	180.61	110.64
Dy	130.34	23.58	65.91	132.11	53.69	28.76	15.22	33.93	370.57	167.91
Ho	137.48	12.74	64.82	174.76	48.03	19.03	8.22	15.48	569.27	170.98
Er	144.27	7.60	65.47	193.55	44.03	15.02	5.65	7.25	847.49	167.15
Tm	121.83	5.25	55.08	180.77	36.94	10.93	3.79	3.86	986.11	150.53
Yb	113.02	4.30	50.71	163.91	33.81	9.26	3.36	2.34	1106.58	141.96
Lu	88.43	3.32	36.51	139.14	19.79	6.26	3.23	1.10	1209.20	97.81
Y	187.94	19.79	87.28	177.65	59.20	24.90	11.37	26.43	665.18	235.27

NCTK10-16B[b] ***Chl schist*** *NAD27, zone 15: 690904E, 5821552N*

ppm	**1**	**4**	**5**	**6**	**7**	**8**
La	0.489	0.043	0.026	0.007	BDL	BDL
Ce	0.298	0.045	0.042	0.000	0.003	0.021
Pr	0.323	0.138	0.164	0.039	0.042	0.044
Nd	0.521	0.355	0.545	0.254	0.406	0.583
Sm	8.30	9.55	10.35	9.23	9.59	9.64
Eu	10.40	8.71	8.08	9.31	8.96	8.88
Gd	45.64	54.11	55.57	64.38	58.56	45.61
Tb	66.79	87.31	82.00	116.15	95.77	67.04
Dy	87.94	118.21	119.50	181.84	143.93	88.77
Ho	79.49	120.97	131.40	210.86	178.16	98.40
Er	74.08	128.33	151.26	264.06	221.28	111.78
Tm	59.19	118.91	139.43	260.38	215.08	110.80
Yb	47.98	106.51	128.03	256.94	225.71	94.63
Lu	33.90	95.44	110.48	244.57	214.43	88.85
Y	109.65	155.19	172.14	271.86	224.98	127.40

Table A4b LA-ICP-MS trace element data (ppm) for garnet in highly deformed rocks of the NCGB, NW Ontario

E591 479 ***Grt schist*** *NAD83, zone 15: 664565E, 5867407N*

ppm[a]	**5RIM**	**5COR**	**2RIM**	**2COR**	**1RIM**	**1COR**
La	BDL	0.032	BDL	0.011	0.012	0.007
Ce	0.004	0.042	0.003	0.016	0.010	0.008
Pr	0.014	0.060	0.016	0.056	0.031	0.053
Nd	0.209	0.304	0.182	0.248	0.187	0.237
Sm	5.57	5.02	5.52	4.46	6.66	4.47
Eu	7.92	6.53	12.55	5.77	13.89	6.50
Gd	20.62	20.76	16.91	20.16	34.80	16.07
Tb	18.99	25.25	10.69	29.25	39.60	14.88
Dy	17.73	23.87	8.17	36.06	42.30	11.58
Ho	14.86	14.72	5.22	38.61	42.11	5.81
Er	13.61	9.60	4.04	44.89	40.38	3.59
Tm	11.98	5.93	3.54	50.72	35.67	2.63
Yb	10.76	4.17	2.86	58.74	32.91	2.21
Lu	9.82	2.58	2.23	63.49	30.48	1.86
Y	15.70	19.82	6.92	45.21	42.20	7.44

NCB11-24 ***Grt-bt schist*** *NAD27, zone 15: 646720E, 5871092N*

ppm	**1RIM**	**1COR**	**2RIM**	**2COR1**	**2COR2**	**3RIM**	**3COR1**	**3COR2**	**3COR3**
La	0.012	0.007	0.077	0.100	0.039	BDL	0.013	0.089	0.023
Ce	0.012	0.020	0.100	0.085	0.044	0.006	0.013	0.088	0.030
Pr	0.148	0.119	0.135	0.131	0.090	0.035	0.072	0.102	0.105
Nd	0.504	0.711	0.281	0.311	0.255	0.349	0.414	0.284	0.419
Sm	2.39	3.25	2.33	2.02	2.84	6.18	4.24	4.45	4.47
Eu	13.56	15.60	6.73	7.62	7.68	7.36	6.96	6.88	9.27
Gd	4.06	4.23	14.14	12.17	16.01	35.65	11.39	18.40	14.76
Tb	4.33	3.96	23.75	18.20	23.30	47.61	12.01	24.45	17.52
Dy	4.91	4.71	36.16	24.49	30.14	58.40	13.49	28.62	20.09
Ho	4.78	4.78	41.76	27.29	32.07	55.77	13.04	26.42	19.27
Er	5.48	5.23	48.65	29.95	33.57	52.32	14.65	24.93	20.16
Tm	4.99	4.59	48.57	27.20	31.28	41.39	12.40	21.64	19.25
Yb	5.16	4.53	49.28	25.23	27.89	34.71	11.26	19.33	16.41
Lu	5.04	4.13	49.93	23.08	25.33	27.96	11.72	17.04	14.34
Y	6.46	5.78	55.99	32.26	38.92	61.73	16.25	32.42	23.82

Table A4b LA-ICP-MS trace element data (ppm) for garnet in highly deformed rocks of the NCGB, NW Ontario

NCB11-28 *Hbld schist* *NAD27, zone 15: 638553E, 5871489N*

ppm[a]	**RIM1**	**COR1**	**COR2**	**RIM2**
La	0.025	0.013	BDL	0.007
Ce	0.080	0.016	0.003	0.081
Pr	0.088	0.066	0.039	0.045
Nd	0.264	0.358	0.337	0.237
Sm	6.08	8.24	9.30	5.25
Eu	7.63	11.02	12.82	7.11
Gd	30.85	39.95	56.89	33.56
Tb	40.97	45.86	72.99	49.61
Dy	54.24	56.78	92.50	72.07
Ho	65.18	66.31	100.36	89.54
Er	81.53	83.23	112.46	112.40
Tm	91.19	88.91	113.07	121.05
Yb	104.27	101.44	119.13	132.27
Lu	123.49	123.10	127.01	140.99
Y	63.44	62.93	97.46	88.65

[a] BDL: below detection limit

[b] This sample is inclusion-rich and could not be differentiated by core and rim.

APPENDIX 5

Geochemistry of fabric forming minerals

METHODS

The JEOL JXA-8230 SuperProbe at the University of Ottawa (Ottawa, Canada) was also used for *in situ* EMPA of chlorite and micas in ten metasedimentary rock samples from in and around the Markop Lake deformation zone as well as the North Caribou-Totogan shear zone. Fabric forming minerals were first identified, and important microstructural context observed with the JEOL 6610LV SEM at the University of Ottawa. Analyses across the contact of chlorite-white mica and chlorite-biotite pairs, as well as analyses of select individual crystals in the matrix, were conducted with an accelerating voltage of 15 kV and probe current of 20 nA to focus and concentrate the beam to a minimum of 5 μm.

Table A5a EMPA major element geochemistry results for white mica in metasedimentary rocks of the NCGB, NW Ontario

	min[a]	mean[b]	max[c]	min	mean	max	min	mean	max
White mica	NCTK10-12B			NCTK10-15			NCTK10-16A		
Wt%[d]	n: 36			n: 31			n: 23		
SiO_2	42.46	45.21	46.70	44.65	46.97	49.02	41.71	45.64	47.04
TiO_2	0.26	0.40	2.28	0.33	0.90	1.88	0.13	0.23	0.34
Al2O3	31.08	34.11	35.51	31.33	33.09	34.51	33.87	35.88	37.03
Al_2O_3	2.00	3.21	8.15	1.54	1.92	4.38	1.26	1.98	7.54
FeO_T	BDL	0.02	0.08	BDL	0.19	1.92	BDL	0.01	0.05
MgO	0.47	0.77	1.89	0.96	1.43	2.52	0.25	0.40	1.38
CaO	BDL	BDL	BDL	BDL	BDL	BDL	BDL	BDL	BDL
Na_2O	0.27	0.53	0.68	0.20	0.26	0.33	0.58	0.83	1.15
K_2O	9.32	10.09	10.60	9.62	10.61	11.08	8.23	9.42	10.01
F	BDL	0.03	0.10	BDL	0.07	0.16	0.06	0.14	0.31
Cl	BDL	0.01	0.07	BDL	0.00	0.02	BDL	0.00	0.02
Total	91.40	94.38	95.38	93.68	95.44	96.34	92.95	94.54	95.79
Ions on the basis of 22 positive charges									
Si	2.952	3.067	3.152	3.022	3.137	3.228	2.907	3.058	3.125
Ti	0.013	0.020	0.117	0.017	0.045	0.094	0.006	0.012	0.017
Al	2.550	2.727	2.860	2.483	2.604	2.701	2.761	2.834	2.937
Fe	0.111	0.183	0.474	0.085	0.107	0.248	0.072	0.112	0.440
Mn	BDL	0.001	0.005	BDL	0.011	0.110	BDL	0.001	0.003
Mg	0.047	0.079	0.196	0.095	0.143	0.255	0.025	0.040	0.143
Ca	BDL	BDL	BDL	BDL	BDL	BDL	BDL	BDL	BDL
Na	0.036	0.070	0.091	0.026	0.033	0.042	0.078	0.108	0.149
K	0.821	0.873	0.910	0.830	0.904	0.953	0.732	0.805	0.855
F	BDL	0.006	0.021	BDL	0.015	0.034	0.000	0.000	0.000
Cl	BDL	0.001	0.008	BDL	0.000	0.002	BDL	0.000	0.000
Cation site distribution									
Si	2.952	3.067	3.152	3.022	3.137	3.228	2.907	3.058	3.125
Ti	0.013	0.020	0.117	0.017	0.045	0.094	0.006	0.012	0.017
Al(IV)	0.848	0.932	1.048	0.772	0.862	0.978	0.875	0.941	1.082
Al(VI)	1.560	1.795	1.870	1.630	1.743	1.824	1.700	1.893	1.942
Mg(M2)	0.031	0.056	0.135	0.073	0.116	0.159	0.014	0.025	0.073
Fe(M2)	0.082	0.129	0.295	0.059	0.087	0.155	0.034	0.070	0.224
Mn(M2)	0.000	0.001	0.005	0.000	0.011	0.110	0.000	0.001	0.003
Mg(M1)	0.009	0.023	0.067	0.010	0.027	0.096	0.007	0.015	0.070
Fe(M1)	0.023	0.054	0.179	0.007	0.021	0.093	0.020	0.042	0.216
v(M1)	0.754	0.923	0.966	0.811	0.953	0.983	0.714	0.944	0.972
K(A)	0.821	0.873	0.910	0.830	0.904	0.953	0.732	0.805	0.855
Na(A)	0.036	0.070	0.091	0.026	0.033	0.042	0.078	0.108	0.149
v(A)	0.011	0.057	0.113	0.017	0.063	0.136	0.047	0.086	0.190
End member composition									
%Musc	75.18%	84.12%	87.34%	82.99%	88.56%	91.78%	75.98%	82.70%	85.65%
%Parag	3.31%	6.74%	9.20%	2.48%	3.25%	4.24%	8.14%	11.12%	15.49%
%Fe-Celad	4.24%	7.57%	17.14%	4.06%	6.12%	10.15%	1.56%	3.69%	11.75%
%Pyroph	0.29%	1.56%	2.98%	0.51%	2.07%	3.90%	1.29%	2.48%	4.13%

Table A5a EMPA major element geochemistry results for white mica in metasedimentary rocks of the NCGB, NW Ontario

	min[a]	mean[b]	max[c]	min	mean	max	min	mean	max
White mica	NCTK10-20A			NCTK10-51A			NCTK10-74A		
Wt%[d]	n: 28			n: 23			n: 17		
SiO_2	44.00	46.39	47.71	44.29	45.39	46.17	44.41	47.09	49.65
TiO_2	0.43	0.49	0.62	0.33	0.40	0.57	0.11	0.65	2.02
Al_2O_3	33.74	35.06	35.93	32.86	35.22	36.15	27.77	33.34	35.27
FeO_T	0.90	1.47	3.50	1.27	1.90	3.69	0.99	1.83	4.83
MnO	BDL	0.02	0.04	BDL	0.02	0.04	0.00	0.03	0.11
MgO	0.71	1.08	2.78	0.39	0.75	1.54	1.06	1.93	5.77
CaO	BDL	BDL	BDL	BDL	BDL	BDL	BDL	0.04	0.63
Na_2O	0.49	0.59	0.84	0.47	0.70	0.96	0.05	0.22	0.29
K_2O	7.88	9.83	10.50	9.25	9.99	10.38	8.45	10.45	11.13
F	BDL	0.04	0.15	BDL	0.03	0.09	BDL	0.06	0.13
Cl	BDL	0.01	0.16	BDL	0.00	0.01	BDL	0.00	0.01
Total	93.40	94.97	95.89	93.17	94.36	94.81	94.16	95.66	96.31
Ions on the basis of 22 positive charges									
Si	2.998	3.089	3.137	3.014	3.055	3.099	3.040	3.131	3.322
Ti	0.022	0.025	0.031	0.017	0.020	0.029	0.006	0.032	0.102
Al	2.691	2.751	2.805	2.671	2.794	2.858	2.190	2.611	2.748
Fe	0.050	0.082	0.199	0.071	0.107	0.213	0.054	0.103	0.273
Mn	BDL	0.001	0.003	BDL	0.001	0.002	BDL	0.002	0.007
Mg	0.070	0.108	0.282	0.039	0.076	0.158	0.105	0.193	0.589
Ca	BDL	BDL	BDL	BDL	BDL	BDL	BDL	0.003	0.045
Na	0.063	0.076	0.107	0.061	0.091	0.124	0.007	0.029	0.037
K	0.681	0.835	0.889	0.800	0.858	0.887	0.737	0.886	0.935
F	BDL	0.009	0.031	BDL	0.006	0.018	BDL	0.013	0.027
Cl	BDL	0.001	0.018	BDL	0.000	0.001	BDL	0.000	0.001
Cation site distribution									
Si	2.998	3.089	3.137	3.014	3.055	3.099	3.040	3.131	3.322
Ti	0.022	0.025	0.031	0.017	0.020	0.029	0.006	0.032	0.102
Al(IV)	0.849	0.910	1.002	0.901	0.944	0.986	0.678	0.863	0.960
Al(VI)	1.720	1.841	1.881	1.726	1.850	1.914	1.476	1.748	1.847
Mg(M2)	0.055	0.076	0.150	0.030	0.054	0.105	0.079	0.146	0.361
Fe(M2)	0.037	0.058	0.106	0.048	0.076	0.142	0.046	0.078	0.171
Mn(M2)	0.000	0.001	0.003	0.000	0.001	0.002	0.000	0.002	0.007
Mg(M1)	0.006	0.031	0.133	0.008	0.022	0.058	0.005	0.047	0.242
Fe(M1)	0.004	0.024	0.094	0.012	0.031	0.079	0.002	0.025	0.112
v(M1)	0.774	0.945	0.990	0.863	0.947	0.979	0.646	0.929	0.993
K(A)	0.681	0.835	0.889	0.800	0.858	0.887	0.737	0.886	0.935
Na(A)	0.063	0.076	0.107	0.061	0.091	0.124	0.007	0.029	0.037
v(A)	0.033	0.089	0.252	0.023	0.051	0.107	0.033	0.085	0.245
End member composition									
%Musc	78.08%	85.97%	88.20%	81.54%	85.35%	88.03%	77.16%	88.34%	92.67%
%Parag	6.45%	7.83%	10.68%	6.10%	9.03%	12.51%	0.60%	2.87%	3.76%
%Fe-Celad	2.07%	3.45%	6.32%	2.48%	4.20%	8.64%	3.00%	6.00%	14.57%
%Pyroph	1.00%	2.76%	7.95%	0.65%	1.42%	2.80%	1.06%	2.79%	6.94%

Table A5a EMPA major element geochemistry results for white mica in metasedimentary rocks of the NCGB, NW Ontario

	min[a]	mean[b]	max[c]	min	mean	max
White mica	NCTK10-75			NCTK10-76		
Wt%[d]	n: 38			n: 37		
SiO_2	42.46	45.17	46.70	44.97	45.98	48.76
TiO_2	0.26	0.39	2.28	0.51	0.62	0.74
Al_2O_3	31.08	34.06	35.51	32.47	34.44	35.44
FeO_T	2.00	3.24	8.15	1.55	1.89	2.90
MnO	BDL	0.02	0.08	BDL	0.01	0.04
MgO	0.47	0.78	1.89	0.59	0.81	1.37
CaO	BDL	BDL	BDL	BDL	BDL	BDL
Na_2O	0.27	0.54	0.83	0.38	0.55	0.71
K_2O	9.32	10.08	10.60	9.87	10.33	10.71
F	BDL	0.03	0.10	BDL	0.03	0.11
Cl	BDL	0.01	0.16	BDL	0.00	0.03
Total	91.40	94.32	95.38	94.00	94.62	95.72
Ions on the basis of 22 positive charges						
Si	2.952	3.068	3.152	3.052	3.090	3.240
Ti	0.013	0.020	0.117	0.025	0.032	0.038
Al	2.550	2.725	2.860	2.543	2.727	2.796
Fe	0.111	0.185	0.474	0.087	0.106	0.164
Mn	BDL	0.001	0.005	BDL	0.001	0.002
Mg	0.047	0.079	0.196	0.059	0.081	0.138
Ca	BDL	BDL	BDL	BDL	BDL	BDL
Na	0.036	0.071	0.110	0.049	0.072	0.093
K	0.821	0.873	0.910	0.849	0.885	0.925
F	BDL	0.006	0.021	BDL	0.007	0.024
Cl	BDL	0.001	0.019	BDL	0.001	0.003
Cation site distribution						
Si	2.952	3.068	3.152	3.052	3.090	3.240
Ti	0.013	0.020	0.117	0.025	0.032	0.038
Al(IV)	0.848	0.932	1.048	0.760	0.909	0.948
Al(VI)	1.560	1.793	1.870	1.755	1.818	1.853
Mg(M2)	0.031	0.056	0.135	0.045	0.065	0.105
Fe(M2)	0.082	0.130	0.295	0.068	0.085	0.122
Mn(M2)	0.000	0.001	0.005	0.000	0.001	0.002
Mg(M1)	0.009	0.023	0.067	0.005	0.016	0.035
Fe(M1)	0.023	0.055	0.179	0.006	0.021	0.044
v(M1)	0.754	0.922	0.966	0.921	0.963	0.989
K(A)	0.821	0.873	0.910	0.849	0.885	0.925
Na(A)	0.036	0.071	0.110	0.049	0.072	0.093
v(A)	0.011	0.056	0.113	0.018	0.043	0.096
End member composition[†]						
%Musc	75.18%	83.97%	87.34%	83.41%	86.57%	88.67%
%Parag	3.31%	6.82%	10.34%	4.76%	7.03%	9.00%
%Fe-Celad	4.24%	7.65%	17.14%	3.75%	5.11%	8.02%
%Pyroph	0.29%	1.55%	2.98%	0.49%	1.29%	3.81%

[a] Minimum value. [b] Average of values from all analyses. [c] Maximum value.
[d] BDL: below detection limit. [†] Calculated from activity determined following Parra et al. (2002).

Table A5b EMPA major element geochemistry results for chlorite in metasedimentary rocks of the NCGB, NW Ontario

	min[a]	mean[b]	max[c]	min	mean	max	min	mean	max
Chlorite	NCTK10-12B			NCTK10-15			NCTK10-16A		
Wt%[d]	n: 26			n: 21			n: 24		
SiO_2	26.32	27.00	27.65	19.86	27.12	28.79	22.26	23.20	24.08
TiO_2	0.00	0.12	0.36	0.02	0.16	0.82	0.03	0.09	0.24
Al_2O_3	19.03	20.30	21.44	15.40	18.87	20.35	21.87	22.89	23.43
FeO_T	23.37	24.61	25.32	20.03	24.49	26.24	31.91	34.11	36.29
MnO	0.20	0.64	1.60	0.32	0.42	0.56	0.12	0.18	0.21
MgO	14.28	14.72	15.45	10.89	15.10	16.44	6.09	7.25	8.06
CaO	0.00	0.07	0.26	BDL	0.07	0.35	BDL	0.02	0.05
Na_2O	BDL	0.02	0.06	BDL	0.05	0.59	BDL	0.02	0.07
K_2O	0.00	0.09	0.45	0.01	0.14	0.93	BDL	0.03	0.08
F	BDL	0.04	0.14	BDL	0.04	0.20	BDL	0.01	0.07
Cl	BDL	0.01	0.03	BDL	0.03	0.31	BDL	0.02	0.05
Total	86.63	87.60	88.36	67.07	86.50	88.41	85.63	87.80	88.89
Ions on the basis of 28 positive char									
Si	2.755	2.836	2.897	2.766	2.888	3.029	2.476	2.567	2.639
Ti	0.000	0.009	0.028	0.001	0.013	0.064	0.003	0.007	0.020
Al	2.354	2.513	2.642	2.199	2.372	2.529	2.860	2.985	3.071
Fe	2.036	2.162	2.219	2.051	2.183	2.332	2.999	3.156	3.381
Mn	0.017	0.057	0.143	0.029	0.038	0.050	0.011	0.017	0.020
Mg	2.237	2.305	2.412	2.243	2.396	2.553	1.010	1.195	1.343
Ca	0.000	0.007	0.029	BDL	0.008	0.040	BDL	0.002	0.006
Na	BDL	0.004	0.012	BDL	0.011	0.121	BDL	0.003	0.016
K	0.000	0.012	0.059	0.001	0.019	0.124	BDL	0.004	0.011
F	BDL	0.012	0.047	BDL	0.014	0.086	BDL	0.003	0.026
Cl	BDL	0.002	0.006	BDL	0.005	0.055	BDL	0.003	0.009
Cation site distribution									
Si(T1)	1.837	1.891	1.931	1.844	1.925	2.019	1.651	1.711	1.759
Si(T2)	0.918	0.945	0.966	0.922	0.963	1.010	0.825	0.856	0.880
Al(T2) (IV)	1.103	1.164	1.245	0.971	1.112	1.234	1.361	1.433	1.524
Al(M4)	1.000	1.000	1.000	1.000	1.000	1.000	1.000	1.000	1.000
Fe(M1)	0.295	0.314	0.322	0.297	0.317	0.338	0.435	0.458	0.490
Mg(M1)	0.324	0.334	0.350	0.325	0.347	0.370	0.146	0.173	0.195
Al(M1) (VI)	0.111	0.169	0.227	0.042	0.175	0.223	0.237	0.272	0.316
v(M1)	0.123	0.183	0.235	0.102	0.161	0.313	0.041	0.097	0.141
Mg(M2+M3)	1.913	1.971	2.062	1.917	2.049	2.183	0.863	1.022	1.148
Fe(M2+M3)	1.740	1.849	1.898	1.754	1.867	1.994	2.565	2.698	2.891
Al(M2+M3)	0.112	0.180	0.241	0.012	0.085	0.217	0.210	0.280	0.351
End member composition[†]									
%Daph	26.93%	37.13%	42.41%	22.79%	35.08%	48.61%	96.38%	97.96%	99.39%
%Clin	46.35%	51.00%	59.24%	41.57%	55.41%	68.16%	0.24%	0.88%	1.74%
%Mg-Am	5.33%	7.94%	12.39%	1.85%	8.06%	10.64%	0.22%	0.54%	0.98%
%Mg-Sud	1.79%	3.93%	8.26%	0.01%	1.46%	9.63%	0.07%	0.61%	1.19%

Table A5b EMPA major element geochemistry results for chlorite in metasedimentary rocks of the NCGB, NW Ontario

	min[a]	mean[b]	max[c]	min	mean	max	min	mean	max
Chlorite	NCTK10-20A			NCTK10-26A			NCTK10-51A		
Wt%[d]	n: 40			n: 8			n: 29		
SiO_2	24.95	25.72	27.54	24.26	25.08	25.89	24.79	26.27	29.77
TiO_2	0.04	0.11	0.32	0.07	0.07	0.07	0.05	0.12	0.54
Al_2O_3	22.28	23.37	24.01	22.08	22.55	23.02	17.50	21.24	23.82
FeO_T	19.54	20.28	21.47	20.22	20.75	21.29	21.51	23.22	26.12
MnO	0.24	0.32	0.36	0.39	0.41	0.43	0.31	0.43	0.51
MgO	16.07	16.75	17.21	15.73	16.24	16.75	14.82	15.94	16.56
CaO	BDL	0.02	0.08	0.02	0.03	0.05	BDL	BDL	0.29
Na_2O	BDL	0.03	0.40	0.00	0.00	0.01	BDL	0.01	0.05
K_2O	0.00	0.16	0.70	0.11	0.17	0.23	BDL	0.16	0.74
F	BDL	0.02	0.09	0.09	0.09	0.09	BDL	0.01	0.07
Cl	BDL	0.02	0.33	0.00	0.01	0.01	BDL	0.00	0.01
Total	85.62	86.81	88.05	83.01	85.36	87.71	85.43	87.43	88.27
Ions on the basis of 28 positive char									
Si	2.605	2.662	2.788	2.643	2.656	2.669	2.576	2.746	3.071
Ti	0.003	0.009	0.025	0.005	0.005	0.005	0.004	0.010	0.042
Al	2.736	2.850	2.955	2.795	2.815	2.835	2.213	2.615	2.917
Fe	1.686	1.755	1.876	1.834	1.838	1.842	1.881	2.030	2.314
Mn	0.021	0.028	0.032	0.034	0.037	0.039	0.028	0.038	0.045
Mg	2.478	2.584	2.649	2.555	2.564	2.573	2.341	2.483	2.571
Ca	BDL	0.002	0.008	0.002	0.004	0.005	BDL	0.003	0.033
Na	BDL	0.006	0.081	0.000	0.001	0.001	BDL	0.002	0.009
K	0.000	0.022	0.092	0.016	0.023	0.030	BDL	0.022	0.098
F	BDL	0.007	0.028	0.028	0.029	0.031	BDL	0.003	0.023
Cl	BDL	0.003	0.057	BDL	0.001	0.002	BDL	0.001	0.003
Cation site distribution									
Si(T1)	1.737	1.775	1.859	1.762	1.771	1.779	1.717	1.831	2.047
Si(T2)	0.868	0.887	0.929	0.881	0.885	0.890	0.859	0.915	1.024
Al(T2) (IV)	1.212	1.338	1.395	1.331	1.344	1.357	0.929	1.254	1.424
Al(M4)	1.000	1.000	1.000	1.000	1.000	1.000	1.000	1.000	1.000
Fe(M1)	0.244	0.254	0.272	0.266	0.267	0.267	0.273	0.294	0.335
Mg(M1)	0.359	0.375	0.384	0.370	0.372	0.373	0.339	0.360	0.373
Al(M1) (VI)	0.132	0.222	0.265	0.233	0.235	0.238	0.083	0.220	0.273
v(M1)	0.095	0.149	0.260	0.124	0.126	0.128	0.073	0.126	0.282
Mg(M2+M3)	2.119	2.210	2.265	2.185	2.192	2.200	2.001	2.123	2.198
Fe(M2+M3)	1.442	1.500	1.604	1.568	1.572	1.575	1.608	1.735	1.978
Al(M2+M3)	0.219	0.290	0.414	0.231	0.236	0.240	0.010	0.141	0.253
End member composition[†]									
%Daph	8.12%	9.73%	14.29%	11.78%	12.55%	13.68%	14.12%	24.57%	45.38%
%Clin	59.16%	67.01%	70.48%	65.25%	66.57%	67.66%	48.09%	60.60%	66.17%
%Mg-Am	7.51%	15.10%	18.99%	15.57%	17.60%	19.18%	3.21%	12.92%	19.09%
%Mg-Sud	2.70%	8.16%	25.21%	2.19%	3.29%	5.14%	0.01%	1.92%	12.07%

Table A5b EMPA major element geochemistry results for chlorite in metasedimentary rocks of the NCGB, NW Ontario

	min[a]	mean[b]	max[c]	min	mean	max	min	mean	max
Chlorite	NCTK10-74A			NCTK10-75			NCTK10-76		
Wt%[d]	n: 13			n: 51			n: 39		
SiO_2	28.25	28.87	30.10	22.74	23.99	25.25	25.01	25.74	26.76
TiO_2	0.00	0.09	0.45	0.04	0.08	0.20	0.03	0.12	0.48
Al_2O_3	19.22	19.86	20.91	21.73	23.11	23.92	20.81	21.63	22.89
FeO_T	17.13	19.36	21.40	23.03	26.31	28.28	22.70	23.76	25.34
MnO	0.53	0.57	0.61	0.37	0.43	0.51	0.38	0.44	0.49
MgO	17.71	18.78	20.97	11.53	12.88	13.39	14.18	15.38	16.51
CaO	BDL	0.10	0.48	BDL	0.01	0.05	BDL	0.01	0.06
Na_2O	BDL	0.01	0.03	BDL	0.04	0.73	BDL	0.02	0.35
K_2O	BDL	0.12	0.80	0.00	0.10	0.85	0.01	0.09	0.88
F	BDL	0.05	0.17	BDL	0.00	0.05	BDL	0.00	0.06
Cl	BDL	0.01	0.02	BDL	0.01	0.19	BDL	0.01	0.06
Total	87.42	87.82	88.80	82.12	86.96	88.42	85.54	87.20	88.18
Ions on the basis of 28 positive char									
Si	2.889	2.932	3.005	2.500	2.571	2.663	2.612	2.706	2.785
Ti	0.000	0.007	0.035	0.003	0.007	0.016	0.002	0.009	0.038
Al	2.285	2.377	2.459	2.762	2.919	3.035	2.575	2.680	2.814
Fe	1.438	1.645	1.830	2.157	2.357	2.528	1.979	2.089	2.260
Mn	0.045	0.049	0.053	0.033	0.039	0.046	0.034	0.039	0.043
Mg	2.635	2.842	3.139	1.837	2.058	2.148	2.254	2.411	2.571
Ca	BDL	0.011	0.052	BDL	0.001	0.005	BDL	0.001	0.006
Na	BDL	0.002	0.006	BDL	0.007	0.153	BDL	0.004	0.070
K	BDL	0.016	0.101	BDL	0.013	0.114	0.001	0.012	0.117
F	BDL	0.015	0.055	BDL	0.001	0.018	BDL	0.001	0.020
Cl	BDL	0.001	0.003	BDL	0.002	0.034	BDL	0.001	0.010
Cation site distribution									
Si(T1)	1.926	1.954	2.003	1.667	1.714	1.775	1.741	1.804	1.857
Si(T2)	0.963	0.977	1.002	0.833	0.857	0.888	0.871	0.902	0.928
Al(T2) (IV)	0.995	1.068	1.111	1.337	1.429	1.500	1.215	1.294	1.388
Al(M4)	1.000	1.000	1.000	1.000	1.000	1.000	1.000	1.000	1.000
Fe(M1)	0.208	0.239	0.265	0.313	0.342	0.367	0.287	0.303	0.328
Mg(M1)	0.382	0.412	0.455	0.266	0.298	0.311	0.327	0.350	0.373
Al(M1) (VI)	0.048	0.146	0.185	0.172	0.265	0.299	0.126	0.234	0.269
v(M1)	0.154	0.204	0.344	0.046	0.094	0.204	0.080	0.113	0.235
Mg(M2+M3)	2.253	2.430	2.683	1.571	1.760	1.837	1.927	2.062	2.198
Fe(M2+M3)	1.229	1.407	1.565	1.844	2.016	2.162	1.692	1.786	1.932
Al(M2+M3)	0.087	0.163	0.416	0.134	0.225	0.359	0.106	0.152	0.234
End member composition[†]									
%Daph	1.80%	6.19%	10.96%	40.00%	57.16%	75.89%	18.20%	27.99%	44.14%
%Clin	62.70%	81.29%	89.08%	15.37%	29.14%	38.93%	43.60%	56.58%	66.84%
%Mg-Am	1.96%	7.95%	10.35%	5.22%	10.83%	13.96%	6.85%	13.64%	17.20%
%Mg-Sud	0.56%	4.56%	30.82%	0.37%	2.87%	11.50%	0.66%	1.79%	8.39%

[a] Minimum value. [b] Average of values from all ana [c] Maximum value.
[d] BDL: below detection limit. [†] Calculated from activity determined following Vidal et al. (2001).

Table A5c EMPA major element geochemistry results for biotite in metasedimentary rocks of the NCGB, NW Ontario

	min[a]	mean[b]	max[c]	min	mean	max	min	mean	max
Biotite	NCTK10-12B			NCTK10-20A			NCTK10-26A		
Wt%[d]	n: 5			n: 25			n: 26		
SiO_2	34.44	35.49	36.84	29.97	36.05	36.87	35.29	35.96	36.36
TiO_2	0.84	1.68	2.22	1.42	1.77	4.63	1.04	1.58	2.07
Al_2O_3	18.19	18.69	18.94	16.29	18.97	19.47	18.74	19.41	20.03
FeO_T	18.16	19.06	20.04	9.77	15.78	17.62	16.31	17.29	18.19
MnO	0.23	0.31	0.40	0.13	0.18	0.27	0.13	0.23	0.32
MgO	10.44	11.02	11.52	10.22	11.70	12.15	10.99	11.33	11.87
CaO	BDL	BDL	BDL	BDL	BDL	BDL	BDL	BDL	BDL
Na_2O	0.04	0.05	0.07	0.05	0.12	0.22	0.21	0.29	0.39
K_2O	5.24	7.94	9.48	6.69	9.31	9.79	8.43	8.83	9.17
F	0.15	0.20	0.25	0.20	0.27	0.39	0.16	0.24	0.34
Cl	0.02	0.02	0.03	0.01	0.01	0.02	BDL	0.01	0.03
Total	92.45	93.94	95.09	77.74	93.40	95.38	92.93	94.46	95.24
Ions on the basis of 22 positive charges									
Si	2.657	2.706	2.813	2.647	2.732	2.760	2.679	2.708	2.737
Ti	0.048	0.096	0.127	0.081	0.102	0.310	0.059	0.090	0.118
Al	1.637	1.679	1.705	1.666	1.695	1.774	1.675	1.722	1.769
Fe	1.146	1.216	1.279	0.726	0.998	1.104	1.022	1.089	1.145
Mn	0.015	0.020	0.026	0.008	0.011	0.020	0.008	0.015	0.020
Mg	1.181	1.252	1.325	1.266	1.322	1.400	1.239	1.272	1.332
Ca	BDL	BDL	BDL	BDL	BDL	BDL	BDL	BDL	BDL
Na	0.006	0.007	0.010	0.008	0.017	0.032	0.031	0.042	0.057
K	0.510	0.772	0.918	0.758	0.899	0.932	0.816	0.848	0.876
F	0.035	0.049	0.062	0.047	0.066	0.111	0.039	0.057	0.081
Cl	0.002	0.003	0.004	0.001	0.002	0.003	BDL	0.001	0.004
Cation site distribution									
Si	2.657	2.706	2.813	2.647	2.732	2.760	2.679	2.708	2.737
Ti	0.048	0.096	0.127	0.081	0.102	0.310	0.059	0.090	0.118
Al(IV)	1.139	1.198	1.275	1.025	1.166	1.270	1.172	1.202	1.232
Al(VI)	0.423	0.481	0.508	0.489	0.529	0.682	0.489	0.520	0.555
Mg(M2)	0.735	0.761	0.792	0.797	0.832	0.850	0.772	0.789	0.825
Fe(M2)	0.714	0.738	0.764	0.453	0.628	0.695	0.635	0.676	0.705
Mn(M2)	0.015	0.020	0.026	0.008	0.011	0.020	0.008	0.015	0.020
Mg(M1)	0.438	0.491	0.533	0.469	0.490	0.556	0.464	0.483	0.508
Fe(M1)	0.432	0.477	0.535	0.273	0.370	0.422	0.387	0.413	0.440
v(M1)	0.000	0.053	0.128	0.023	0.140	0.217	0.053	0.104	0.129
K(A)	0.510	0.772	0.918	0.758	0.899	0.932	0.816	0.848	0.876
Na(A)	0.006	0.007	0.010	0.008	0.017	0.032	0.031	0.042	0.057
v(A)	0.075	0.221	0.484	0.046	0.084	0.223	0.081	0.110	0.151
End member composition[†]									
%Fe-Al-cel	20.79%	27.90%	31.91%	22.43%	29.95%	32.30%	25.79%	29.71%	31.83%
%Ann	30.66%	34.40%	37.53%	9.04%	21.18%	28.00%	23.17%	27.12%	30.90%
%Phl	33.70%	37.69%	41.68%	42.29%	48.87%	58.66%	39.84%	43.17%	49.36%

Table A5c EMPA major element geochemistry results for biotite in metasedimentary rocks of the NCGB, NW Ontario

	min[a]	mean[b]	max[c]	min	mean	max	min	mean	max
Biotite	NCTK10-51A			NCTK10-74A			NCTK10-75		
Wt%[d]	n: 18			n: 4			n: 26		
SiO_2	34.33	35.64	36.21	35.44	36.14	37.19	33.48	34.85	37.66
TiO_2	1.51	1.72	1.87	0.49	1.28	2.22	1.74	2.04	2.46
Al_2O_3	18.59	19.07	19.40	19.24	19.62	20.13	17.76	18.49	19.23
FeO_T	17.50	18.22	19.63	12.77	14.83	15.86	19.74	21.11	22.53
MnO	0.24	0.27	0.33	0.39	0.42	0.44	0.18	0.23	0.27
MgO	10.49	10.72	11.04	12.46	13.62	14.68	7.44	8.58	8.99
CaO	BDL	BDL	BDL	BDL	BDL	BDL	BDL	BDL	BDL
Na_2O	0.03	0.09	0.18	0.04	0.06	0.08	0.03	0.12	1.06
K_2O	8.52	9.66	10.07	7.58	8.51	9.35	8.16	9.14	9.87
F	0.06	0.13	0.20	0.03	0.09	0.22	0.01	0.10	0.16
Cl	BDL	0.01	0.02	0.01	0.02	0.04	BDL	0.01	0.06
Total	93.27	94.81	95.71	93.33	94.06	94.91	91.20	94.05	96.85
Ions on the basis of 22 positive charges									
Si	2.639	2.699	2.721	2.672	2.696	2.734	2.643	2.699	2.805
Ti	0.088	0.098	0.106	0.027	0.072	0.124	0.102	0.119	0.145
Al	1.661	1.702	1.729	1.687	1.725	1.743	1.643	1.687	1.720
Fe	1.106	1.154	1.262	0.785	0.926	1.000	1.280	1.367	1.459
Mn	0.015	0.017	0.021	0.025	0.027	0.028	0.012	0.015	0.018
Mg	1.183	1.210	1.261	1.382	1.514	1.608	0.827	0.991	1.035
Ca	BDL	BDL	BDL	BDL	BDL	BDL	BDL	BDL	BDL
Na	0.004	0.014	0.026	0.006	0.009	0.012	0.005	0.017	0.153
K	0.839	0.933	0.971	0.729	0.809	0.877	0.807	0.903	0.969
F	0.014	0.032	0.049	0.006	0.020	0.051	0.002	0.024	0.039
Cl	BDL	0.001	0.002	BDL	0.001	0.001	BDL	0.002	0.008
Cation site distribution									
Si	2.639	2.699	2.721	2.672	2.696	2.734	2.643	2.699	2.805
Ti	0.088	0.098	0.106	0.027	0.072	0.124	0.102	0.119	0.145
Al(IV)	1.182	1.203	1.270	1.172	1.232	1.260	1.076	1.182	1.249
Al(VI)	0.438	0.498	0.539	0.474	0.493	0.514	0.432	0.505	0.612
Mg(M2)	0.747	0.760	0.778	0.860	0.919	0.987	0.536	0.622	0.651
Fe(M2)	0.699	0.725	0.772	0.481	0.562	0.599	0.798	0.858	0.917
Mn(M2)	0.015	0.017	0.021	0.025	0.027	0.028	0.012	0.015	0.018
Mg(M1)	0.436	0.450	0.490	0.522	0.596	0.622	0.290	0.369	0.399
Fe(M1)	0.408	0.429	0.490	0.303	0.364	0.406	0.452	0.509	0.545
v(M1)	0.020	0.121	0.157	0.000	0.048	0.115	0.071	0.122	0.258
K(A)	0.839	0.933	0.971	0.729	0.809	0.877	0.807	0.903	0.969
Na(A)	0.004	0.014	0.026	0.006	0.009	0.012	0.005	0.017	0.153
v(A)	0.021	0.053	0.157	0.112	0.181	0.264	0.015	0.080	0.179
End member composition[†]									
%Fe-Al-cel	22.60%	30.22%	33.53%	17.56%	20.28%	26.37%	25.10%	33.16%	48.92%
%Ann	29.92%	32.43%	38.74%	8.58%	15.20%	18.60%	39.70%	48.34%	55.56%
%Phl	35.43%	37.35%	40.14%	55.02%	64.53%	73.86%	10.67%	18.50%	21.38%

Table A5c EMPA major element geochemistry results for biotite in metasedimentary rocks of the NCGB, NW Ontario

	min[a]	mean[b]	max[c]
Biotite		NCTK10-76	
Wt%[d]		n: 17	
SiO_2	34.89	35.52	36.69
TiO_2	1.71	2.09	2.64
Al_2O_3	17.57	18.15	18.81
FeO_T	18.61	19.48	20.18
MnO	0.20	0.25	0.31
MgO	9.16	9.82	10.44
CaO	BDL	BDL	BDL
Na_2O	0.01	0.05	0.10
K_2O	8.90	9.54	9.87
F	BDL	0.07	0.13
Cl	BDL	0.01	0.07
Total	93.07	94.29	94.97
Ions on the basis of 22+ charges			
Si	2.693	2.722	2.772
Ti	0.099	0.121	0.153
Al	1.589	1.639	1.688
Fe	1.187	1.249	1.298
Mn	0.013	0.016	0.020
Mg	1.048	1.122	1.199
Ca	BDL	BDL	BDL
Na	0.001	0.007	0.014
K	0.874	0.933	0.962
F	BDL	0.017	0.030
Cl	BDL	0.001	0.009
Cation site distribution			
Si	2.693	2.722	2.772
Ti	0.099	0.121	0.153
Al(IV)	1.118	1.157	1.199
Al(VI)	0.435	0.482	0.526
Mg(M2)	0.671	0.711	0.745
Fe(M2)	0.748	0.791	0.818
Mn(M2)	0.013	0.016	0.020
Mg(M1)	0.377	0.411	0.454
Fe(M1)	0.430	0.457	0.480
v(M1)	0.069	0.132	0.165
K(A)	0.874	0.933	0.962
Na(A)	0.001	0.007	0.014
v(A)	0.030	0.060	0.119
End member composition[†]			
%Fe-Al-cel	27.55%	32.48%	37.36%
%Ann	34.23%	39.10%	42.41%
%Phl	22.93%	28.43%	33.53%

[a] Minimum value. [b] Average of values from all analyses. [c] Maximum value.
[d] BDL: below detection limit. [†] Calculated from activity determined following Parra et al. (2002).